Fluid Property Effects on Spray Cooling: An Experimental and Numerical Study

by

Andrea C. Ashwood

A thesis submitted in partial fulfillment of
the requirements for the degree of

Master of Science
(Mechanical Engineering)

at the

UNIVERSITY OF WISCONSIN-MADISON
2006

Fluid Property Effects on Spray Cooling: An Experimental and Numerical Study

Andrea C. Ashwood, M.S.
Department of Mechanical Engineering
University of Wisconsin-Madison, 2006
Professor Timothy A. Shedd, Advisor

Spray cooling is a process where liquid is atomized into droplets and sprayed onto a surface that is hotter than the saturation temperature of the fluid. The droplets impact the surface and spread, causing a thin liquid film to form. This liquid film is capable of removing large heat loads from the surface. The purpose of this study is to investigate the behavior of the spray film on the chip surface. Both pure fluids and mixtures were analyzed in an effort to ascertain the effects of fluid properties and to increase the performance of traditional spray systems. Measurements of the applied heat flux and temperatures at 8 locations per chip were taken. Measurements were also recorded for the conditions of the fluid being delivered to the die. From these, heat transfer coefficients and surface temperature distributions were obtained.

Separately, the first step toward a general model of spray cooling was developed. The velocity distribution was characterized by two layers: the viscous sublayer, characterized by a linear profile, and the fully turbulent region, characterized by a power law profile. A numerical model and correlation for the thin film were both derived based on the two layer theory using a velocity profile predicted by a computational fluid dynamics (CFD) model in an effort to ascertain the fundamental behaviors behind the spray cooling phenomena. The model included mass flow and momentum equations integrated through the thickness of the thin liquid film and was implemented in an iterative software program (EES) with good agreement to previous empirical data. The correlation was also in good agreement to the data obtained in this work.

Acknowledgments

First, I'd like to thank God for all of the blessings that He has bestowed on me thus far. I'd especially like to thank my advisors, Professors Tim Shedd and Greg Nellis, for their constant encouragement both through my undergraduate and graduate studies. I know that it hasn't been an easy journey, but thank you both so much for helping me to grow as a student, an engineer and person. Thank you to Professor Frank Pfefferkorn for being on my defense committee and for his advocacy for me as a student. Ich danke Ihnen vielmals.

The decision to continue in higher education couldn't have been made without the eternal support of my family: my parents Lachelle Ashwood and Anthony Leflore, my aunt Kimberly Ashwood, my grandmothers Mary Jones and Elmira Canady, my brother Anthony Ashwood and my cousin Nicole Enoch. I'd also like to thank my friends for listening to me even when they had no idea what I was talking about. Thank you all for your support, advice and love. I couldn't have gotten this far without it.

During the course of this project I received help from an undergraduate student, Sander Hunter. I'd like to thank him for all of his hard work in the machine shop as well as the lab. I'd also like to thank undergraduates Ben Regner and Amy Stoikes for keeping me entertained during countless hours of data acquisition.

Thank you to Cray, Inc. and the Center for Power Electronic Systems (CPES) for funding this project and the Graduate Research Scholars (GERS) community. Lastly, I'd like to thank my friends and colleagues (both new and old) from the Solar Energy Lab and the Multiphase Flow Visualization Analysis Lab. Especially Adam, Curtis, Diego, Kate, Rodrigo, Rory, Ryan, Scott, and Terry. Thank you for the hilarity, the camaraderie and the fun. Without it life would have been very dreary indeed.

Table of Contents

List of Tables

List of Figures

Nomenclature

Symbol		Description	Units
Symbols			
A	=	area	[cm^2]
CHF	=	critical heat flux	[W cm^{-2}]
C_p	=	specific heat	[J g^{-1} C^{-1}]
δ	=	boundary layer thickness	[m]
$\delta\Delta T_{surf}$	=	uncertainty in T$_{surf}$ - T$_{in}$	[^{o}C]
δh	=	uncertainty in heat transfer coefficient	[W cm^{-2} K^{-1}]
δP	=	uncertainty in power measurement	[W]
δ^+	=	non-dimensional boundary layer thickness	[m]
δq	=	uncertainty in heat flux	[W cm^{-2}]
δV	=	uncertainty in voltage measurement	[V]
δ_M	=	momentum boundary layer thickness	[m]
δ_ν	=	viscous sublayer thickness	[m]
δ_T	=	thermal boundary layer thickness	[m]
ΔP	=	pressure difference across the system manifold	[psid]
ΔT_{sat}	=	T$_{surf}$ - T$_{sat}$	[^{o}C]
ΔT_{surf}	=	T$_{surf}$ - T$_{in}$	[^{o}C]
dx	=	length of each node	[m]
h	=	heat transfer coefficient	[W cm^{-2} K^{-1}]
h_fg	=	heat of vaporization	[J g^{-1}]
i	=	node value	
k	=	thermal conductivity	[W m^{-1} C^{-1}]
L	=	node interval length	[m]
$\dot{m}''_{drop}$	=	droplet mass flux	[kg s^{-1} cm^{-2}]
$\dot{m}''$	=	mass flux	[kg s^{-1} cm^{-2}]
MC	=	percent of momentum in x-direction	
N	=	number of nodes	
P	=	pressure	[kPa]
Pr	=	Prandtl number	

Q''	=	droplet flux	[mL cm^{-2} s^{-1}]
$\overline{Q''}$	=	average droplet flux	[mL cm^{-2} s^{-1}]
T_{bub}	=	bubble temperature	[^{o}C]
T_{in}	=	inlet temperature	[^{o}C]
T_{sat}	=	saturation temperature	[^{o}C]
T_{surf}	=	surface temperature	[^{o}C]
u_{drop}	=	velocity of droplet	[m s^{-1}]
U_{δ_T}	=	thermal sublayer velocity	[m s^{-1}]
U_{∞}	=	viscous sublayer velocity	[m s^{-1}]
u^{+}	=	non-dimensional velocity	
u^{*}	=	friction velocity	[m s^{-1}]

Greek symbols

α	=	thermal diffusivity	[m^2 s^{-1}]
ϵ	=	cooling effectiveness	[J mL^{-1}]
μ	=	liquid dynamic viscosity	[cP]
ν	=	liquid kinematic viscosity	[m^2 s^{-1}]
ρ	=	density	[g mL^{-1}]
τ	=	solid surface shear stress	[Pa]
τ_w	=	wall shear stress	[Pa]

Chapter 1

Introduction

In this technological age, consumers yearn for sleeker products, from MP3 players to hybrid vehicles. This slimming down directly impacts the design of next generation electric drives and their control electronics. But getting higher heat loads out of smaller modules is rapidly becoming a design limitation for power electronics as well as other applications incorporating microelectronic devices. Amazingly, this trend was predicted in 1965 by Dr. Gordon Moore [1]. Moore's law, as it is commonly called, predicted an exponential increase in the number of components on a computer chip. This exponential growth has continued for decades despite repeated warnings that the physical limits of microelectronics are approaching rapidly. However, what Moore failed to realize is that the power density of the integrated circuits would increase exponentially as well, which requires the removal of high heat fluxes from very small packages.

Liquid or two-phase cooling configurations have been proposed as potential thermal management strategies for high heat flux removal using either direct contact between the fluid and the electronics or indirect methods that involve water or refrigerant-cooled plates attached to the electronics package at the module or chip level [2, 3]. Indirect methods are challenged by the large temperature drop required to overcome the contact resistance between the package and the plate at high heat flux. The contact resistance can be reduced using a chilled liquid or by incorporating the heat exchanger directly into the electronic device; both of these approaches require additional research and development before they can be applied in a practical system [3]. Direct liquid cooling options include forced single-phase liquid or two-phase evaporation energized by jet or spray impingement of a dielectric fluid. Various forms of direct liquid cooling have been implemented in practical systems and these

systems have been proven very effective at removing heat dissipation at the device level [4].

Spray cooling represents a liquid cooling configuration that shows promise for the removal of high heat fluxes. The working fluid in a spray cooling system is pumped to a nozzle, or array of nozzles arrayed over the surface generating heat. These nozzles atomize the fluid by forcing it through orifices of small diameters so that small droplets strike the surface at high velocity. Upon impact, the droplets merge into a thin turbulent film that, under typical operating conditions, will completely cover the surface. Thermal transport to this turbulent thin film is characterized by high heat transfer coefficients, which means that high heat fluxes may be removed with a relatively small temperature difference between the surface and the fluid.

Chen et al. [5] found that the mean droplet velocity had the strongest effect on the heat transfer coefficient, followed closely by the mean droplet flux. Unfortunately, simple generalized correlations based on droplet flux have not been identified. Rybicki and Mudawar [6] found that the heat transfer coefficient was a function of the Sauter mean diameter, volumetric flux and various liquid properties. They developed a correlation for the Nusselt number based on these findings and found that their heat transfer data could be correlated within 13% using this correlation. No work has been done, to the authors knowledge, to study mixtures in spray cooling technology.

The advantage of spray cooling systems is that they have the potential to be compact and lightweight, as well as simple and essentially maintenance-free, as can be seen with the commercial success of the implementation of the Cray X1 vector supercomputers [7]. Our knowledge of spray cooling, however, is limited. Namely, it is not clear how fluid properties impact spray cooling performance. Moreover, there are very few generally applicable empirical or numerical models documented in the literature.

Since spray cooling is characterized by an extremely thin fluid layer moving at very high velocity, the fluid layer is continuously subjected to a high rate of droplet impingement.

Therefore, it is expected that the heat transfer coefficient degradation reported for flow boiling of refrigerant mixtures will not manifest itself in spray cooling. This degradation is due to the development of concentration gradients. In spray cooling, the fluid will remain well-mixed, eliminating these concentration gradients and therefore avoiding the associated loss of performance.

1.1 Thesis Summary

This work presents the results of an experimental investigation of the heat transfer performance of pure Fluorinerts FC-72, FC-74 , FC-40 and segregated hydrofluoroethers HFE-7000 and HFE-7001 using conical spray nozzles and their respective mixtures. This thesis also presents a numerical model that was developed as an initial step toward predicting the heat transfer behavior of the sprays. A correlation was developed to try to understand the actual mechanisms behind the spray film and to relate this performance to fluid properties that are easily measured. This thesis includes a review of previous spray cooling research, mixture boiling and numerical modeling of turbulent flows. Experiments that are closely related to some components of spray cooling with mixtures, such as pool boiling and liquid film boiling, were also researched in order to gain insight into mixture behavior. A complete description of the experimental test facility is given. Also, a detailed experimental method is provided along with the results from the experiment and the models. Finally, conclusions are drawn using the results from the experiments together with the models in order to understand the mechanisms of heat transfer that are at work in spray cooling.

1.2 Objectives

The overall objectives of this project are:

To determine the effects of fluid properties on spray cooling performance. Based on a comparison of water and Fluorinert data, it was hypothesized that the thermal conductivity would be the most important parameter in terms of heat transfer performance.

To evaluate the use of mixtures in spray cooling. Sensible heating is the heat removal mechanism that dominates in pure components [8], but evaporation should become more significant in mixtures at lower saturation temperatures.

To investigate the fundamental mechanisms of spray cooling. The numerical model and correlation were both derived in an effort to ascertain the fundamental behaviors behind the spray cooling phenomena.

Chapter 2

Background

Spray cooling has been shown to yield heat flux removal rates that are approximately an order of magnitude higher than can be achieved by pool boiling using the same fluid [9]. Unfortunately, the heat removal requirements of electronics technology are fast outpacing the capabilities of traditional spray systems. The purpose of this work is to extend the life of traditional spray cooling systems. A literature review of spray cooling, evaporation of mixtures, and numerical modeling of thin turbulent films is presented in this chapter.

2.1 Spray Cooling

Spray cooling, and more generally, liquid impingement cooling, represents a direct liquid cooling configuration that is capable of removing high heat fluxes. The working fluid in a spray cooling system is pumped through a nozzle or nozzles that are arrayed over the surface generating heat; for electronics cooling this surface is ideally the back side of a device or integrated circuit. The nozzles atomize the fluid so that small droplets strike the surface at high velocity. Upon impact, the droplets merge into a thin turbulent film that, under typical operating conditions, will completely cover the surface. Thermal transport to this turbulent thin film is characterized by heat transfer coefficients on the order of 1 W cm^{-2} K^{-1} for dielectric liquids.

Previous work suggests that the heat transfer coefficient (i.e., heat transfer performance) can be correlated to the fluid droplet diameter [6]. However, more recent data from extensive studies using gas-subcooled Fluorinert FC-72 by Pautsch and Shedd [10, 11], shows minimal influence of the drop size and also hypothesized that the thickness of the liquid that forms on the surface was not directly related to the local heat transfer performance [12]. Chen et al.

independently varied numerous spray parameters including flow rate, droplet size, droplet flux and droplet velocity and found that the droplet velocity had the largest effect on the heat transfer coefficient [5]. Kopchikov et al. [13] correlated the heat transfer coefficient in a thin liquid film using fluid properties and a non-dimensional fitting parameter for a single wall jet and achieved good agreement to their experimental data. However, this correlation does not predict spray cooling heat transfer data. This is an expected result due to the fact that Kopchikov et al. derived their correlation based on a nucleation site length scale which doesn't capture the physical behavior of spray cooling.

Some studies have been done on the effects of evaporation on the spray cooling performance. Rini found that, at low heat fluxes on the order of 1 W cm^{-2}, phase change could account for 36% of the total heat flux [14]. However, Pautsch and Shedd's data indicate that, although two phases are present in the sprays and within the liquid film, the thermal energy is carried away from the heated surface primarily through sensible heating of the impinging liquid rather than the formation of vapor [10, 15]; Estes and Mudawar [16] have made similar observations. Using a novel, high resolution local heat transfer measurement technique, Freund et al. [17] have shown that the heat transfer coefficient beneath the spray can vary by a factor of 10 to 20 within the spray impact region. Due to the predominance of sensible heating as a heat removal mechanism, large temperature variations can exist across the heater surface, even when the surface is completely covered by impinging droplets [15].

The Sauter mean diameter, correlated by Mudawar and Estes [16], is a common length scale used for correlating heat transfer performance. It relates the orifice diameter to the Weber and Reynolds number based on orifice flow conditions. This is done so that data can be compared between experiments with very different nozzles. Another length scale has been recently suggested by Jiang and Dhir [18]. They sprayed deionized and degassed water through a single nozzle in an environment where the partial pressure of the vapor and the total system pressure were both varied. They found a temperature dependent Reynolds

number and Prandtl number using the diameter of the heated surface as a length scale and were able to correlate the Nusselt number in the single phase region within ± 10% of their data.

Although spray cooling systems exhibit high heat transfer performance, they are still limited by a critical heat flux at which the surface dries out and the surface temperature rapidly rises, preventing re-wetting. Mudawar and Estes [6, 19] systematically studied and correlated the critical heat flux for conical sprays of FC-72, FC-87 and water impinging on a square heater. This correlation, which has been independently verified [20], provides some insight into the effects of subcooling and geometry, but the mechanisms leading to the critical heat flux (CHF) condition are still unclear. Chen et al. found that the droplet velocity had the most dominant effect on the onset of critical heat flux [5].

Horacek et al. [20] provide the most detailed study to date on the near-wall mechanics of spray cooling and critical heat flux through the use of a micro-heater array. They used a high speed digital camera and a tele-microscopic lens to capture the images and a unique total internal reflection imaging technique to analyze the areas of liquid-solid contact areas. They found that thermal subcooling did not have a significant effect on CHF, but that so-called gas-subcooling[1] was significant. Furthermore, through the analysis of plots illustrating the relationship between the wetted area fraction and the wall superheat, the authors concluded that critical heat flux did not appear to be caused by a deficit of liquid flux to the surface; rather, CHF is correlated to the lengthening of the total length of the three-phase contact lines observed.

Previous work also shows that fluid management is an important consideration when using spray cooling technology in a closed system. Pautsch and Shedd indicated that the performance of the system was limited by the area of the die that exhibited the worst

[1] gas subcooling occurs when a non-condensible, such as nitrogen, is used to pressurize the system above the saturation pressure for the liquid temperature

performance. In multi-nozzle arrays this area was often the center region of the die due to flow interactions from neighboring nozzles. Using a single nozzle, this occurred at the edges of the die where there was no continual addition of cooler fluid and less mixing in the film due to a lack of droplets perturbing the free surface of the film [10]. They also found that their single nozzle data could be modeled using the superposition of the contribution from single phase convection in the impact region and a contribution from the thin film in the boiling region outside of the impact zone. Their multiple nozzle data were modeled similarly with the addition of a constant that was used to represent the spray interaction between the nozzles [15]. Rybicki and Mudawar found a single phase Nusselt number correlation for their full cone nozzles that matched their experimental results with an overall mean absolute error of 13 %. They also found that orientation had virtually no effect on the spray cooling performance provided that the liquid management was sufficient to prevent liquid build up on the test surface [6].

Mudawar and Valentine correlated critical heat flux to volumetric flux and Sauter mean diameter for water. Their data precluded any definitive assessment of the impact of key fluid properties because they only used one fluid, water, and varying flow rates [21]. Estes and Mudawar looked at FC-72 and FC-87 and found an increase in single phase heat transfer coefficient and critical heat flux with increasing the droplet flux and decreasing the Sauter mean diameter. They also found that critical heat flux was influenced by the thermophysical properties of the fluid, flow parameters, orifice parameters, and heater length [16]. Chen et al., however, found that the Sauter mean diameter had no definitive effect on heat transfer performance or the onset of critical heat flux [5].

The spray nozzle geometry, for example nozzle height, has also been studied. Estes and Mudawar looked at spray cooling with a single nozzle and found that the optimum cooling performance occurred when the nozzle height was such that the spray impact zone just inscribes the heated surface [22]. Horacek et al. had the nozzle oriented at such a

height that they oversprayed the heater surface in their experiment. However, they looked at critical heat flux rather than cooling performance and found that the critical heat flux increased with increasing gas content which was controlled by varying the pressure within the test section. They compared their experimental results to the correlation found by Estes and Mudawar and found agreement within 30% absolute error [20].

Silk et al. conducted a study on enhanced surfaces and found that the the performance of enhanced surfaces in the single phase region exceeded that of the flat surface. A straight fin array performed best, followed by a cubic pin fin array, and finally a pyramid pin fin array had the poorest performance. The straight fin and cubic fin had the same wetted area, so it was hypothesized that the difference must have been due to fluid management or the efficiency with which the wetted surface was utilized. They also looked at spraying at different angles and found that the spray angles greater than 15° eliminated the excess liquid on the heater surface due to the multiple nozzle stagnation zone phenomena [23].

2.2 Mixtures

The use of mixtures in spray cooling is attractive because it may be possible to preferentially evaporate one component and keep the surface wetted with the other component. The development of concentration gradients is possibly one reason behind the degradation in mixture performance when compared with that of pure components in horizontal tube boiling [24]. Collier and Thome [24] also found that that the onset of boiling was delayed with increased wall superheats. They hypothesized that the temperature gradients set up in the pool to accommodate the corresponding gradients in the liquid composition caused the heat transfer coefficient in the nucleate boiling region to be sharply reduced.

Based on the knowledge of spray cooling behaviors and mechanisms presented above, it was hypothesized that spray cooling with mixtures of miscible liquids would demonstrate

both improved heat transfer performance as well as elevated critical heat flux. For example, since the mechanism for heat removal in spray cooling appears to be dominated by sensible heating over a large range of conditions, adding a latent heat storage component (such as evaporation) could maintain a lower liquid temperature during heat removal, even with the temperature glide. This behavior should be advantageous for the minimization of temperature gradients across a heated surface and for the management of so-called hot spots: localized evaporation could prevent large temperature changes when uneven heat flux patterns are encountered. Since critical heat flux appears to be related to the failure of the liquid to maintain a large net contact line length [20], mixtures could elevate the onset of the critical heat flux due to the more volatile liquid in the mixture encouraging evaporation while maintaining less-volatile liquid between bubbles. In addition, the difference between the dewpoint and the bubble point at a given concentration yields the temperature glide at a constant pressure. This can be useful in mixtures to reduce the entropy generation due to heat transfer by matching the temperature variation of the surface with that of the heat transfer fluid [25].

Conventional pool boiling and flow boiling experimental results for mixtures of refrigerants and glycol/water mixtures described in the literature appear to contradict this hypothesis of improved heat transfer performance. In virtually every case, heat transfer performance decreases with the use of mixtures, sometimes by as much as 50% or more [24]. The reduction in performance is thought to be related to a stratification of components of the mixture during the evaporation process. As the liquid is heated, a temperature gradient is produced that drives the more volatile liquid away from the heated surface. The layer of liquid left behind is rich in the less volatile component and acts as a resistance to further transport by the more volatile component. Stephan et al. found that the actual heat transfer coefficients of binary and ternary mixtures (of acetone/methanol and ethanol/water) were found to be lower than the ideal case, which was found using the assumption that the heat transfer

coefficient would vary linearly with mole fraction. The deviations in the heat transfer coefficient from ideal are considerable when the equilibrium compositions of vapor and liquid differ substantially, but decrease as the azeotropic point is approached [26].

Ross et al. looked at boiling in horizontal tubes [27]. In annular two-phase flow, heat is conducted across the liquid layer and, especially in a horizontal geometry, the liquid film at the bottom of the tube is thicker than at the top of the tube due to gravity. For pure components, the wall temperature at the bottom is higher than at the top because of increased resistance to heat conduction. The result is a higher heat transfer coefficient at the top of the heated tube.

In mixtures, the heat transfer coefficient at the bottom was higher than at the top. It was hypothesized that this was due to varying mixture concentrations along the circumference of the tube. Ross et al. found that more R13B1 (the more volatile component) accumulated at the bottom of the tube due to gravity-assisted draining of the bulk fluid. This led to an opposition between the depletion of the more volatile component and the film thickness, which led to a higher heat transfer coefficient toward the bottom of the heated tube.

Mixture behavior has been studied extensively in horizontal flow boiling. It appears that the fluid properties vary greatly with the addition of the second component. This results in the so called Marangoni effect. The more volatile component (or the component with the lower boiling point) has the lowest surface tension. Thus it becomes exhausted in the thin liquid layer between two adjacent vapor bubbles. This results in a high local value of the surface tension compared to the rest of the bubble wall and coalescence of the bubbles is avoided due to contraction of both bubble walls. This delay in coalescence of the bubbles is thought to be what delays the onset of critical heat flux at the wall.

Van Strahlen showed that the individual components of a mixture pass from liquid to vapor phase in different proportions. The faster evaporation of the more volatile component results in the enrichment of the bubble forming boundary layer with the less volatile compo-

nent. As a result, the local bubble point temperature is increased [28]. In addition, Stephan et al. found significant changes in the transport properties of the mixture composition that could significantly impact the heat transfer performance [26].

Van Strahlen [28] also noted that the rate of bubble growth in pure components depends on the heat flow toward the bubble boundary to satisfy the heat requirement for evaporation. In mixtures, the heat diffusion is linked with mass diffusion of the more volatile component, which is rapidly depleted in the liquid immediately adjacent to the bubble. This results in a slowing of the bubble growth because the mass diffusivity is an order of magnitude smaller than the thermal diffusivity.

Fujita and Tsutsui looked at mixtures of R123 and R134a, R142b and R123, and R134a and R142b and developed a correlation for the heat transfer coefficient in binary mixtures that could predict experimental results within 4.1% absolute error, but this predictive ability was reduced substantially with increasing temperature glide. Moreover, the correlation incorporated the use of two parameters which were varied to fit each individual data set. Therefore, this correlation did not capture the effects of fluid properties and mixture behavior [29].

Celato et al. hypothesized that the heat transfer deterioration observed for mixtures was controlled by the heat diffusion and mass diffusion and that the mass diffusivity for the more volatile component was generally an order of magnitude smaller than the thermal diffusivity. The mass diffusion effect diminished as subcooling increased, and they hypothesized that this was due to two effects: the increasing contribution of single phase natural convection in energy transfer and the condensation of vapor bubbles at or near the heated wall as subcooling increased. The latter of these would reduce the depletion of the more volatile component in the liquid phase close to the wall [30]. The bubble growth in binary mixtures is limited by the rate at which heat can diffuse to the interface to provide latent heat of vaporization (as in a single component system) and also by the depletion of the more volatile

component of the liquid mixture closest to the bubble interface [31].

Thome looked at bubble growth in liquid argon and liquid nitrogen and binary mixtures of the two. He found that the bubble departure waiting time for mixtures was twice that found for either pure component. This contributed to a general decrease in the latent and sensible heat rates in the mixtures. This decrease was also evident in the heat transfer coefficients of the mixtures. Thus, he hypothesized that the effect of mass diffusion controlled bubble growth in binary mixtures is the retardation of the main heat transport mechanisms (i.e., the vapor-liquid exchange and evaporative mechanisms) [32].

Spray cooling, however, is characterized by an extremely thin fluid layer moving at very high velocity. Also, the fluid layer is continuously subjected to a high rate of droplet impingement. Therefore, it is expected that the heat transfer coefficient degradation reported for flow boiling of refrigerant mixtures will not manifest itself in spray cooling. The fluid will remain well-mixed, eliminating the concentration gradients that occur in more traditional boiling applications. The literature is unclear whether or not critical heat flux would actually increase or decrease with mixtures [33], but this was not the focus of this study.

2.3 Numerical Modeling

Despite the large amount of experimental work on spray cooling systems, the underlying physical processes responsible for its high thermal performance are not well understood and a detailed model that is suitable for the design and optimization of these systems does not currently exist. There have been few documented attempts to create an engineering model of a spray cooling system that accurately captures the fluid dynamics and thermal transport associated with the atomized droplets and thin turbulent fluid film. Fundamentally, spray cooling is a complex convective heat transfer problem; however, the governing equations of mass, momentum and energy conservation are quite familiar. The spray models that do

exist use turbulent wall functions or other empirical correlations in order to approximate the velocity profile in the fluid film. This approach is required due to a lack of detailed knowledge of the characteristics of the turbulent thin film which is created by, and interacts with, the impinging droplets. Models that use such empirical techniques can produce accurate results for a specific configuration and operating condition, but, this type of model is very case-specific and not entirely suitable for design and optimization.

Yang et al. modeled droplets of n-heptane and water impacting the heated surface. The technique adopted in this model involved an Eulerian, fixed grid, finite volume algorithm coupled with level set methods that track the deformation of the droplet surface. Comparisons with experimental results found in the literature were in good agreement (i.e., the droplet deformation process and surface temperature variation agreed well) [34].

Selvam et al. [35] used computer modeling to model the liquid and vapor during nucleate boiling and used the level set method introduced by Sussman et al. [36] for bubble dynamics, which was modified by Son and Dhir [37] to accommodate phase change. The collapse of the vapor bubble in the liquid layer either by the liquid droplet impingement at high speed or the vapor bubble breaking during the merging of the vapor on the top of the thin film both had a major impact on the heat transfer. Selvam et al. hypothesized that the major phenomena in spray cooling is as a complex interaction of transient conduction of heat from the surface into the liquid and convection of the liquid during droplet impact or the breaking of the vapor bubble [35].

Stanton and Rutland [38] created a multi-dimensional model of the dispersion of liquid fuel droplets in a combustion cylinder. In order to account for the fuel distribution along the surface of the engine they used thin film assumptions that were achieved by solving the continuity, momentum and energy equations for the fuel film. Included in the model were the interactions with the fuel film created by impinging droplets on the cylinder wall, droplet splashing, interfacial shear, piston acceleration, dynamic pressure, conduction, and

convective heat and mass transfer. Their model showed good agreement with experimental results.

Chapter 3

Experimental Description

Five fluids were investigated in this work. The first, fluorocarbon perfluorohexane, is a dielectric fluid used in electronics cooling applications and commonly known as the 3M specialty fluid FC-72. The second is a more viscous dielectric fluid with a much higher boiling point, known as FC-40. The third fluid is closely related to FC-72 and is known as FC-74. The final fluids are segregated hydrofluoroethers known as HFE-7000 and HFE-7100. All of these fluids are engineered by 3M and their saturated liquid properties are summarized in Table 3.1 [39].

Table 3.1: Thermal Properties of Fluids at P=1 atm.

Fluid	ρ [g mL^{-1}]	k [W m^{-1} C^{-1}]	μ [cP]	C_p [J g^{-1} C^{-1}]	h_{fg} [J g^{-1}]	T^o_{sat} [C]
FC-72	1.68	0.057	0.64	1.05	88	57
FC-74	1.77	0.064	0.79	1.05	92	101
FC-40	1.85	0.065	3.4	1.1	68	155
HFE-7000	1.40	0.075	0.45	1.3	142	34
HFE-7100	1.47	0.073	0.38	1.13	111.6	61

Mixtures of these fluids were generated volumetrically. Measured volumes of FC-72, FC-40, FC-74, HFE-7100 and HFE-7000 were mixed together and added to the test facility with an uncertainty of ± 2 mL, leading to an uncertainty in composition of $\pm 0.15\%$.

3.1 Test Facility

The spray cooling test facility was donated by Cray Inc. and consists of two integrated sub-systems: the fluid delivery system and the instrumentation system. The fluid delivery system was modified for these testing purposes and includes a chiller, a Coriolis flow meter, a system manifold, a spray cap, a spray plate, and a heat exchanger. A schematic of this

facility is shown in Fig. 3.1.

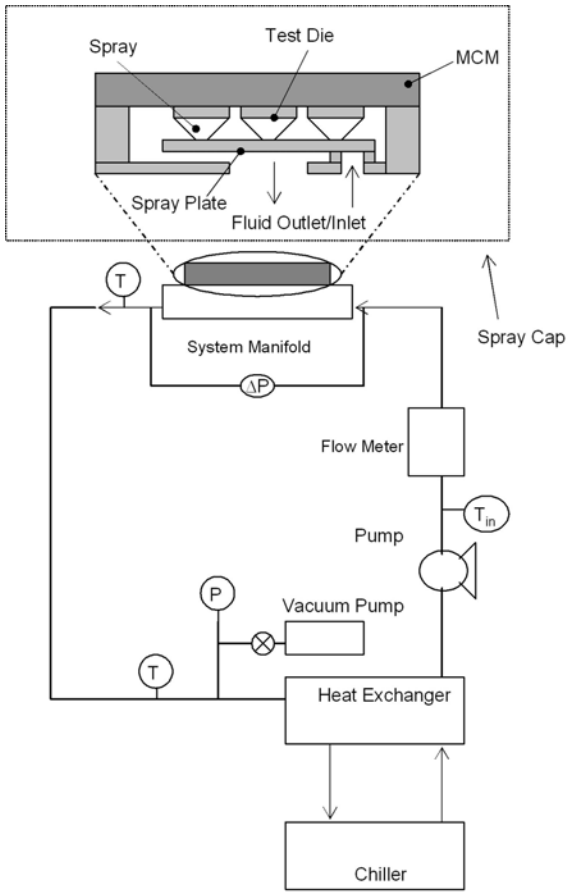

Figure 3.1: Schematic of spray cooling test facility

The chiller was a Neslab model 3310511-2 chiller. The heat exchanger was a model number FP3X8-1K plate heat exchanger from Flat Plate Inc. The pump was a custom designed gear pump manufactured by MicroPump and was magnetically coupled to a Leeson 1/2 horsepower AC motor (model number PR000108). The flow meter was a Model F025 MicroMotion BASIS coriolis flow meter, which measured the volumetric flow rate (Q) and temperature (T_{in}). The device measured the temperature of the fluid to ± 0.1°C and the volumetric flow rate to ± 3 mL min^{-1}. The fluid was then delivered to the system manifold through a quick-disconnect fitting where it flowed into the spray cap. Type T thermocouples

were placed at the inlet of the flow meter, the drain of the spray cap and downstream of the spray cap. A pressure transducer was placed downstream of the spray cap and used to monitor the pressure of the fluid, specifically for use with the non-gas-saturated data.

3.2 Spray Nozzles and Thermal Test Dies

Multiple swirl-atomizing, full cone spray nozzles were custom designed and manufactured by Parker-Hannifin, and incorporated into a steel spray plate. Two types of nozzle arrangements were included on a single spray plate, as shown in Fig. 3.2; single nozzles are located in the corners while sets of 4 nozzle arrays located in the more central regions. The nozzles are 0.3 mm in diameter and placed 6.8 mm directly below the centers of the test dies. The spray plate is secured onto a stainless steel system manifold that contains the fluid inlet and outlet ports as well as the mounting flange. The system manifold, or spray cap, is sealed to a modified multi-chip module (MCM) substrate using an O-ring. The entire spray manifold assembly is oriented so that the fluid is sprayed upward (against gravity) onto the test dies and draining of the fluid is gravity assisted. This arrangement was necessary to prevent pooling of coolant on the substrate, which significantly decreases the heat transfer performance of this spray system design. The fluid then drains back into the heat exchanger, as seen in Figure 3.1.

The MCM consists of eight thermal test dies that are located above the 8 nozzle arrays on the spray plate (see Fig. 3.2). The thermal test dies were custom developed and manufactured by the IBM Corporation. Each test die is 15 mm on a side and contains four resistive heating elements and nine solid-state diode temperature sensors that are integrated into the silicon substrate (Fig. 3.3). The four heating elements divide the die into quarters. The placement of the temperature sensors is indicated in Fig. 3.3. These diode sensors have been calibrated to $\pm 0.2^{\circ}$C in a precision environmental chamber [8]. One of the corner tem-

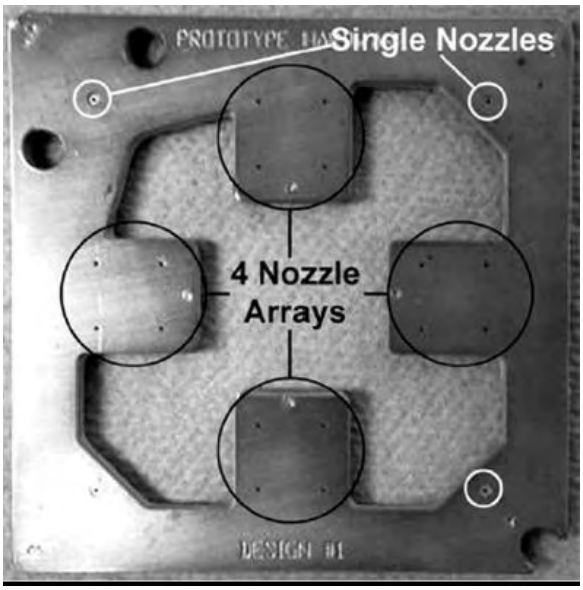

Figure 3.2: Spray plate containing 4-nozzle arrays and single nozzles in the corners

perature sensors is used exclusively by the thermal shutdown circuit and is not monitored by the data acquisition system.

3.3 Data Acquisition

The data acquisition system included all of the necessary electronic equipment to drive the fluid delivery system, to power the eight test dies, and to acquire any necessary measurements. The test stand is controlled and monitored using a LabView based program. The program controls the power level that is applied to all of the test dies as well as the speed of the pump. A National Instruments SCXI data acquisition system is used to acquire and save experimental measurements. The SCXI modules are used to obtain temperature measurements from the test dies, voltage and current measurements, pressure readings, flow rate readings, and thermocouple temperature measurements of the air and the fluid [8]. The test die power levels are actively controlled using a Xantrex XFR 60-20 as the main power supply. The Xantrex supplies nominally 48 VDC to four DC-DC converter units that were

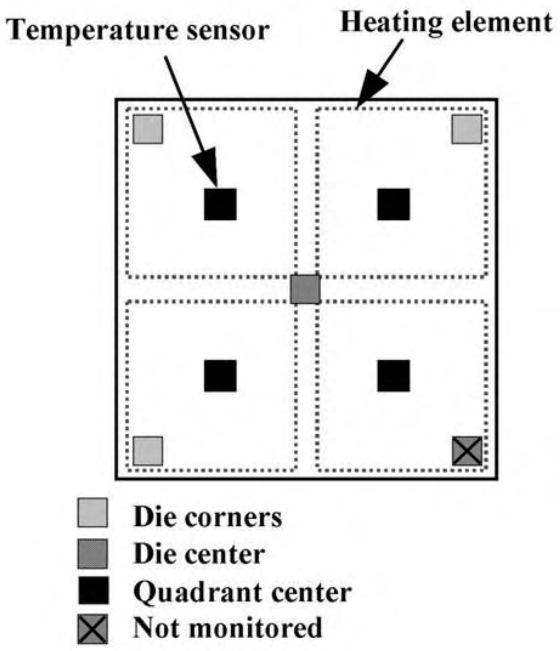

Figure 3.3: Thermal test die containing 4 resistive heating elements and 9 diode temperature sensors. One thermal test die is located above each of the nozzle arrays in the spray plate shown in Fig. 3.2

custom fabricated by Cray, Inc.

3.4 Test Procedure

The test facility is designed to protect the test dies from thermal failure. A minimum fluid flow rate must be detected (using a differential pressure measurement across the nozzles) before it is possible to apply power to the heating elements. Also, the maximum allowable surface temperature is 110°C; exceeding this temperature results in an automatic shutdown of power to the heating elements in order to protect the integrity of the electrical elements used in testing. The desired fluid flow rate is set by adjusting the speed of the pump. The initial power level to an individual die starts at 5 W for each run. The test facility is maintained at each power level for at least 40 seconds before acquiring data so that the

system reaches steady state. The power level is increased in 5 W increments until a thermal limit is reached and system shut-off occurs.

The thermal limit can occur in two ways. In some tests, the surface temperatures are uniformly and significantly below the maximum allowable safe temperature (110°C) at one level of heat flux but rapidly rise when the heat flux is increased by 5 W for the next data point. This rapid and dramatic rise in surface temperature is characteristic of exceeding the critical heat flux, which results in the incipience of dryout at some location on the heater. In other tests, the surface temperatures smoothly increase with applied heat flux until the surface temperature at some location reaches 110°C and the system shuts off. This occurs without a sudden, significant increase in temperature; therefore the CHF is not reached. Rather, the temperature limit of the test dies has been encountered before the system reaches CHF.

3.5 Data Reduction

The average heat transfer coefficient (h) is defined as the ratio of the heat flux (q'') to the difference between the inlet fluid temperature (T_{in}) and the average die surface temperature (T_s)

$$h = \frac{q''}{T_s - T_{in}} \tag{3.1}$$

The average surface temperature was determined by averaging the measurements at the eight different locations on the test die (see Figure 3.3). It should be emphasized that the heat transfer coefficient is an average value based on the conventional, though somewhat arbitrary, definition in Eqn. (3.1). The local heat transfer coefficient could not be calculated because the local liquid film temperature was not known. Each nozzle array was duplicated four times per spray plate, because four of the eight test dies were cooled by each nozzle design. Therefore, the values of heat transfer coefficient were not only an average of the locations on

the die, but also an average of the four dies. The large number of sample locations increases the statistical reliability of the results.

$$\begin{aligned} x_A P_A^{sat} &= y_A P \\ x_B P_B^{sat} &= y_B P \\ x_A + x_B &= 1 \\ y_A + y_B &= 1 \end{aligned} \tag{3.2}$$

In order to correlate the data and display the results in the form of boiling curves, molar concentration averaged properties were used for the mixture calculations. The equations from Raoult's law (shown in Eqn. (3.2)), relating the partial pressure in the vapor phase to the concentration of the component in the liquid phase [40], were solved simultaneously to determine the vapor pressure and the bubble temperature (T_{bub}) of the mixture.

3.6 Uncertainty Analysis

Equation (3.1) shows that the heat transfer coefficient is dependent on the average heat flux (q A^{-1}) and the temperature difference between the heater surface and the incoming liquid (ΔT_{surf}). Thus, the total uncertainty in the heat transfer coefficient (δh), according to the standard procedures for propagating uncertainty [41], is

$$\delta h = \sqrt{\left(\frac{\partial h}{\partial q}\delta q\right)^2 + \left(\frac{\partial h}{\partial A}\delta A\right)^2 + \left(\frac{\partial h}{\partial \Delta T_{surf}}\delta \Delta T_{surf}\right)^2} \tag{3.3}$$

The average heat flux is the ratio of the applied electrical power to the area of the chip. The test dies were fabricated by the IBM Corporation using standard methods for integrated

circuit production and die separation, so the uncertainty in the area (δA) is assumed to be less than one micron, and thus, negligible.

The uncertainty in the electrical power is dependent upon the uncertainty in the voltage and current measurements, which are measured indirectly because the National Instruments SCXI 1102 analog input accessory can only measure values between -10 and 10 volts. The manufacturer lists a worst-case uncertainty of 0.035% of reading for the SCXI 1102 accessory, and the uncertainty of the 6023E 12 bit data acquisition card can be calculated by finding the resolution for each measurement (δV).

$$\delta V \;=\; \frac{range}{2^{12}} \;=\; 0.00488V \tag{3.4}$$

Combining these values, the uncertainty in the voltage measurement due to the data acquisition system is (δV_{DAQ}) is 0.00600 V.

The test facility contains circuitry custom-designed by Cray, Inc. that converts the actual voltage and current to indicating voltages that can be measured by the data acquisition system. It is estimated that the total uncertainty due to the scaling circuitry is less than 0.1% of reading. At worst, then, this leads to a total uncertainty in the voltage measurement of δV= 0.0603 V and a total uncertainty in the current δI= 0.012 A. Using the propagation of uncertainty method,

$$\delta q = \sqrt{(\delta V I)^2 + (\delta I V)^2}. \tag{3.5}$$

With V_{max} = 60 V and I_{max} = 12 A, the maximum uncertainty in the power was found to be $\pm$1 W.

The final uncertainty that needs to be considered in Equation (3.3) is that of the temperature difference. To minimize this uncertainty, the difference between the liquid inlet measurement thermocouple and the average die temperature was calibrated using many

independent samples. The standard deviation of the difference between these two measurements when no power was applied to the heaters was 0.05 °C.

Thus, using Eqn. (3.3), the maximum uncertainty in the heat transfer coefficient was found to be, ± 0.030 W cm^{-2} K^{-1} at the lowest heat flux.

Chapter 4

Experimental Results and Discussion

4.1 Pure Fluids

Data were obtained for nitrogen-saturated pure fluids in order to provide a baseline to compare with the mixture data. Nitrogen-saturated FC-72 is currently used in high-end computer systems and has been extensively studied, so there are significant data related to its performance in the test facility [10]. Figure 4.1 shows the measured heat transfer coefficient as a function of flow rate for both the single nozzle and four nozzle arrays. Note that these data were taken in separate, independent tests; during tests with the single-nozzle arrays, the test dies under the four-nozzle arrays were not powered and vice versa.

Each data point in the heat transfer coefficient plots represents the average of 10 measurements over a range of heat fluxes far from the peak heat flux. The data in Fig. 4.1 and the fluid properties illustrated in Table 3.1 show that heat transfer performance increases with decreasing T_{sat}, but also that it increases with lower viscosity, higher heat of vaporization and higher thermal conductivity; definitive conclusions as to the most influential liquid properties are thus hard to draw.

Boiling curves were also generated for the saturated pure fluids where ΔT_{sat} is defined as the difference between the surface temperature and the saturation temperature at operating pressure ($\sim$1 atm for gas-saturated conditions).

Figure 4.2 illustrates the behavior of pure, nitrogen saturated FC-72. The smoothness and linearity of both curves indicates predominately single phase behavior. This is further illustrated in Figure 4.3.

Here it is clear that there is some heat flux dependence on the heat transfer coefficient

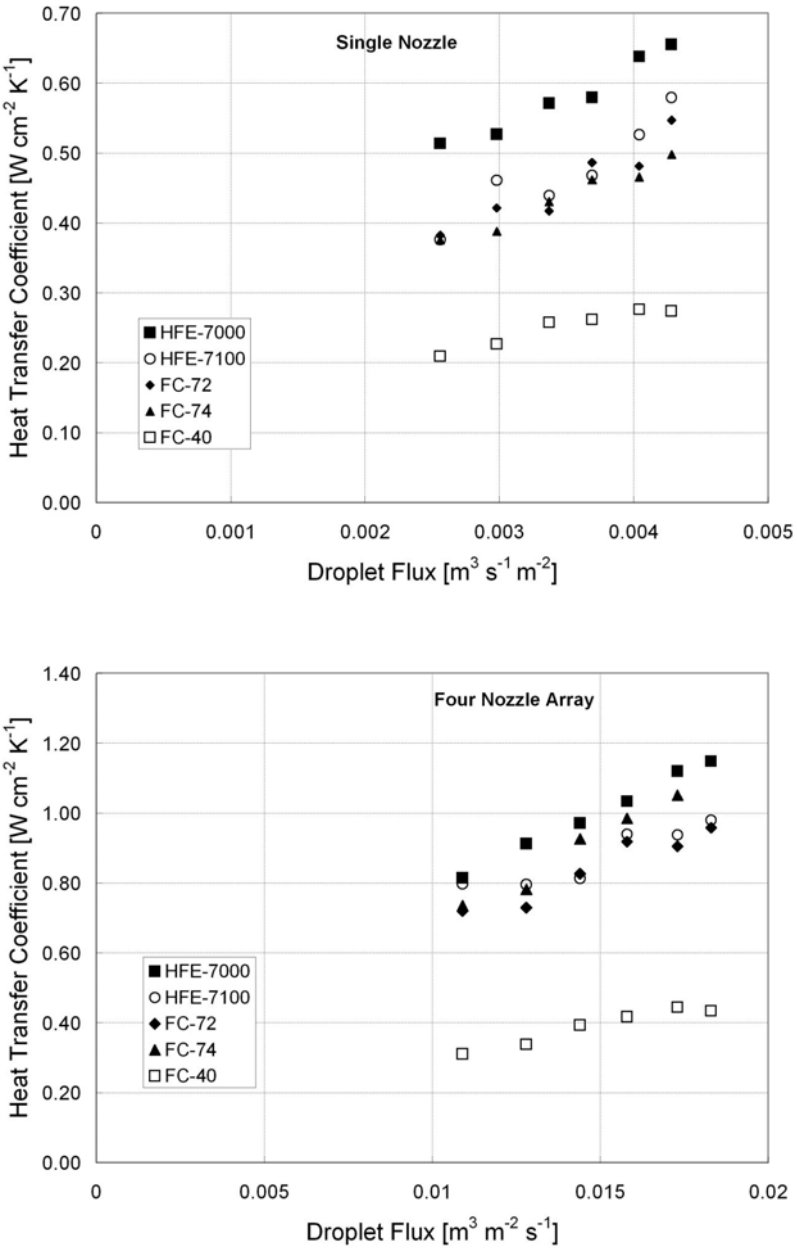

Figure 4.1: Heat transfer performance of the four nozzle and single arrays for nitrogen saturated pure fluids.

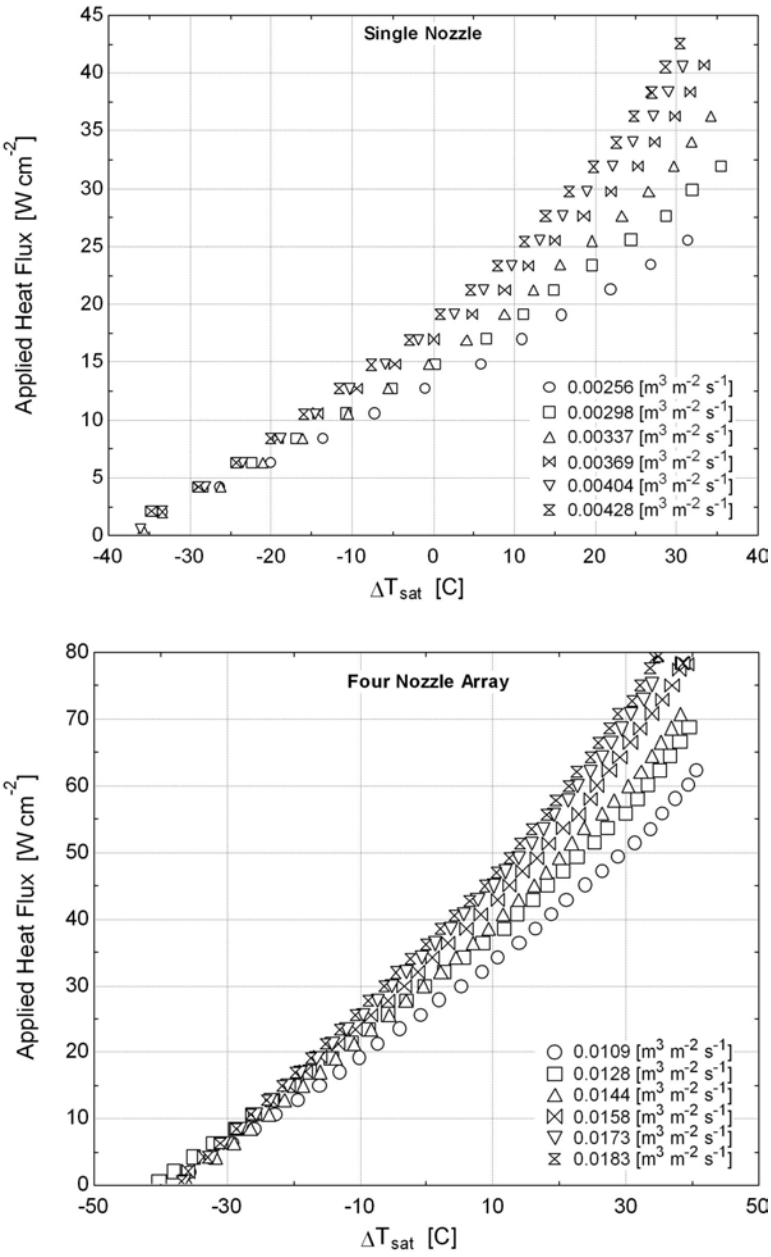

Figure 4.2: Boiling curves for FC-72 using the single nozzle and four nozzle array at 1 atm

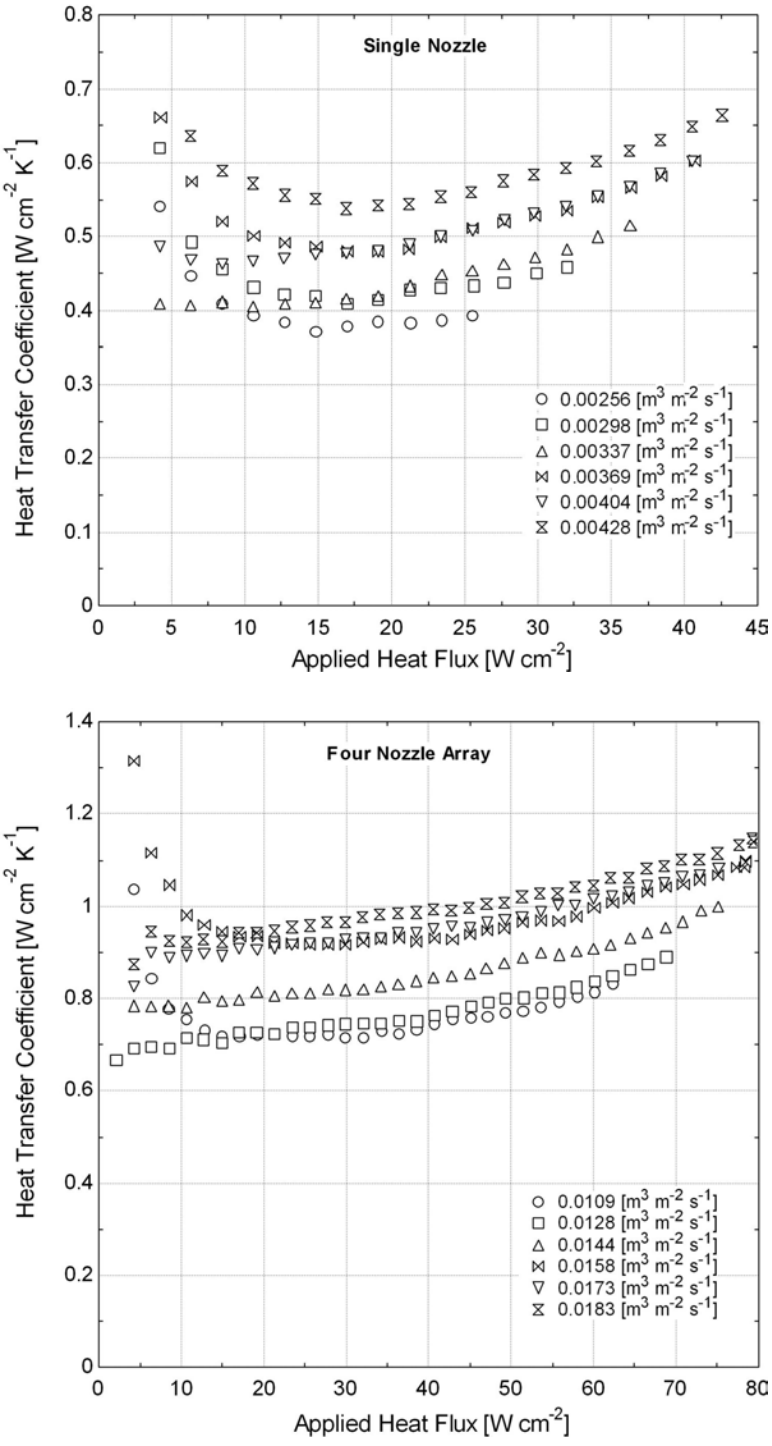

Figure 4.3: Heat transfer performance for FC-72 for the single nozzle and four nozzle array at 1 atm

at both low and high heat fluxes. However, not enough is known to explain the low heat flux behavior. At higher heat flux, the rise could be due to increased evaporation from the surface of the liquid film or from bubbles entrained within the film. A final possibility is that the rise is due to temperature dependent property variation in the liquid.

Figure 4.4 indicates that FC-74 is also predominately single phase during the duration of testing. As is shown in Figure 4.5, FC-74 with a T_{sat}=101°C does not exhibit as strong a

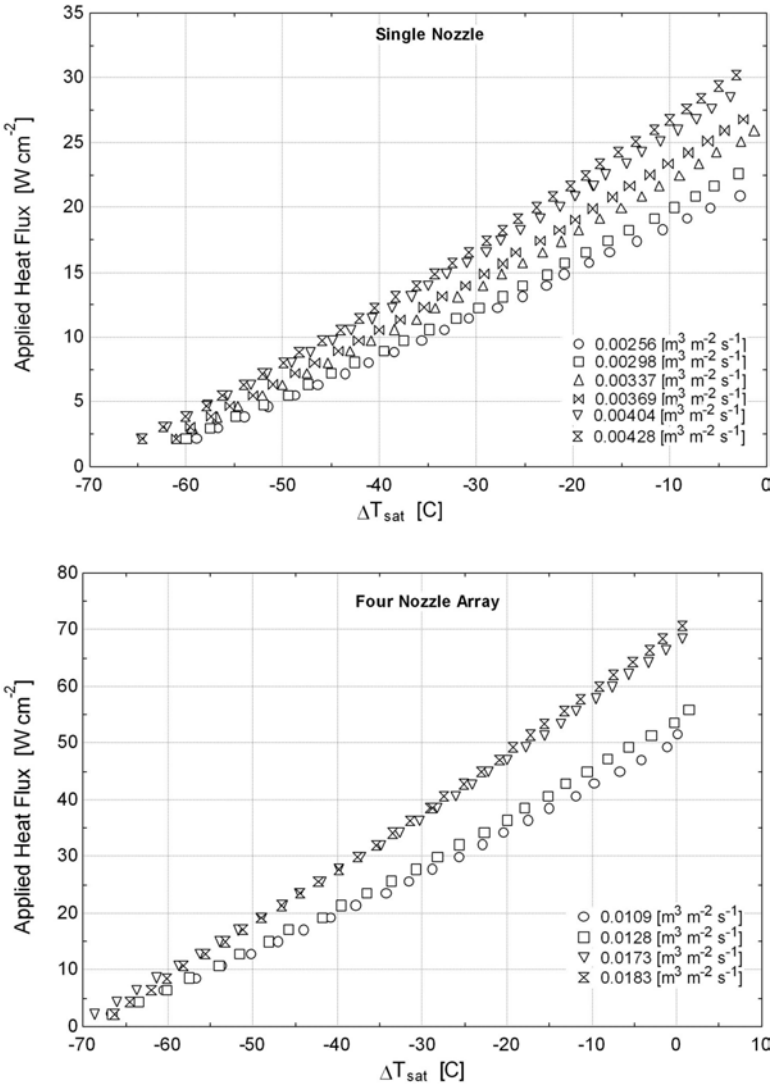

Figure 4.4: Boiling curves for FC-74 using the single nozzle and four nozzle array at 1 atm

heat flux dependence at high heat fluxes. This suggests that evaporation plays a significant role in the heat flux dependence of the FC-72 data since its saturation temperature is 56°C.

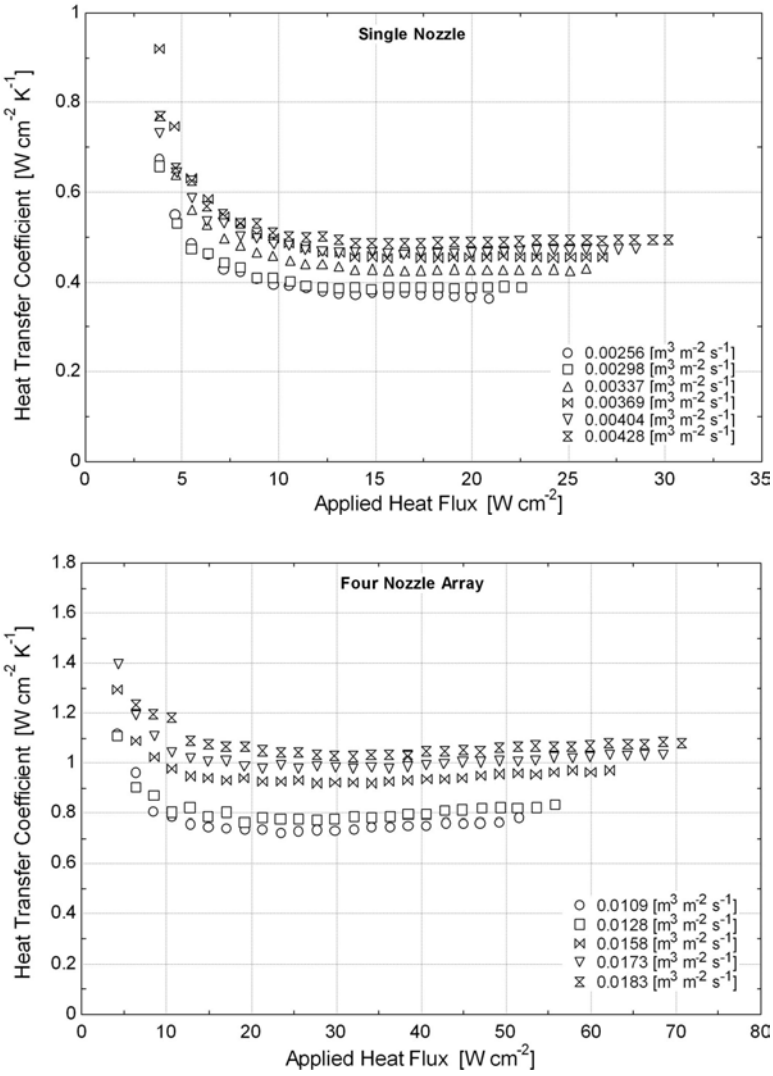

Figure 4.5: Heat transfer performance for FC-74 for the single nozzle and four nozzle array at 1 atm

The FC-40 boiling curves (see Figure 4.6) are quite a bit more linear than that of the FC-72 and FC-74 at all droplet fluxes. This would seem to indicate that the fluid behavior is not the same. Due to the high viscosity of the fluid, it is possible that the FC-40 is actually not being atomized by the nozzle(s). Nozzle development for another application shows

that it is unlikely for a fluid with similar viscosity to atomize [42]. This jet impingement behavior could explain the different trend of the FC-40, although it does appear that the fluid remains single phase throughout the duration of the testing. Figure 4.7 illustrates a significantly lower performance for the FC-40 when compared to that of both the FC-72 and the FC-74 at a given droplet flux.

The hydrofluoroether (HFE-7000 and HFE-7100) boiling curves indicate phase change more than did those of the Fluorinerts, as can be seen in Figures 4.8 and 4.9.

The slow rise in the heat transfer coefficient with increasing heat flux of these data suggests a secondary role for fluid property variations. The FC-40 data had the highest liquid surface temperature and the lowest heat transfer coefficient, amplifying the effects of heating on properties such as viscosity.

The phase change is indicated by the presence of two distinct slopes in the boiling curves. This phase change may not be the reason why the hydrofluoroethers outperform the perfluorohexanes (see Figures 4.10 and 4.11). The sensible heating mechanism is joined with a latent heat component, allowing heat flux removal along the surface of the chip at a more constant liquid temperature. The increased levels of evaporation, however, do not necessarily indicate the presence of nucleate boiling. If the vapor were evaporating from the surface of the chip, one would expect the greatest change in slope to occur with increasing ΔT_{sat} and decreasing droplet flux. This is because the number of activated nucleation sites for bubble growth increases with increasing ΔT_{sat} and decreasing velocity gradients.

Since the slope of both boiling curves appear to get steeper with increasing droplet flux, it is hypothesized that the bubbles where evaporation occurs are entrained in the thin film, aiding in the heat transfer performance. In addition, the hydrofluroethers have larger thermal diffusivities than the perfluorohexanes which discourages nucleation by preventing the fluid along the surface from heating as fast.

A parameter that normalizes the performance against the flow required by different nozzle

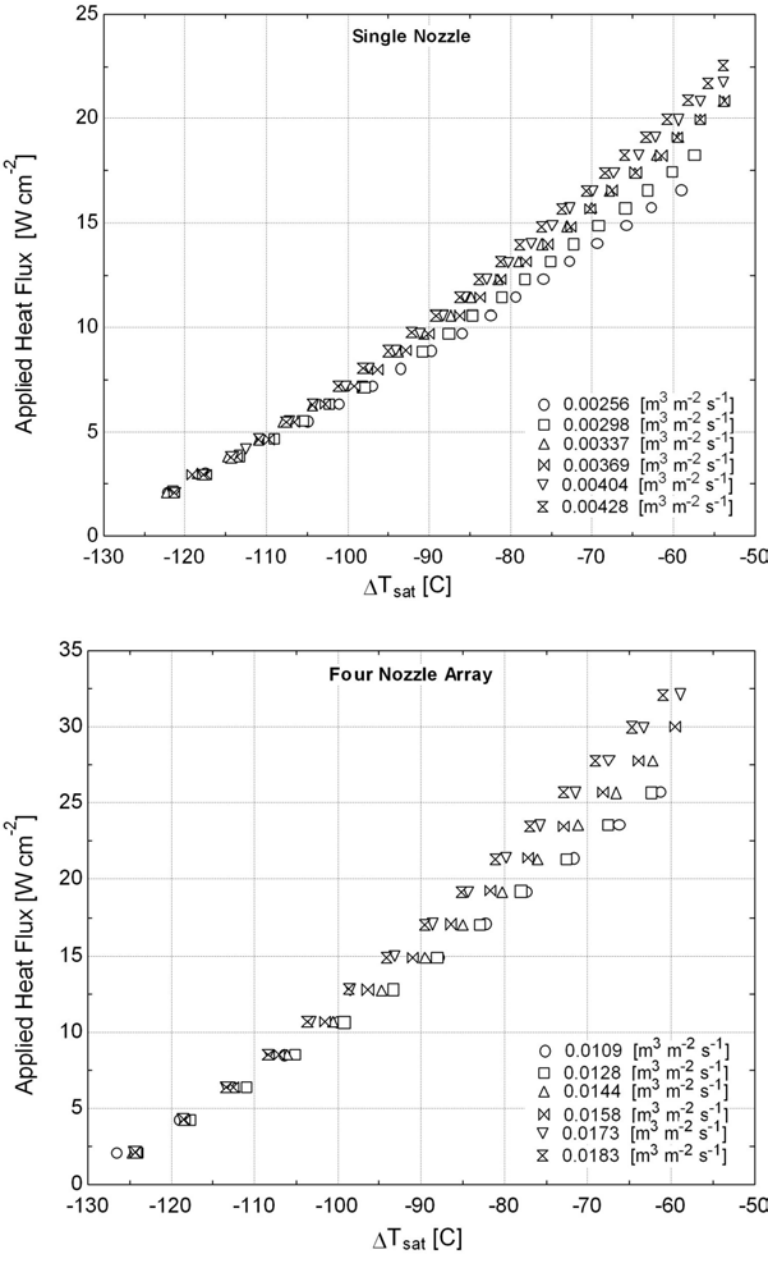

Figure 4.6: Boiling curves for FC-40 using the single nozzle and four nozzle array at 1 atm

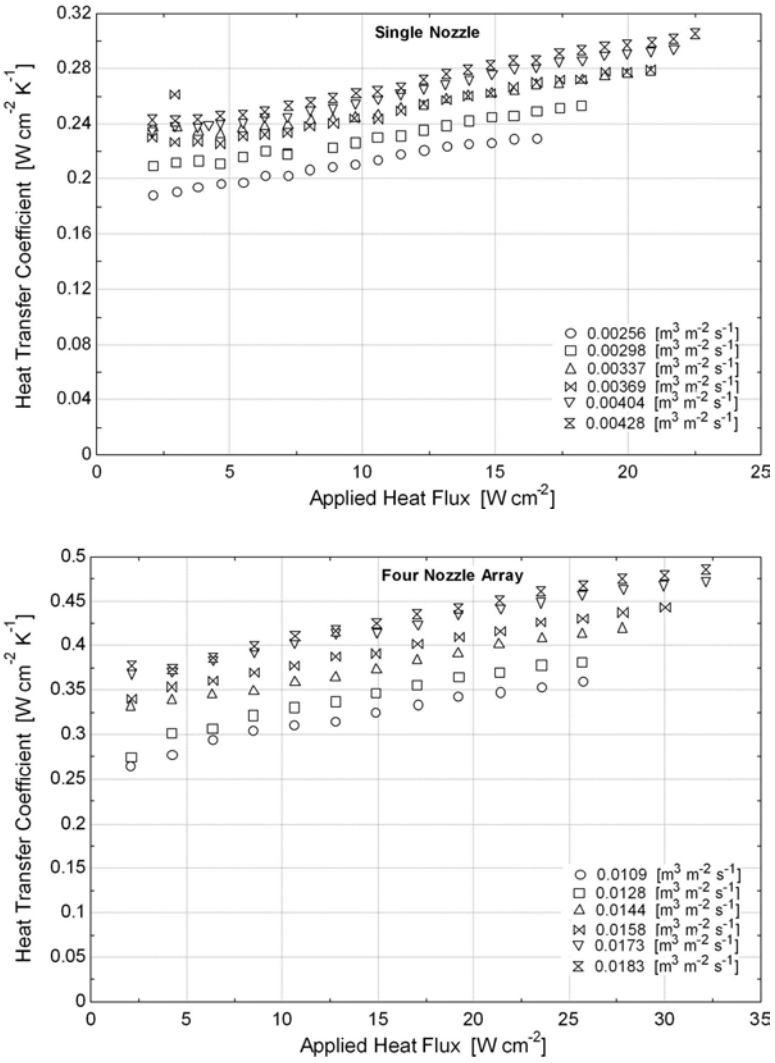

Figure 4.7: Heat transfer performance for FC-40 for the single nozzle and four nozzle array at 1 atm

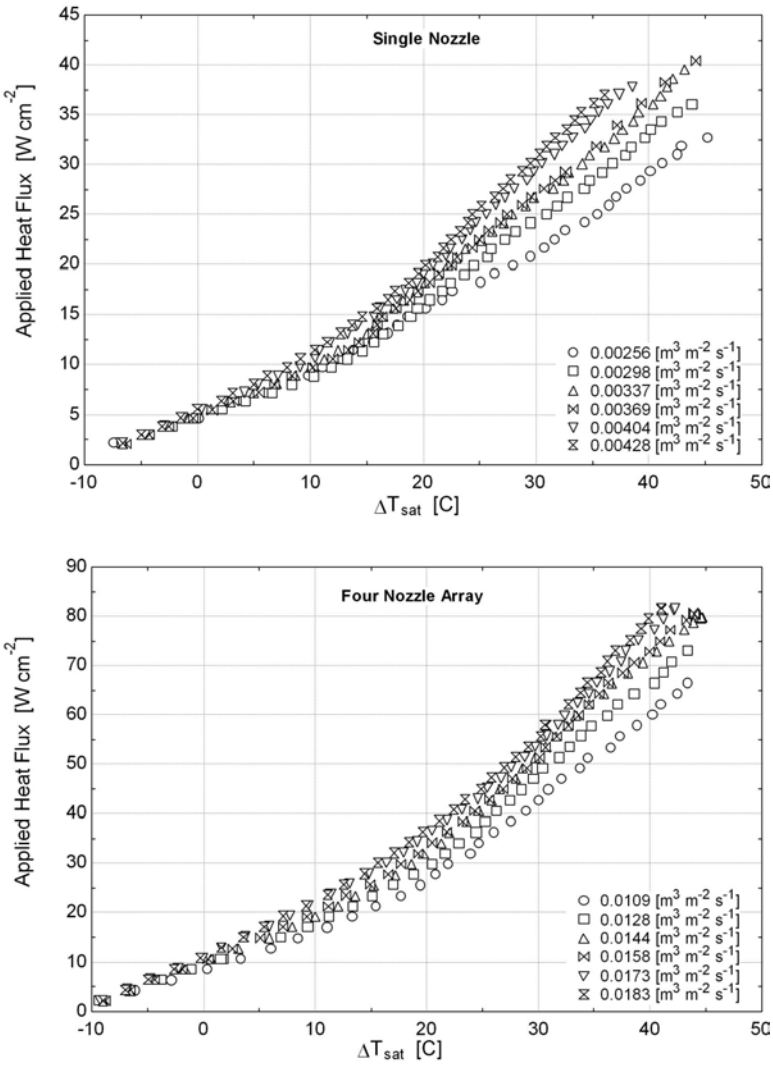

Figure 4.8: Boiling curves for HFE-7000 using the single nozzle and four nozzle array at 1 atm

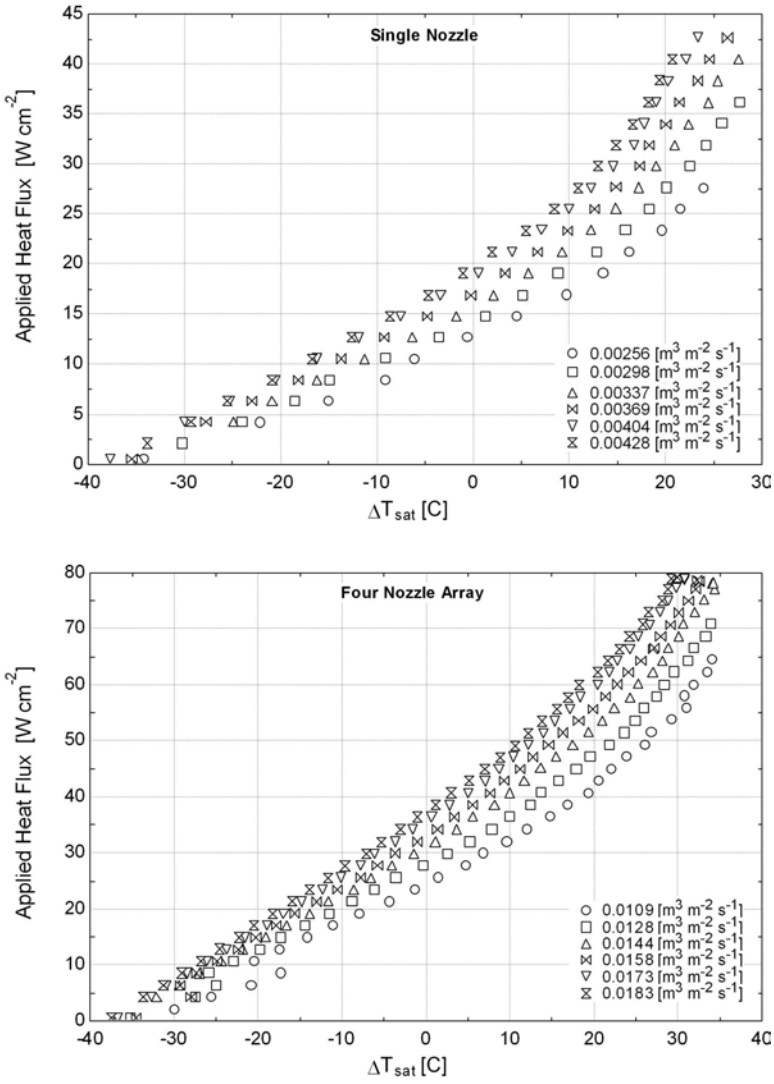

Figure 4.9: Boiling curves for HFE-7100 using the single nozzle and four nozzle array at 1 atm

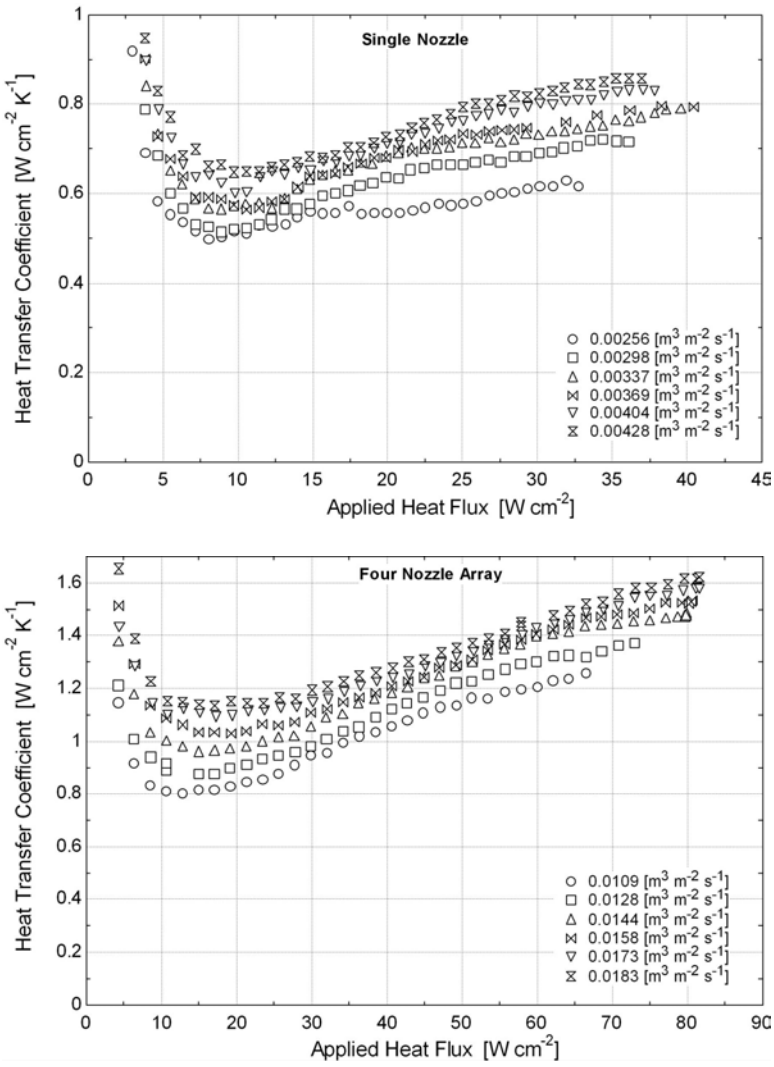

Figure 4.10: Heat transfer performance for HFE-7000 using the single nozzle and four nozzle array at 1 atm

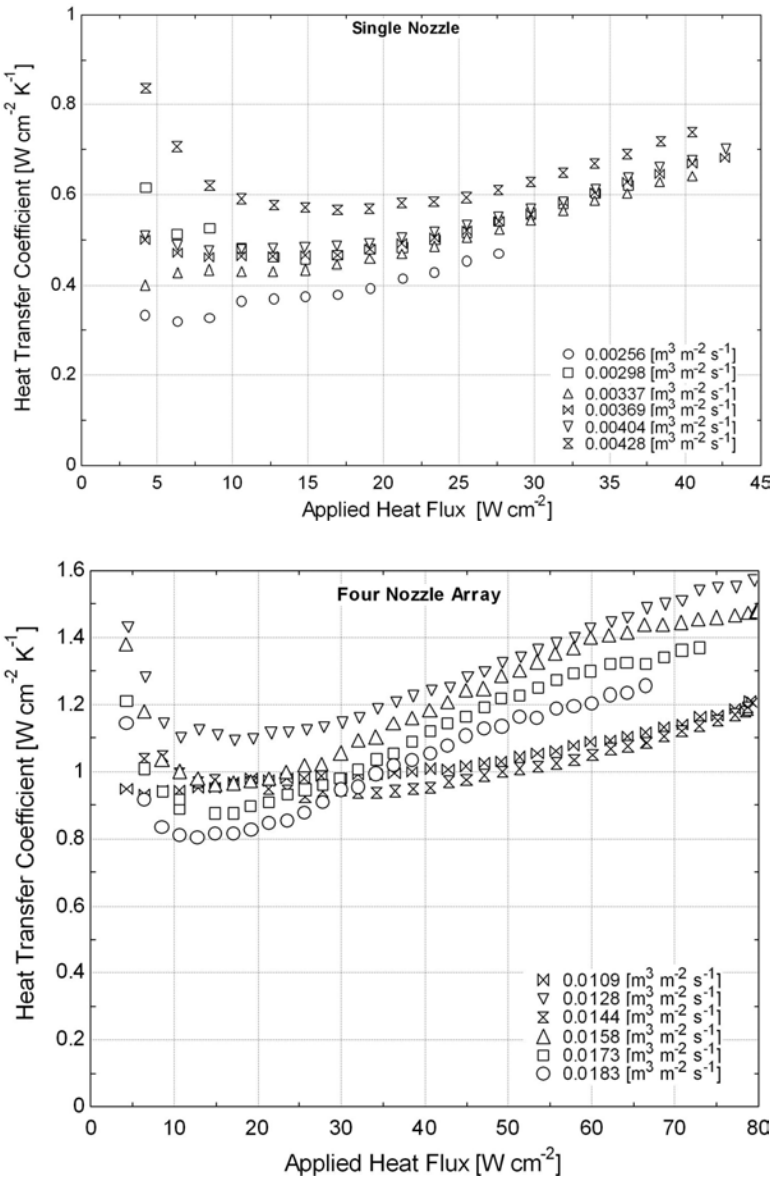

Figure 4.11: Heat transfer performance for HFE-7100 using the single nozzle and four nozzle array at 1 atm

designs and heat fluxes is the cooling effectiveness (ϵ) given in Equation 4.1, where A is the die surface area, Q is the volumetric flow rate, and q'' is the applied heat flux.

$$\epsilon = \frac{q''A}{Q} \tag{4.1}$$

Since ϵ is a measure of how effectively the fluid removes energy, one would expect ϵ to increase with increasing ΔT_{sat}. Or, more explicitly, for ϵ to increase with more evaporation. As is illustrated in Figure 4.12, this is the trend that is observed. It is interesting to note, however, that the HFE-7100 tends toward the HFE-7000 even though Table 3.1 clearly indicates that ΔT_{sat} for the HFE-7000 is equal to that of FC-72. This seems to indicate that there is an additional effect due to other fluid properties.

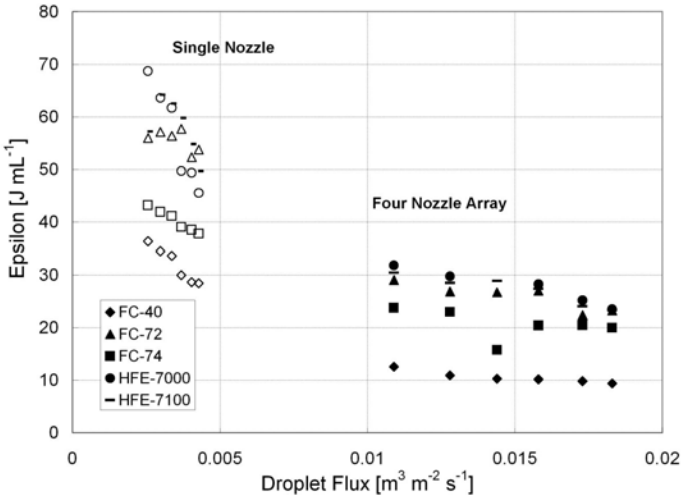

Figure 4.12: Effectiveness of varying fluids at 1 atm

4.2 Non-gas-saturated Pure Fluids

All of the data above were obtained for nitrogen-saturated fluids and fluid mixtures at approximately 1 atm. However, it is not precisely known how the nitrogen itself affects the heat transfer of the fluids in spray cooling. Thus, non-nitrogen saturated data were collected as well for the FC-72 and the HFE-7000. Namely, the system was evacuated until the saturation pressure of the fluid was reached. It should be noted that, while this procedure greatly reduces the nitrogen content, it does not completely eliminate it from the liquid.

It can be seen by observing Fig. 4.13 that the HFE-7000 heat transfer coefficients increase by 10 to 20% when the nitrogen is removed from the system, but the FC-72 performance is virtually unaffected. This further suggests that evaporation from the HFE-7000 liquid may be occurring, which keeps the average liquid temperature lower, improving the heat transfer performance.

On the other hand, it is interesting to note that the HFE-7000 boiling curves show somewhat less of a heat flux effect than the gas saturated curves in Figure 4.8. In addition, comparing the single nozzle FC-72 boiling curves seems to indicate that the non-gas-saturated boiling curves could be an extension of the gas-saturated curve in Figure 4.2. More explicitly, the boiling curves look similar in shape and behavior compared at the same ΔT_{sat}. The non-gas-saturated FC-72 heat transfer coefficients show the same trends as the gas-saturated except with much less low heat flux effects. All of these observations, combined with Figure 4.18, seem to indicate that the presence of nitrogen in the system has little to no effect on the heat transfer performance of the fluids. This is further supported by the work of Horacek et al. [20] who studied subcooling with Fluorinerts, and Jiang and Dhir [18], who studied the effects on non-condensibles in water.

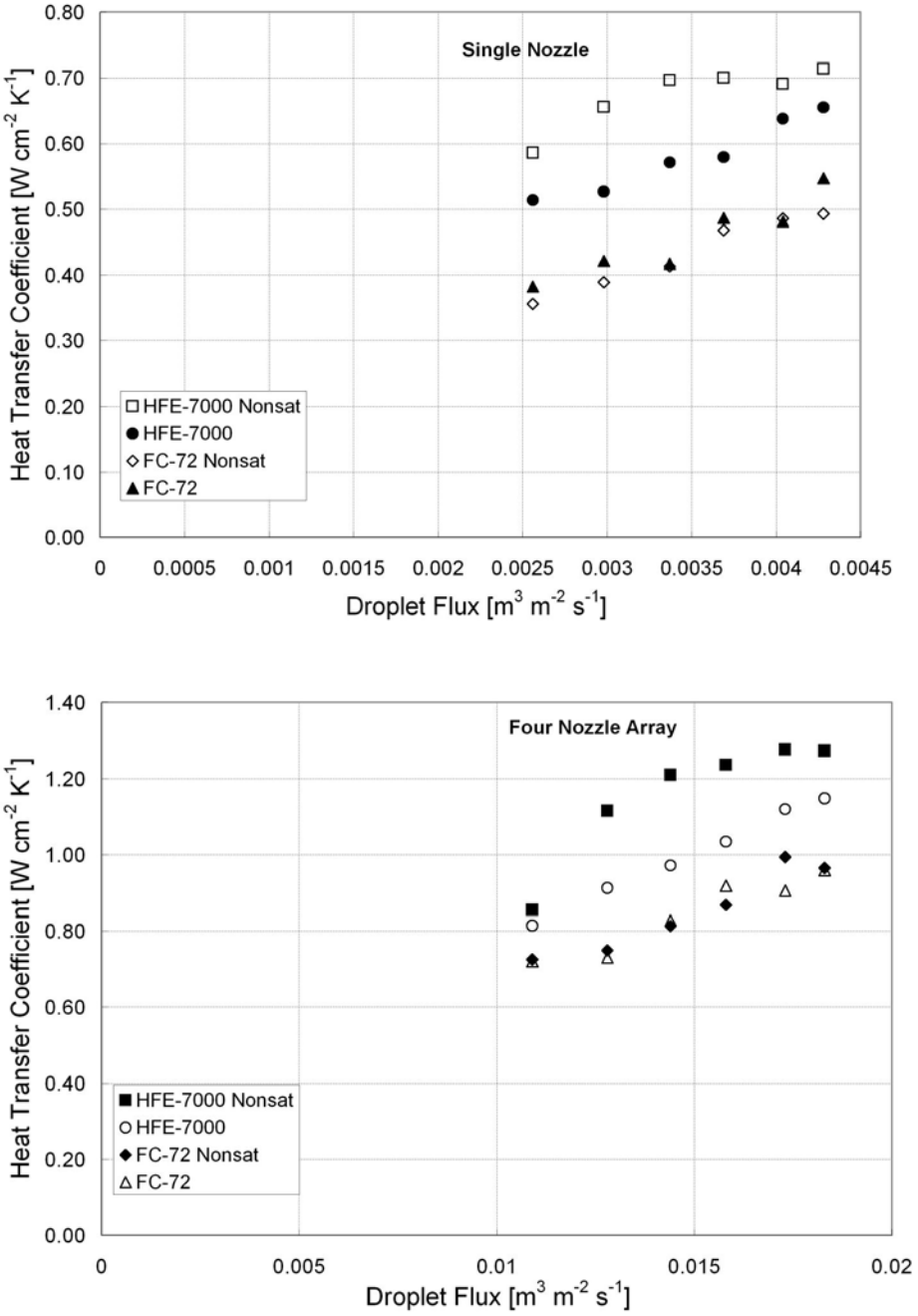

Figure 4.13: Heat transfer performance of the four nozzle and single arrays for nitrogen saturated and non-nitrogen saturated pure fluids.

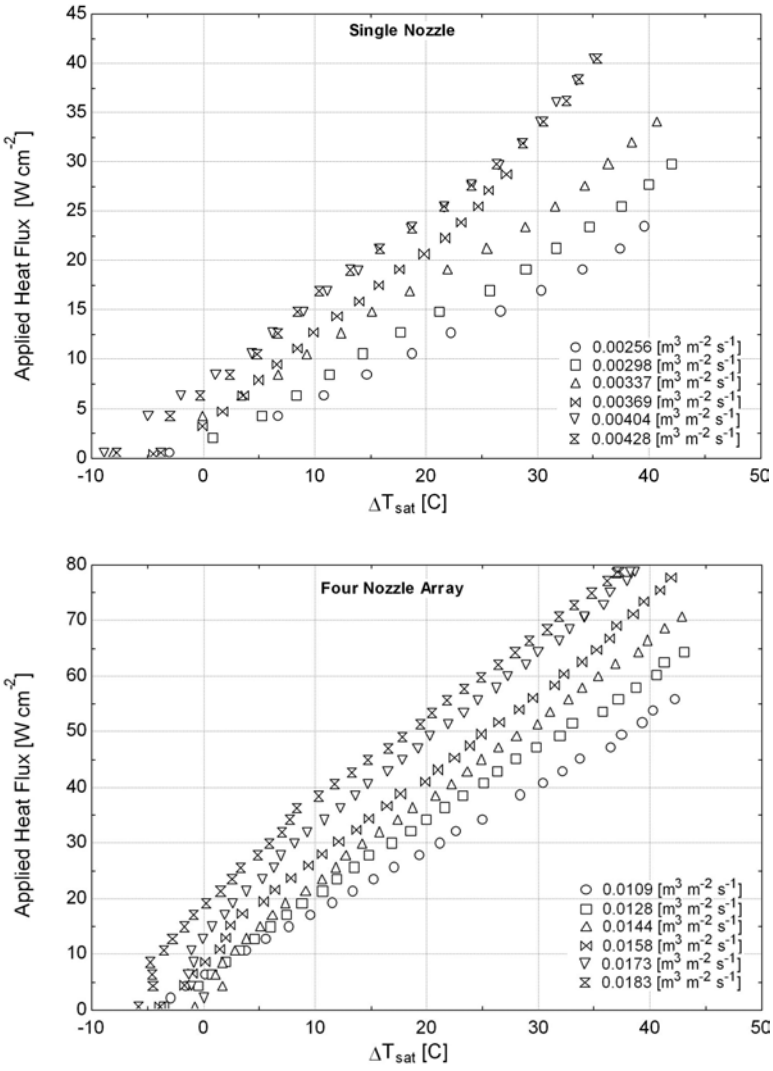

Figure 4.14: Boiling curves for FC-72 using the single nozzle and four nozzle array at saturation pressure

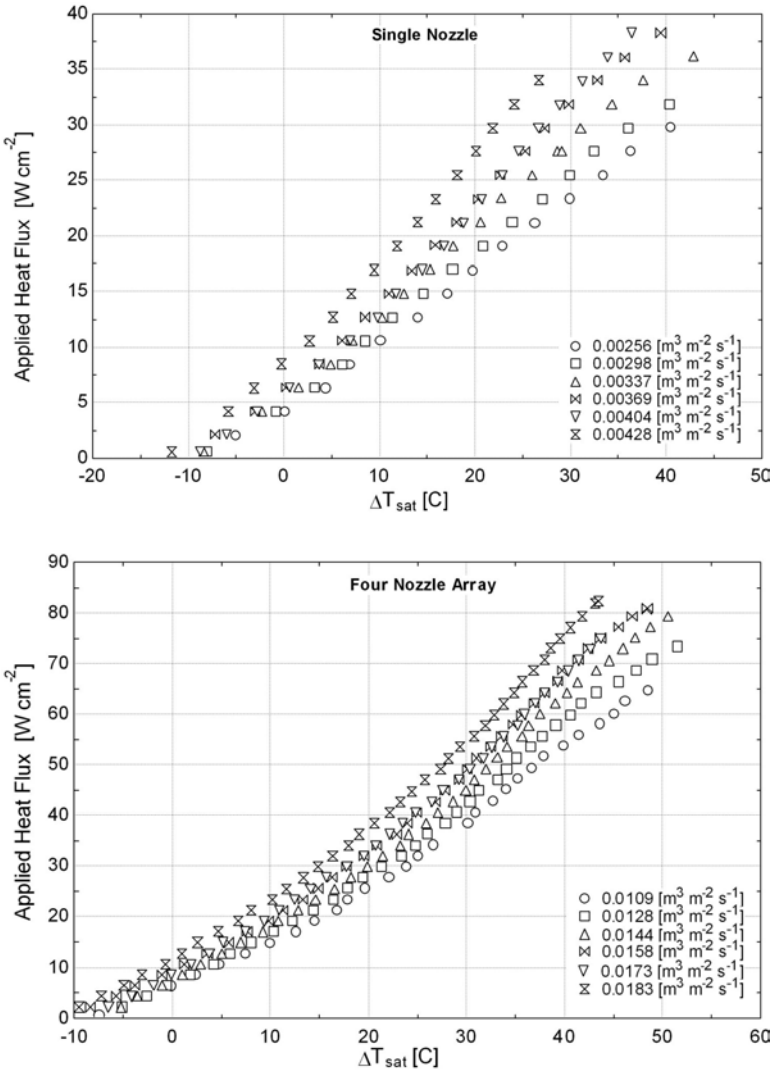

Figure 4.15: Boiling curves for HFE-7000 using the single nozzle and four nozzle array at saturation pressure

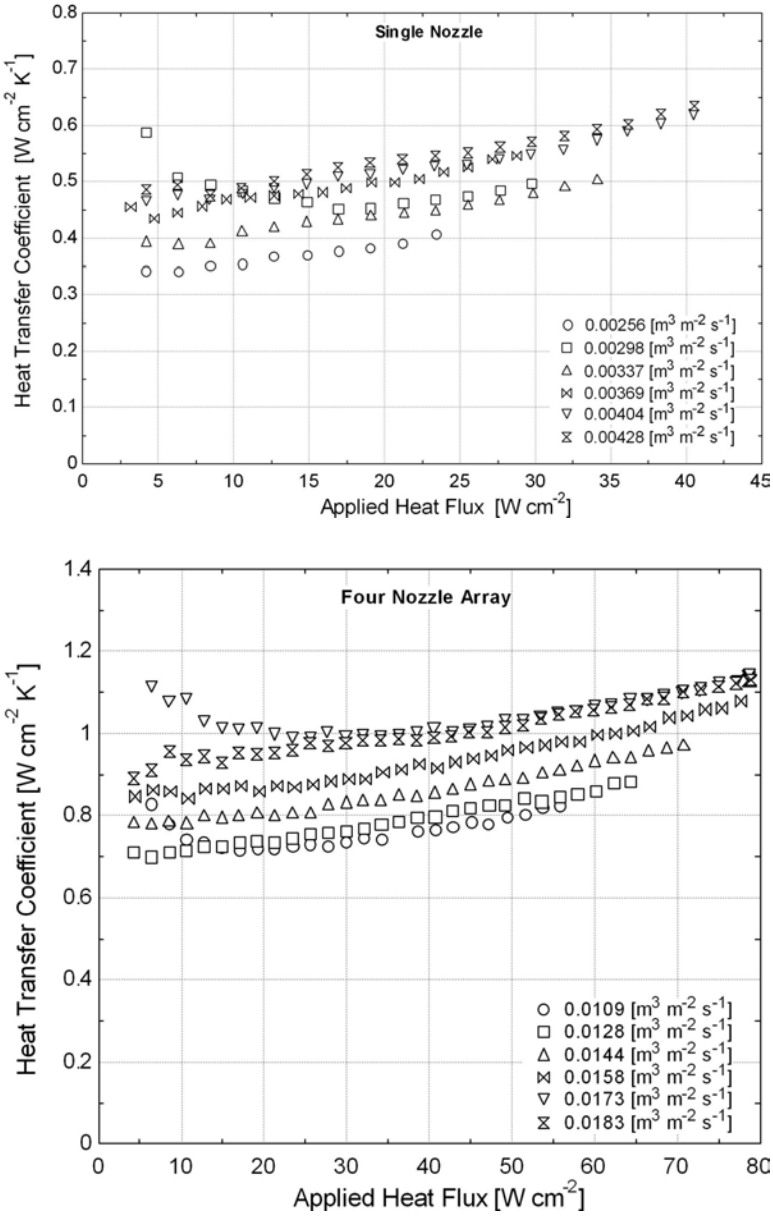

Figure 4.16: Heat transfer performance for FC-72 using the single nozzle and four nozzle array at saturation pressure

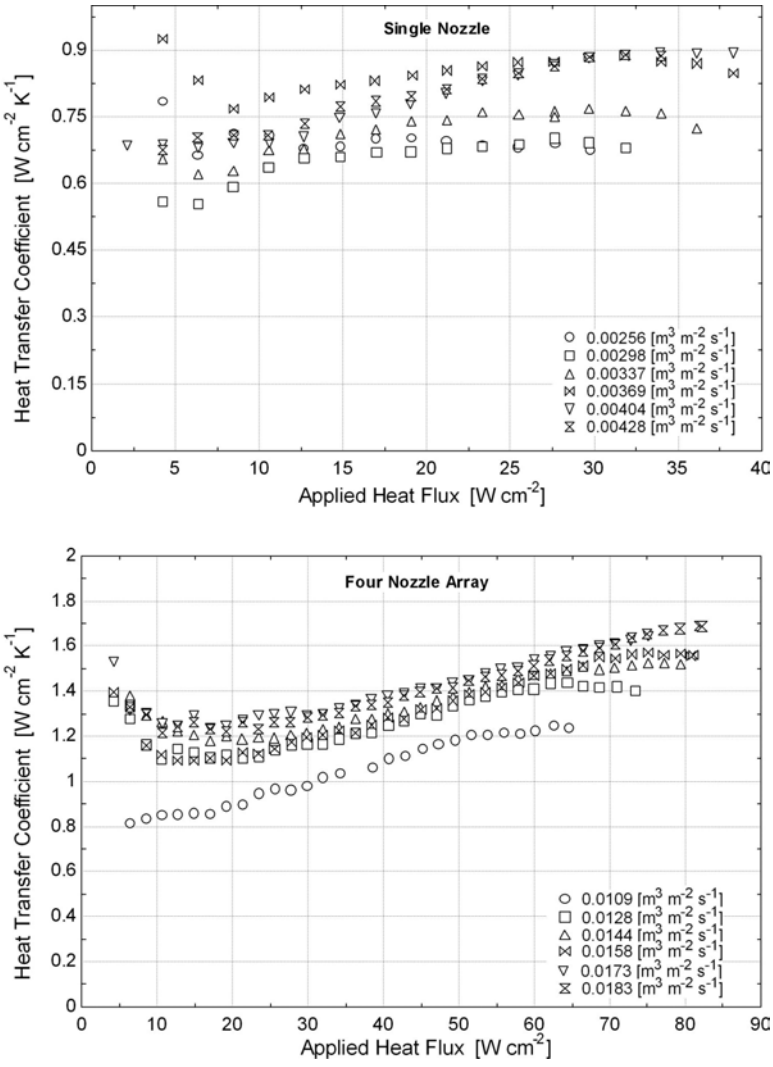

Figure 4.17: Heat transfer performance for HFE-7000 using the single nozzle and four nozzle array at saturation pressure

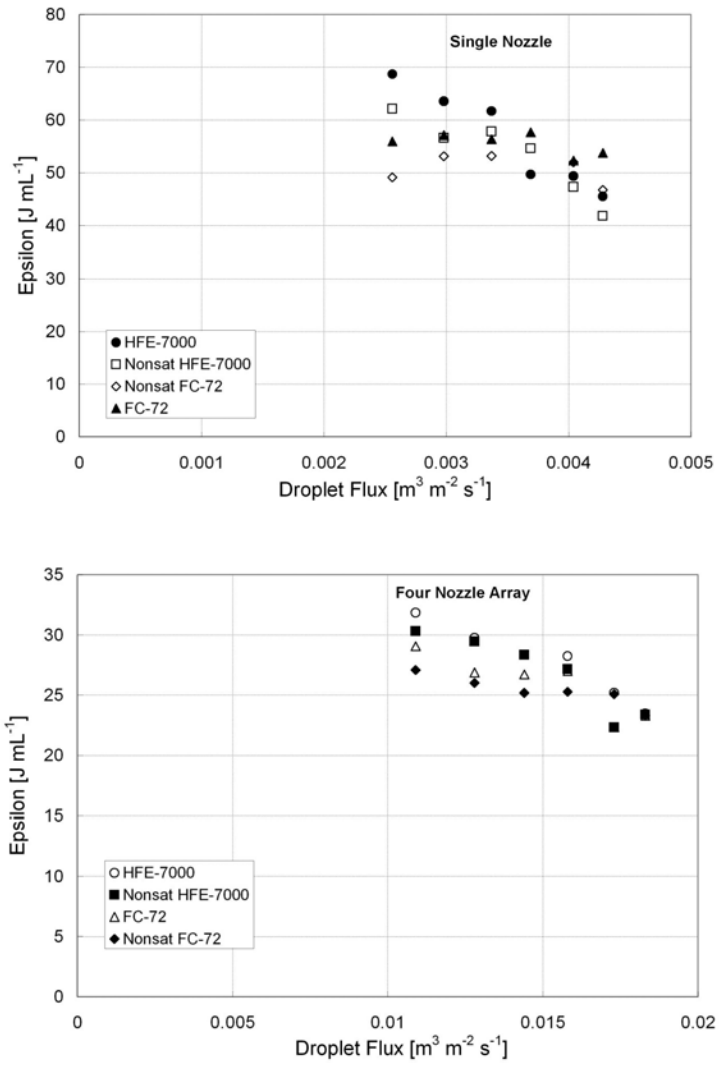

Figure 4.18: Effectiveness of non-gas-saturated FC-72 and HFE-7000 compared to gas-saturated FC-72 and HFE-7000

4.3 Mixtures

It was hypothesized that fluid combinations with very different properties would uncover the effects of fluid properties on mixture performance. FC-72 was chosen initially because a lot of data exists in the literature that utilizes it. The properties behind the decision to use which fluid combination is illustrated in Table 4.1. For example, FC-40 was chosen because it has a very high boiling point when compared to FC-72. It also has a much higher viscosity, and it was thought that this trait might aid in increasing the heat transfer coefficient of the mixture by maintaining a liquid film on the surface.

Table 4.1: Fluid selection for mixtures.

Fluid	T_{sat} Effects	Viscosity Effects	Conduction Effects	Chemical Composition Effects
FC-72/FC-40	x	x		
FC-72/FC-74	x	x		
FC-72/HFE-7000	x		x	
FC-72/HFE-7100			x	x
HFE-7000/HFE-7100			x	x

In order to completely study the mixture behavior, a full range of concentrations were chosen for each fluid combination: 25%-75%, 50%-50%, and 75%-25%. To date, mixtures have been studied only for applications involving heat transfer in tubes or small passages where the use of mixtures in flow boiling applications has been accompanied by a significant degradation in heat transfer performance. However, the data presented in Figs. 4.19-4.22 do not show any degradation in the heat transfer coefficient for either nozzle configuration compared with the lowest performing pure fluid of the fluid pair. The mixture data, in fact, strongly trend toward the data of the lowest performing pure fluid in each case (except the FC-40 mixtures), with no consistent, significant improvement beyond this.

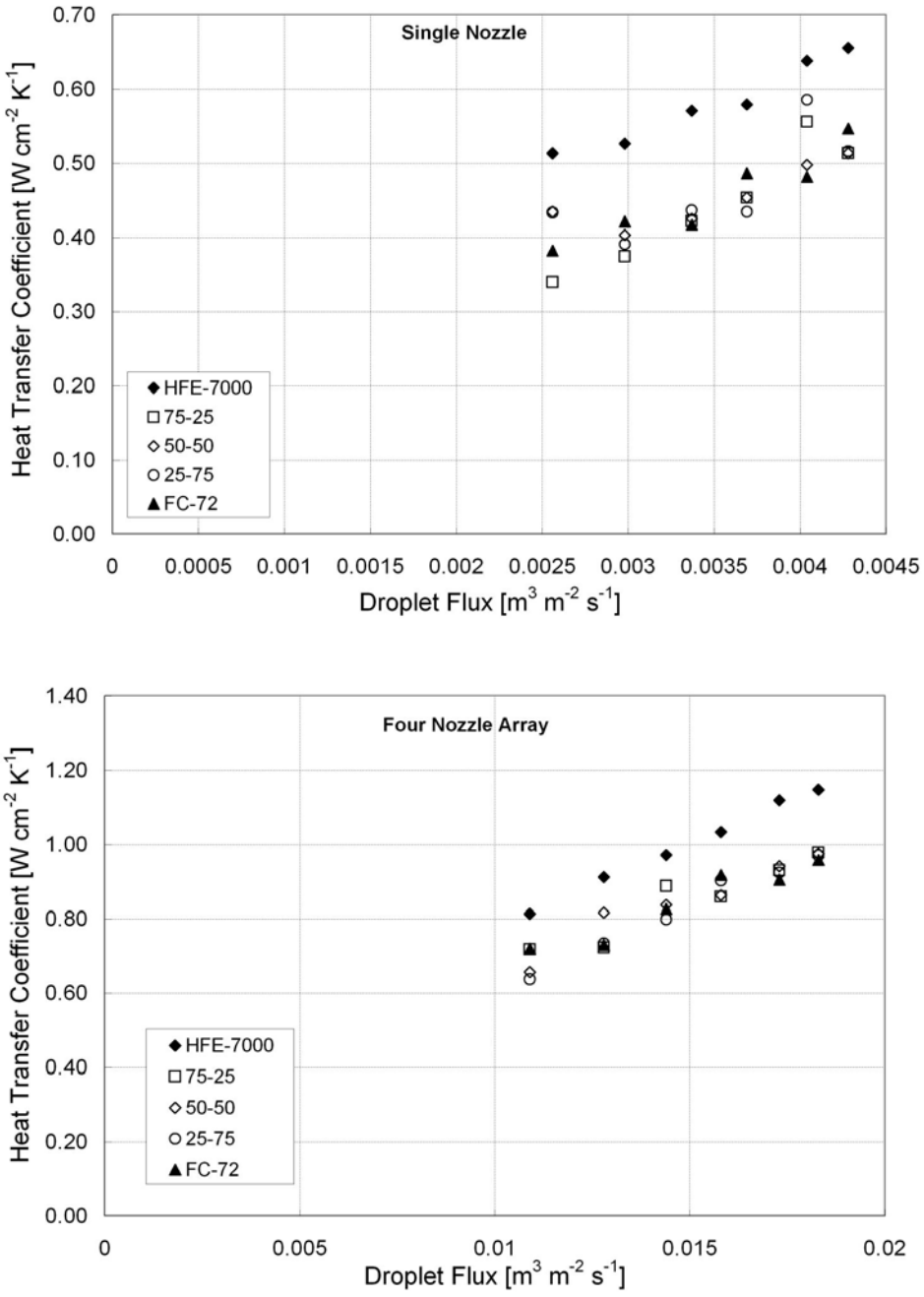

Figure 4.19: Heat transfer performance of the four nozzle and single arrays for FC-72/HFE-7000 mixtures.

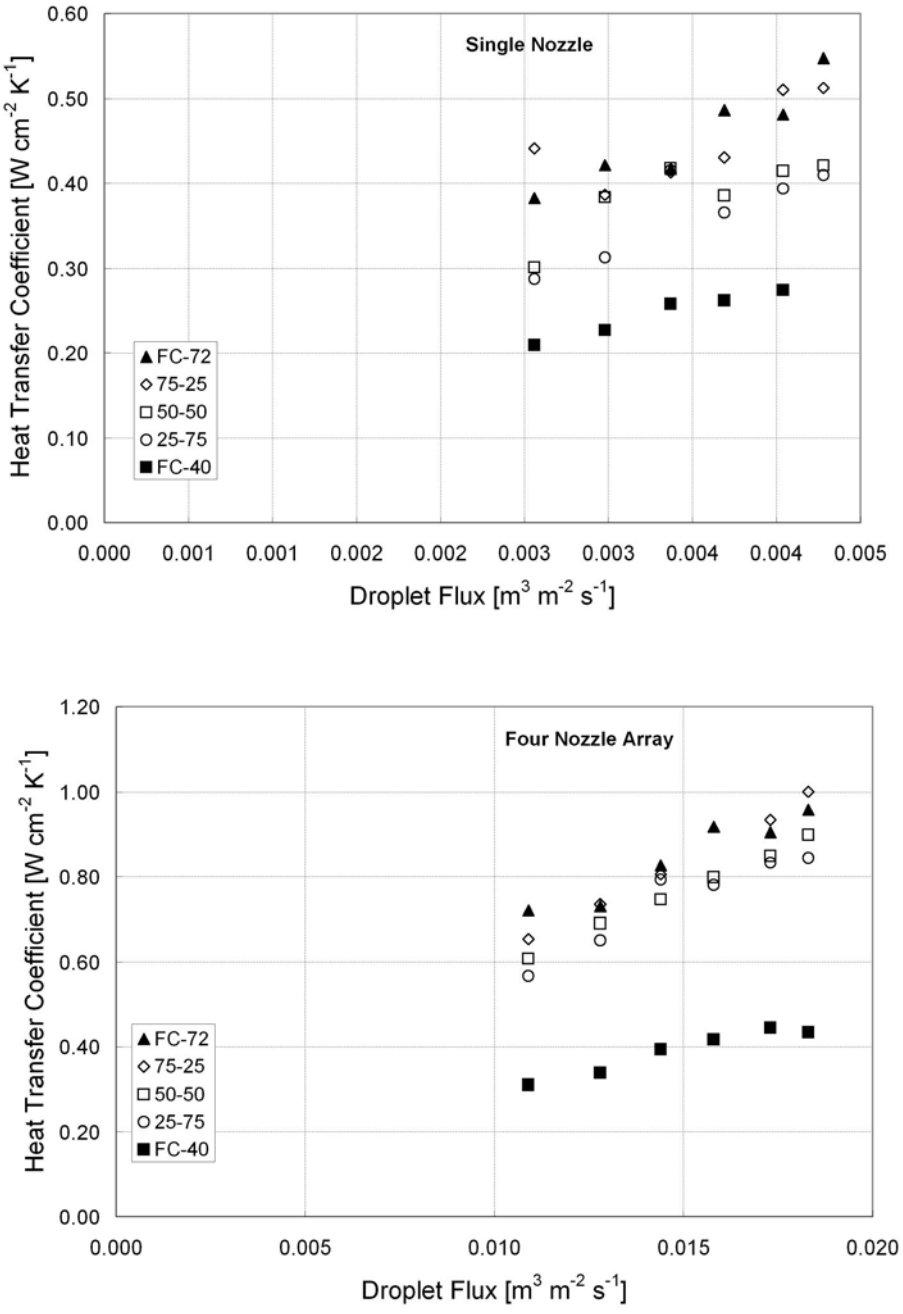

Figure 4.20: Heat transfer performance of the four nozzle and single arrays for FC-72/FC-40 mixtures.

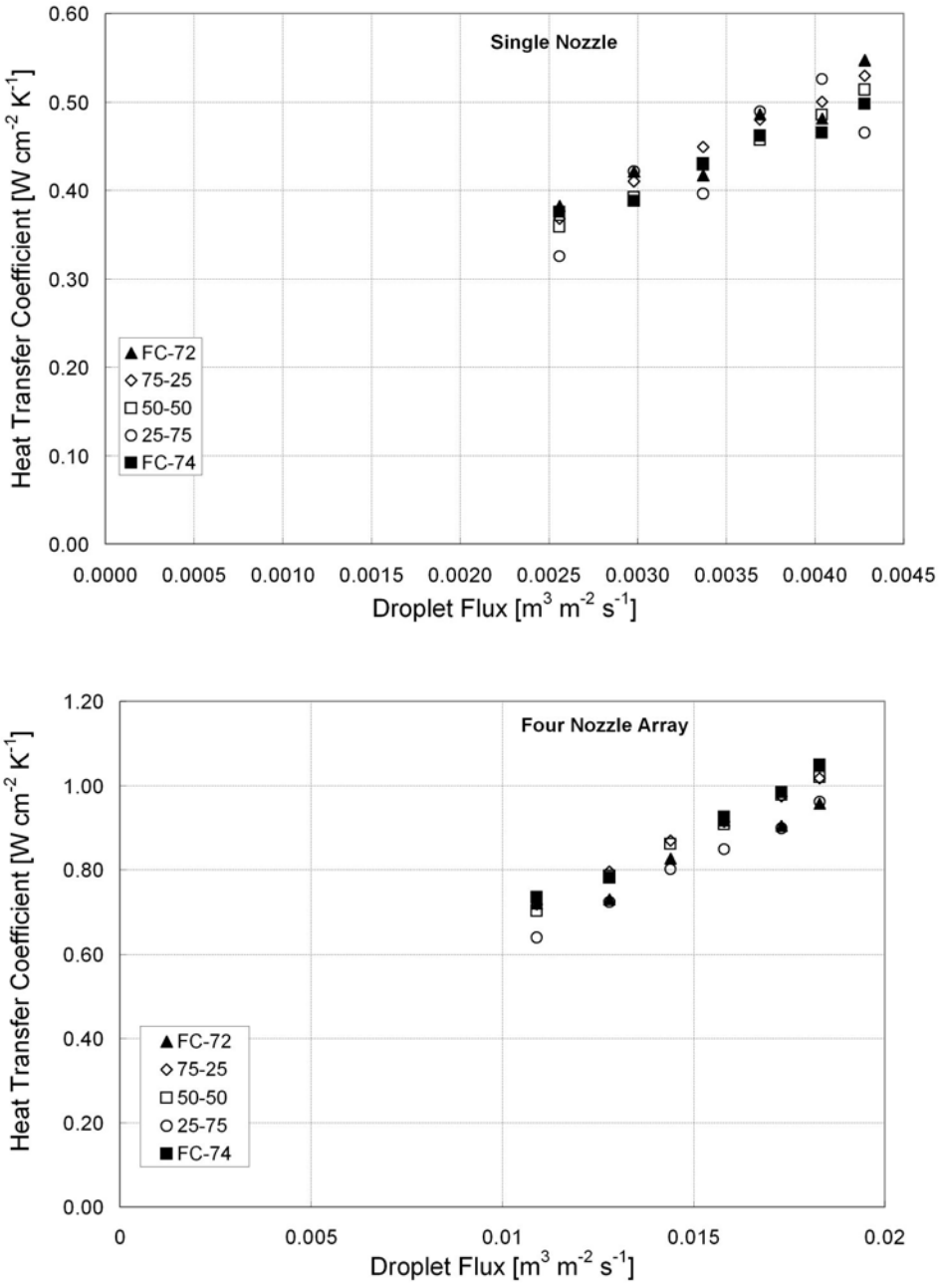

Figure 4.21: Heat transfer performance of the four nozzle and single arrays for FC-72/FC-74 mixtures.

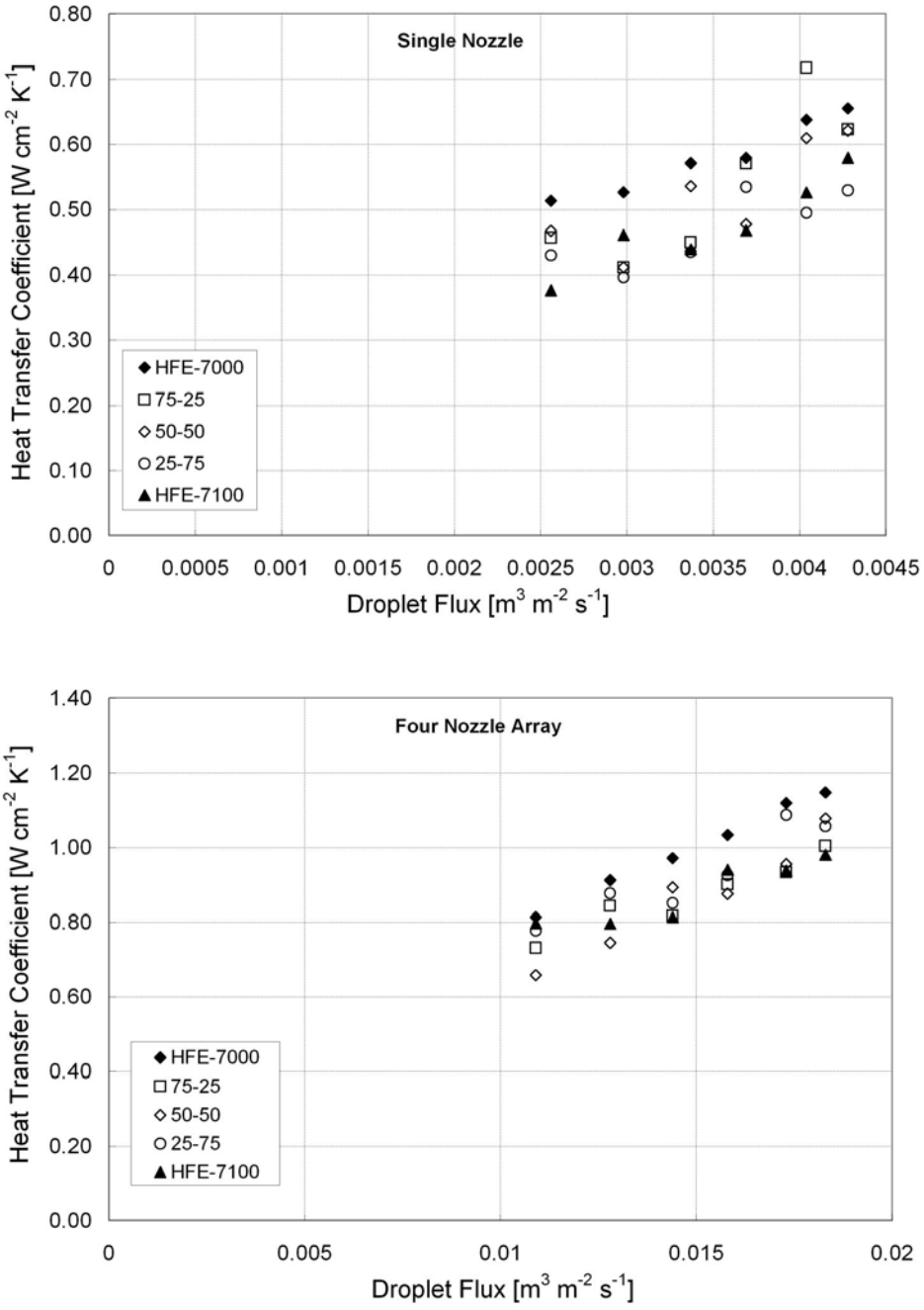

Figure 4.22: Heat transfer performance of the four nozzle and single arrays for HFE-7000/HFE-7100 mixtures.

4.4 Non-gas-saturated Mixtures

Non-nitrogen saturated data were collected for the FC-72 and the HFE-7000 mixtures. Namely, the system was evacuated until the saturation pressure of the fluid was reached. It should be noted that the nitrogen was eliminated from the test facility atmosphere, but not completely from the fluid.

The mixture data still trend toward the FC-72 data, but the single nozzle heat transfer with 75% HFE-7000 shows a significant improvement over this, as is illustrated in Figure 4.23. It is likely that this is because the single nozzles under-spray the square heater and there is a significant amount of heater area covered by a thin, slower moving film. This film could heat enough to sufficiently exceed the bubble point temperature where surface evaporation or nucleate boiling could occur. The heaters above the four nozzle arrays are completely covered by impinging drops, so evaporation may be suppressed because the liquid temperature may never exceed the bubble point temperature enough to allow for evaporation. For further non-gas-saturated mixture data, please refer to Appendix B.

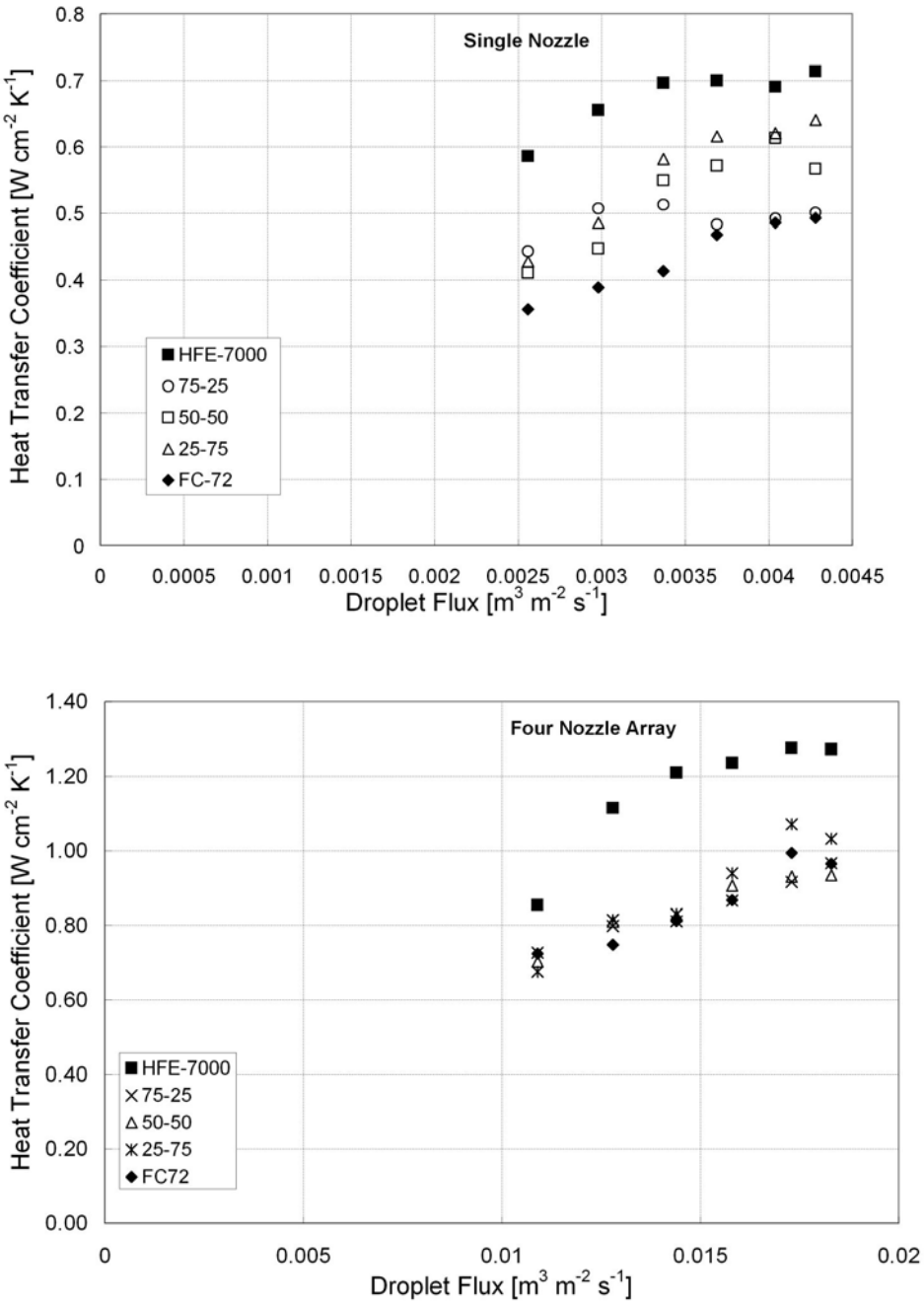

Figure 4.23: Heat transfer performance of the four nozzle and single arrays for non-nitrogen saturated FC-72/HFE-7000 mixtures.

Chapter 5

Numerical Model

5.1 Velocity Profiles

Preliminary calculations using the law of the wall velocity profile, a traditional means for evaluating the forces exerted on a surface due to turbulent flow, showed that it was not able to predict experimental heat transfer data well [43]. To find a more appropriate velocity profile, a CFD model was generated that simulated droplets falling through air and impinging on a liquid film. The liquid film could be approximated as having two layers; a viscous sublayer and a turbulent bulk [44].

The CFD data obtained from Lane [44] were generalized using non-dimensional parameters in order to compare the velocity profiles in wall units. Dimensionless velocity and dimensionless height are commonly referred to as u^+ and y^+ respectively, and are defined as

$$u^+ = \frac{u}{u^*} \tag{5.1}$$

and

$$y^+ = \frac{y}{\nu} u^*, \tag{5.2}$$

where u^* is the friction velocity defined by

$$u^* = \sqrt{\frac{\tau_w}{\rho}}. \tag{5.3}$$

Here, τ_w is the shear stress at the wall and ρ is the fluid density.

A test facility utilizing linear nozzles was designed to generate a liquid film flowing uniformly in one direction [44]. The droplets are nominally evenly distributed across the

surface of the liquid film, creating a highly mixed region in the liquid. Near the heated surface, however, viscosity will become important, and molecular diffusion processes will control the thermal and momentum transport. For simplicity, the structure of the liquid film beneath the sprays is envisioned as shown in Fig. 5.1, a turbulent, well-mixed layer and a viscous sublayer.

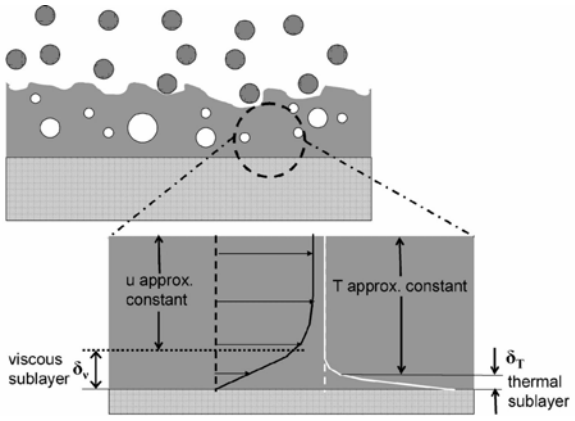

Figure 5.1: Simplified depiction of the liquid film beneath the sprays assuming a two-layer model

Since $Pr \sim 10$ for the dielectric fluids used here, the temperature profile can also be assumed to have two layers of conduction; a conduction sublayer with large temperature gradients and a layer of nearly uniform temperature. If the velocity profile across the thermal sublayer can be approximated as linear, the temperature gradient will be linear as well, and a power law shaped curve can represent the transition and fully developed turbulent region of the profile. The exponent 1/7 is frequently used in the modeling of turbulent pipe flow, and it provided the best agreement with the CFD data, therefore it was used in the power law portion of the profile. Thus, the equation for the two layer model can be best described as

$$u^+ = \begin{cases} y^+ & \text{for } y^+ < y_{crit} \\ C(y^+)^{1/7} & \text{for } y^+ > y_{crit} \end{cases} \tag{5.4}$$

where y^+_{crit} is the transition point from the linear viscous region to the turbulent power law region. This value was found to be 22.7 from the CFD simulation, and the constant C was found to be 14.8.

5.1.1 Derivation of Numerical Equation

Using the two layer velocity distribution derived from the CFD analysis, a numerical model was created that attempts to mathematically characterize the flow by satisfying the integral forms of the mass and momentum conservation equations. The momentum and mass balance on the differential control volume in the fluid is illustrated in Figs. 5.2 and 5.3.

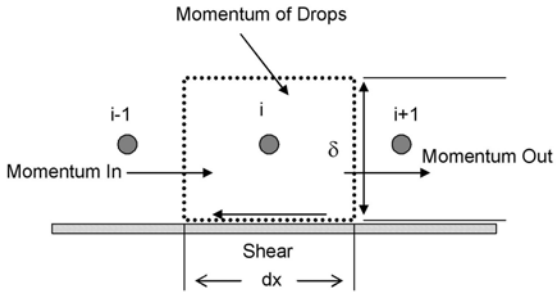

Figure 5.2: Momentum balance on the differential control volume

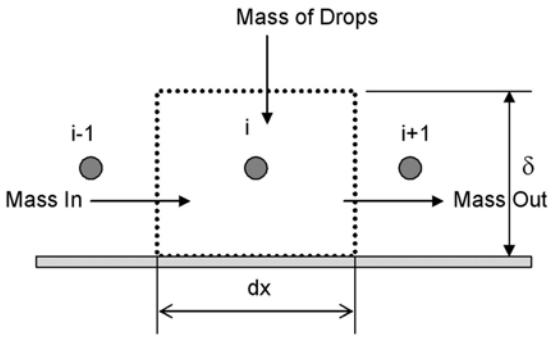

Figure 5.3: Mass balance on the differential control volume

Both of these terms were integrated both through the viscous sublayer and the fully

turbulent region in order to complete the nodal balance at each location. Given the velocity distribution assumed in Eqn. (5.4), the net momentum at any location is related to the film thickness by integrating across the liquid flow.

$$\Delta\text{Momentum} = \int_0^{y_{crit}} \rho u^2 w dy + \int_{y_{crit}}^{\delta} \rho u^2 w dy \tag{5.5}$$

Equation (5.5) can then be rewritten in dimensionless coordinates in order to make the model more general. The basic wall coordinates were defined previously in Eqns. (5.1) and (5.2). The film thickness δ and dy also need to be defined in order for this simplification to be completed.

$$dy = \frac{\nu}{u^*} dy^+ \tag{5.6}$$

$$\delta = \frac{\nu \delta^+}{u^*} \tag{5.7}$$

Thus, Eqns. (5.1,5.2, 5.6), and Eqn. (5.7), can be put into equation 5.5 to yield

$$\Delta\text{Momentum} = \int_0^{y^+_{crit}} \rho {u^*}^2 {y^+}^2 w \frac{\nu}{u^*} dy^+ + \int_{y^+_{crit}}^{\delta^+} \rho C^2 {y^+}^{2/7} {u^*}^2 w \frac{\nu}{u^*} dy^+ \tag{5.8}$$

The integration of Eqn. (5.8) and algebraic simplification yields the net momentum at any location as

$$\Delta\text{Momentum} = \frac{1}{3}\rho u^* w \nu y^{+3}_{crit} + \frac{7}{9}\rho u^* C^2 w \nu {\delta^+}^{9/7} - \frac{7}{9}\rho u^* C^2 w \nu {y^+}^{9/7}_{crit} \tag{5.9}$$

Similarly, the net mass flow at any location can be derived for the differential control volume shown in Figure 5.3.

$$\dot{\text{m}} = \int_0^{y_{crit}} \rho u w dy + \int_{y_{crit}}^{\delta} \rho u w dy \tag{5.10}$$

Using previously defined wall coordinates and dimensionless parameters this equation becomes

$$\dot{\mathrm{m}} = \int_0^{y^+_{crit}} \rho y^+ u^* w \frac{\nu}{u^*} dy^+ + \int_{y^+_{crit}}^{\delta^+} \rho C {y^+}^{1/7} u^* w \frac{\nu}{u^*} dy^+ \tag{5.11}$$

The integration of Eqn. (5.11) and algebraic simplification shows that

$$\dot{\mathrm{m}} = \frac{1}{2}\rho w \nu y^{+^2}_{crit} + \frac{7}{8}\rho C w \nu {\delta^+}^{8/7} - \frac{7}{8}\rho C w \nu y^{+^{8/7}}_{crit} \tag{5.12}$$

A momentum balance in terms of shear, droplet momentum, and momentum at i and i-1 (as seen in Figure 5.2) is the next step. The result of this nodal balance allows for the momentum to be tabulated locally for a specified number of nodes.

$$\Delta Momentum_i = \Delta Momentum_{i-1} + \Delta Momentum_{drop} - \tau_i dx w \tag{5.13}$$

where

$$dx = \frac{L}{N} \tag{5.14}$$

$$\Delta Momenum_{drop} = \dot{m}''_{drop} u_{drop} \mathrm{MC} w dx \tag{5.15}$$

and

$$\dot{m}''_{drop} = Q''\rho \tag{5.16}$$

L is the length of the chip surface, N is the number of nodes, and Q'' is the droplet flux defined as

$$Q'' = \frac{Q}{A} \tag{5.17}$$

where Q is the volumetric flow rate, A is the surface area of the heated surface, and u_{drop} is the initial velocity of the droplets, and MC is a parameter that denotes the percentage of

the droplet momentum that is nominally converted into the x-direction. This momentum conversion number is somewhat physical in that it was less than one for each set of nozzles. The 250 micron diameter nozzles also had a higher MC value than the 200 micron diameter nozzles. This further indicates that this parameter is physical in that you would expect more droplets to be converted into the x-direction with the 250 micron diameter nozzles since larger droplets are generated for the same droplet flux.

Similarly, a mass balance in terms of droplet mass ($\dot{m}''_{drop}$) and mass at i ($\dot{m}$) and i-1 ($\dot{m}_{i-1}$) is needed.

$$\dot{m} = \dot{m}_{i-1} + \dot{m}''_{drop} w dx \tag{5.18}$$

Given these nodal balances, the numerical model is implemented in the iterative software Engineering Equation Solver (EES). The inputs necessary to run the model are the volumetric flow rate (Q) in L min^{-1}, y_{crit}, the width of the heater surface directed into the page (w), the distance between nozzles, the fluid density (ρ) in kg m^{-3} and viscosity (ν) in m^2 s^{-1}.

5.2 Experimental Verification

The nozzles for the linear spray arrays are manufactured using 1.59 mm aluminum tubing with an inner diameter of 0.71 mm. These tubes were cut to a desired length, mounted onto a substrate and then cut with a circular saw to create slits at 45°. Orifices were then drilled through the remaining material in the slits. The length of the orifice was made to be much less than the diameter of the orifice which causes the fluid to "fan" out in the slit and atomize into a spray as it leaves the nozzle. The experiment utilized an array of 56 nozzles, arranged in an alternating pattern to ensure that the entire surface is covered evenly with drops. The slits were cut at a 45° angle with a 0.25 mm thick circular saw to a depth of approximately 0.53 mm. The orifices were drilled using a 200 or 250 micron drill bit and the substrate was mounted to a plate such that the backside of the tubing was sealed using

a gasket. For more in depth coverage of the experiment itself see [46].

5.3 Results

The wall shear was found using the previous numerical analysis so that the numerical model could be directly compared to the experimental results. Figure 5.4 shows the comparison between the measured shear data and the shear predicted from the numerical model for 250 micron diameter and 200 micron diameter nozzles respectively.

This comparison yields an absolute average error of 18% for the 250 micron diameter orifice and 9% for the 200 micron diameter orifice. This seems to indicate that there is a limit to the assumption that the nozzles are always spraying. It may be that to 250 micron diameter orifice is jetting rather than spraying. This would affect the thickness of the thin film and could imply that there is a limit to the two layer assumption. At some film thickness a three layer model may be more appropriate to mathematically capture the fluctuations and other turbulent phenomena in the near wall region.

Clearly this model will not predict heat transfer coefficients due to the fact that no temperature profile was derived from the CFD simulations. As such, this analysis serves as a first step toward predicting the behavior of the sprays.

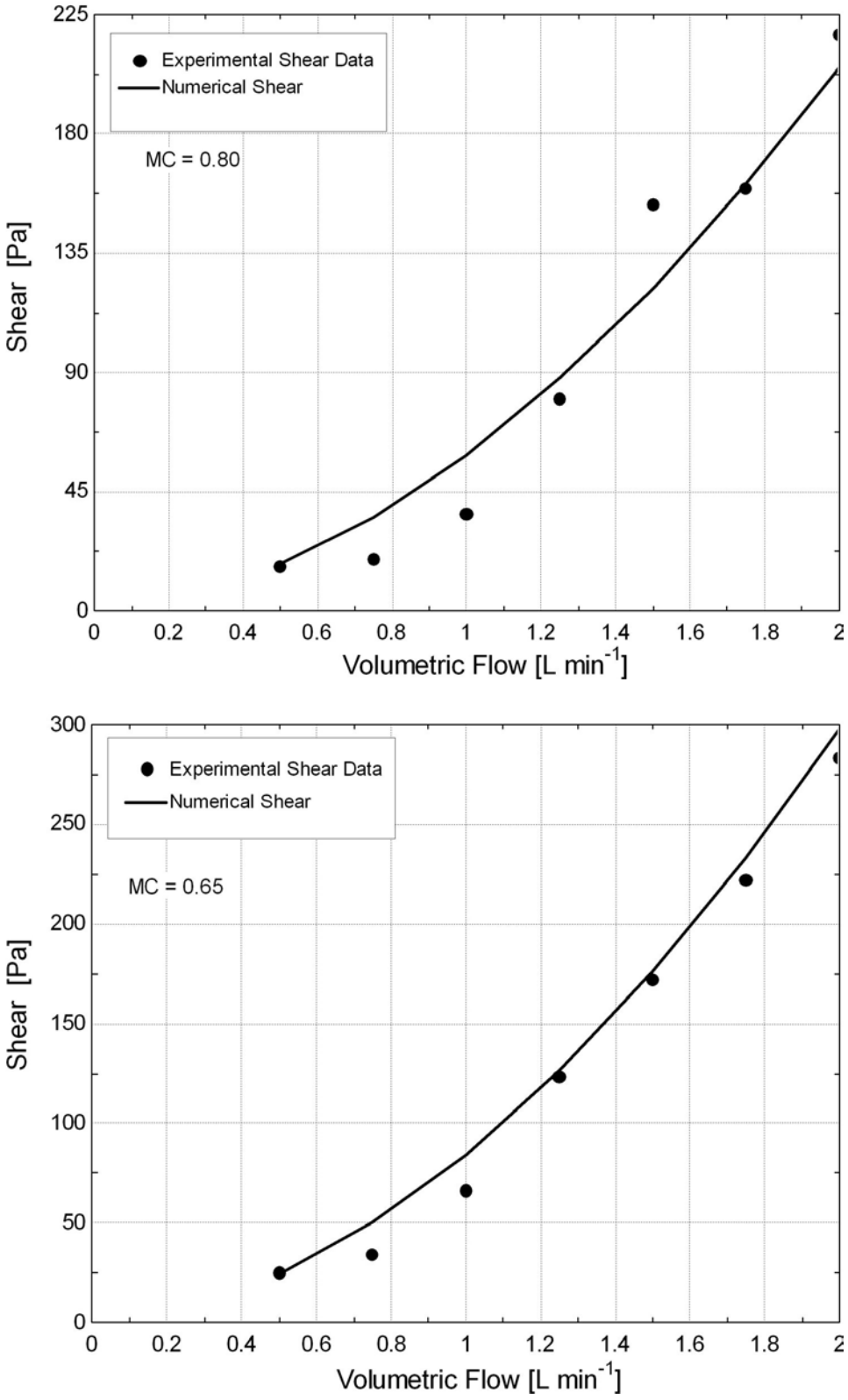

Figure 5.4: Numerical shear stress compared to experimental shear stress

5.4 Heat Transfer Correlation

Studying the complete sets of data obtained in this project, it was hypothesized that the heat transfer behavior for the conical nozzles could be described in a manner similar to the linear sprays, by thinking of the liquid film that forms as consisting of two layers: a turbulent, well-mixed layer and a viscous sublayer. This is depicted schematically in Fig. 5.1. By this model, the thermal sublayer, i.e., the region encompassing nearly all of the temperature gradient that drives the thermal transport, will occur entirely within the viscous sublayer. If the velocity profile across the thermal sublayer can be approximated as linear, the temperature gradient will be linear as well, and the heat transfer conductance (heat transfer coefficient) can be written with no further approximation as

$$h = \frac{k}{\delta_T} \tag{5.19}$$

where k is the thermal conductivity of the fluid and δ_T is the thermal sublayer thickness.

In general boundary layer flow, a relationship between momentum and enthalpy transport can be derived [45]. To begin, momentum transport is assumed to be analogous to enthalpy transport such that,

$$\frac{Advected\ Momentum\ Rate}{Momentum\ Diffusion\ Rate} = \frac{Advected\ Enthlapy\ Rate}{Enthalpy\ Diffusion\ Rate} \tag{5.20}$$

Then, assuming a linear velocity and temperature profile with the viscous sublayer visualized in Figure 5.5, we can write

$$\frac{\rho U_\infty \delta_\nu w}{U \frac{U_\infty}{\delta_\nu} x w} = \frac{\rho U_{\delta_T} C \delta_{nu} w (T_s - T_\infty)}{\frac{k}{\delta_T} x w (T_s - T)} \tag{5.21}$$

Here U_∞ is the velocity of the viscous sublayer and U_{δ_T} is the velocity at the top of the

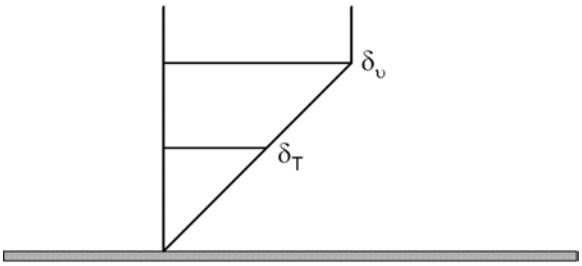

Figure 5.5: Geometric interpretation of viscous and thermal sublayers

thermal sublayer. Eqn. (5.21) can be simplified algebraically to yield

$$\frac{C\mu}{k} = \frac{U_\infty \delta_\nu^2}{U_{\delta_T} \delta_T^2} \tag{5.22}$$

Since the Prandtl number is defined as follows

$$\mathrm{Pr} = \frac{C\mu}{k}, \tag{5.23}$$

Eqn. (5.22) can be simplified to yield

$$\mathrm{Pr} = \frac{U_\infty}{U_{\delta_T}} \frac{\delta_\nu^2}{\delta_T^2} \tag{5.24}$$

The similar triangles of Figure 5.5 can be used to further reduce this so that the thermal sublayer is related to the viscous sublayer by the Prandtl number such that

$$\mathrm{Pr} \propto \left(\frac{\delta_\nu}{\delta_T} \right)^3 \tag{5.25}$$

or, in general,

$$\delta_T = \delta_\nu \mathrm{Pr}^{-n} \tag{5.26}$$

where n is equal to 1/3. Then the heat transfer coefficient can be approximated as

$$h = \frac{k}{\delta_T} = \frac{k}{\delta_\nu}\mathrm{Pr}^n \tag{5.27}$$

where δ_ν is the viscous sublayer thickness and n is an exponent appropriate for scaling the ratio of the two sublayer thicknesses. Assuming that this liquid film can be represented as a turbulent boundary layer,

$$\delta_\nu = \frac{\delta^+ \nu}{u^*} \tag{5.28}$$

where δ^+ is the non-dimensional thickness of the viscous sublayer, ν is the liquid kinematic viscosity and

$$u^* = \sqrt{\frac{\tau}{\rho}} \tag{5.29}$$

Here, u^* is the friction velocity, τ is the shear stress at the solid surface and ρ is the liquid density. Setting $\delta^+ = 5$ as is common in some turbulent boundary layer models and $n = 0.4$ based on turbulent heat transfer correlations for pipe flow,

$$h \approx 0.2\frac{k}{\nu}\sqrt{\frac{\tau}{\rho}}\mathrm{Pr}^{0.4} \tag{5.30}$$

Since all of the fluid properties are known, this relationship for heat transfer coefficients can be verified by direct measurement of the shear stress. It was not possible to obtain shear data for the conical sprays, however dimensional analysis in the boundary layer shows that

$$\frac{\tau}{\rho} = \nu\frac{V}{\delta_\nu} \tag{5.31}$$

where V is a velocity term and δ_ν is the momentum boundary layer thickness term associated with this velocity. The velocity term in Eqn. (5.31) is a function of the average droplet flux over the entire heater surface ($\overline{Q''}$), which may or may not be the same as Q'' because of

over/under spraying, and some constant which also contains the viscosity term (ν). Thus, the thickness associated with this velocity term is the thickness of the viscous sublayer δ_ν

$$\frac{\tau}{\rho} = C_2\overline{Q''} \tag{5.32}$$

The viscous sublayer thickness (δ_ν) is not known a priori, but, for a given flow rate, is primarily a function of the viscosity. Therefore this term can be assumed to be a new constant. So,

$$h = 0.2\frac{k}{\nu}Pr^{0.4}\overline{Q''}^{0.5}C_3 \tag{5.33}$$

Using the heat transfer data, the best fit for the exponent on the Prandtl number was 0.5 rather than 0.4 and C_3 is a dimensional parameter with units of $\mathrm{m}^{-0.5}$ $\mathrm{s}^{-0.5}$. Two separate parameters were found, one for the four nozzle array and another for the single nozzle array. These parameters were found at a low applied heat flux such that the only method for heat transfer is single phase transport. The end result was a parameter of 0.645 and 0.745 for the four nozzle and single nozzle arrays respectively. Thus, the correlations are

$$h = 0.129\frac{k}{\nu}\mathrm{Pr}^{0.5}\overline{Q''}^{0.5} \tag{5.34}$$

for the four nozzle array and

$$h = 0.149\frac{k}{\nu}\mathrm{Pr}^{0.5}\overline{Q''}^{0.5} \tag{5.35}$$

for the single nozzle. These correlations agree within 6% and 5% absolute average error of the experimental result as seen in Figure 5.6.

The mixture data were also correlated, resulting in parameters of 0.62 and 0.69 $\mathrm{m}^{-0.5}$ $\mathrm{s}^{-0.5}$ for the four nozzle array and single nozzle, respectively. The properties were calculated using the molar concentrated averages and yielded results within 8% and 9% absolute error, as is illustrated in Figure 5.7.

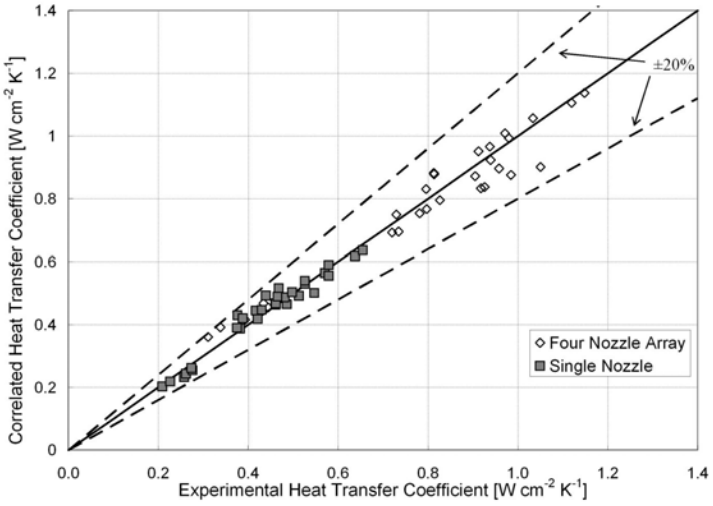

Figure 5.6: Correlated Heat Transfer Performance compared to Experimental Heat Transfer Performance

The only gas saturated Fluorinert data found in the literature for comparison was that of Horacek et al. [20] who looked at gas subcooled FC-72. Using the correlation found in Eqn. (5.35), since the study utilized a single nozzle, it was found that the heat transfer coefficient could be accurately predicted. Data was found using gas saturated water. Work done by Jiang and Dhir [18] looked at spraying water through a single nozzle configuration in a closed system. Their experimental data could also be correlated well.

It is interesting to note that the parameter found for Horacek's data is very close to the value found in this experiment for the single nozzle (Table 5.1). This seems to indicate that the distance between the heater surface and the nozzle has minimal effect in the prediction of the heat transfer performance. The accuracy of the correlation also seems to indicate that the two layer model accurately depicts the spray cooling behavior in the turbulent boundary layer. If the thickness of the viscous sublayer could somehow be accurately measured it would be the largest factor in the parameter that is needed to make this correlation work better. Eqn. (5.33) the correlation parameter is an indication of how effectively droplet flux

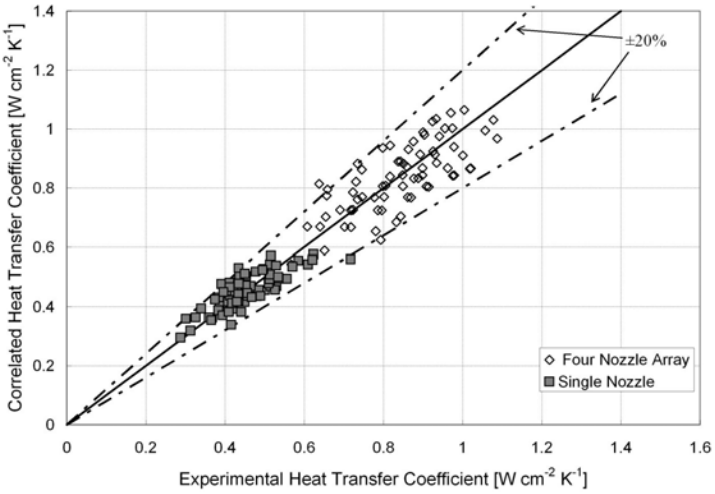

Figure 5.7: Correlated Mixture Heat Transfer Performance compared to Experimental Mixture Heat Transfer Performance

creates a thin viscous sublayer.

Table 5.1: Correlated Heat Transfer Coefficients

Nozzle Type	h_{exp} [W cm^{-2} s^{-1}]	h_{cor} [W cm^{-2} s^{-1}]	Parameter (C_3) m$^{-0.5}$ s$^{-0.5}$	Author(s)
Conical Single	-	-	0.745	Ashwood
Conical Four	-	-	0.645	
Conical Single Mixture	-	-	0.69	
Conical Four Mixture	-	-	0.62	
Conical Single	0.791	0.798	0.753	Horacek et. al [20]
	0.806	0.798	0.753	
Conical Single	5.621	5.621	0.325	Jiang et. al [18]
Linear at 45°	1.397	1.50	1.049	Regner et. al [46]
	1.764	1.731		
	1.96	1.937		
	2.20	2.123		

Also of interest is the performance of the single nozzle compared to the four nozzle array. For a given flow rate, the single nozzle outperforms the four nozzle array. This can be attributed to fluid management. Pautsch and Shedd visualized gas saturated FC-72 using this same multi-chip module [10]. Their data indicate a rather large area of both

fluid stagnation (or pooling of fluid) and re-circulation of fluid in the four nozzle array. This stagnation area was seen to some degree in the single nozzle, but was not nearly as prominent and seemed to occur at the corners of the test die. This seems to indicate that the single nozzle more effectively maintains a thin viscous sublayer. This theory is corroborated by the Linear Spray Nozzles as well. Since these nozzles only spray in one direction more momentum is nominally injected into the film. Thus, the film itself is more accurately continuously maintained as is illustrated with a constant of 1.049 $m^{-0.5}$ $s^{-0.5}$ (see Table 5.1).

Chapter 6

Conclusion

The first objective was to determine the effects of fluid properties on spray cooling performance. It was found that the data are represented by an empirical correlation of the form

$$h = C\frac{k}{\nu}\mathrm{Pr}^{0.5}\overline{Q''}^{0.5} \tag{6.1}$$

which can be simplified to

$$h = \left(\frac{kC_p}{\nu}\right)^{0.5}\dot{m}''^{0.5} \tag{6.2}$$

Thus, it appears that k, C_p, and ν are of equal importance for this system. Of these, k and C_p directly impact the thermal transport while ν affects both the thermal transport and the spray characteristics.

Another objective was to evaluate the use of mixtures in spray cooling. It was found that the heat transfer coefficients were not at all degraded by the use of mixtures and that the presence of non-condensibles in the system does not affect the heat transfer performance of the fluid.

The last objective was to investigate the fundamental mechanisms of spray cooling. A correlation based on a two-layer model of the liquid film predicts all of the data well, as well as other data in the literature. This suggests that this is a useful model for the thermal transport. A numerical model was developed based on this concept and a viscous sublayer of $y^+ = 23$ predicts the experimental shear values very accurately.

Bibliography

[1] G. E. Moore. Cramming more components onto integrated circuits. *Electronics*, 8(38):1–4, 1965.

[2] H. Baumann, P. Heinemeyer, W. Staiger, M. Töpfer, K. Unger, and D. Müller. Optimized cooling systems for high-power semiconductor devices. *IEEE Transactions on Industrial Electronics*, 48(2):298–306, 2001.

[3] M. J. Ellsworth and R. E. Simons. High powered chip cooling,air and beyond. *Electronics Cooling*, 11(3):14–22, 2005.

[4] I. Mudawar. Assessment of high-heat-flux thermal management schemes. *IEEE Transactions on Components and Packaging Technologies*, 24(2):122–141, 2001.

[5] R.-H. Chen, L. C. Chow, and J. E. Navedo. Effects of spray characteristics on critical heat flux in subcooled water spray cooling. *International Journal of Heat and Mass Transfer*, 45:4033–4043, 2002.

[6] J. R. Rybicki and I. Mudawar. Single-phase and two-phase cooling characteristics of upward-facing and downward-facing sprays. *International Journal of Heat and Mass Transfer*, 49(1-2):5–16, 2006.

[7] G. Pautsch. An overview on the system packaging of the CRAY SV2 supercomputer. In *Proceedings of IPACK'01, The Pacific Rim/ASME International Electronic Packaging Technical Conference and Exhibition*, pages 617–624. ASME, 2001.

[8] A. G. Pautsch. Heat transfer and film thickness characteristics of spray cooling with phase change. Master's thesis, University of Wisconsin-Madison, Madison, Wisconsin, 2004. Available at *http://sel.me.wisc.edu*.

[9] D. P. Rini, R.-H. Chen, and L. C. Chow. Bubble behavior and nucleate boiling heat transfer in saturated FC-72 spray cooling. *Journal of Heat Transfer*, 124:63–72, 2002.

[10] A. G. Pautsch and T. A. Shedd. Spray impingement cooling with single- and multiple-nozzle arrays Part I: Heat transfer data using FC-72. *International Journal of Heat and Mass Transfer*, 48:3167–3175, 2005.

[11] D.-C. Cheng and H. Burkhadt. Bubble tracking in image sequences. *International Journal of Thermal Sciences*, 42:647–655, 2003.

[12] A. G. Pautsch and T. A. Shedd. Adiabatic and diabatic measurements of the liquid film thickness during spray cooling with fc-72. *To appear in the International Journal of Heat and Mass Transfer*, 2006.

[13] I.A. Kopchikov, G.I. Voronin, T.A. Kolach, D.A. Labuntsov, and P.D. Lebedev. Liquid boiling in a thin film. *International Journal of Heat and Mass Transfer*, 12:791–796, 1969.

[14] D. P. Rini, R.-H. Chen, and L. C. Chow. Bubble behavior and heat transfer mechanism in FC-72 pool boiling. *Experimental Heat Transfer*, 14:27–44, 2001.

[15] T. A. Shedd and A. G. Pautsch. Spray impingement cooling with single- and multiple-nozzle arrays. Part II: Visualization and empirical models. *International Journal of Heat and Mass Transfer*, 48:3176–3184, 2005.

[16] K. A. Estes and I. Mudawar. Correlation of Sauter mean diameter and critical heat flux for spray cooling of small surfaces. *International Journal of Heat and Mass Transfer*, 38(16):2985–2996, 1995.

[17] S. Freund, A. G. Pautsch, T. A. Shedd, and S. Kabelac. Local heat transfer coefficients in spray cooling systems measured with temperature oscillation IR thermography. *Submitted to the International Journal of Heat and Mass Transfer*, -(-):–, 2006.

[18] S. Jiang and V. K. Dhir. Spray cooling in a closed system with different fractions of non-condensibles in the environment. *International Journal of Heat and Mass Transfer*, IN Press:In Press, 2004.

[19] I. Mudawar and K. A. Estes. Optimizing and predicting CHF in spray cooling of a square surface. *Journal of Heat Transfer*, 118:672–679, 1996.

[20] B. Horacek, K. T. Kiger, and J. Kim. Single nozzle spray cooling heat transfer mechanisms. *International Journal of Heat and Mass Transfer*, 48:1425–1438, 2005.

[21] I. Mudawar and W. S. Valentine. Determination of the local quench curve for spray-cooled metallic surfaces. *Journal of Heat Treatment*, 7:107–121, 1989.

[22] K. A. Estes and I. Mudawar. Comparison of two-phase electronic cooling using free jets and sprays. *Transactions of the ASME–Journal of Electronic Packaging*, 117:323–332, December 1995.

[23] K. Kiger E. A. Silk, J.H. Kim. Spray cooling of enhanced surfaces and impact of structured surface geometry and spray axis inclination. *To appear in the International Journal of Heat and Mass Transfer*, August 2006.

[24] J. G. Collier and J. R. Thome. *Convective Boiling and Condensation*. Oxford University Press, Oxford, third edition, 1994.

[25] L. Cheng and D. Mewes. Review of two phase flow and flow boiling of mixtures in small and mini channels. *International Journal of Heat and Mass Transfer*, pages 183–207, 2006.

[26] K. Stephan and P. Preusser. Heat transfer and critical heat flux in pool boiling of binary and ternary mixtures. *German Chemical Engineering*, 2:161–169, 1979.

[27] H. Ross, R. Radermacher, and M. DiMarzo. Horizontal flow boiling of pure and mixed refrigerants. *International Journal of Heat and Mass Transfer*, 30(5):979–992, 1987.

[28] S. Van Strahlen and R. Cole. *Boiling Phenomena*. Hemisphere Publishing Corp, 1979.

[29] Y. S. Fujita and M. Tsutsui. Nucleate boiling of two and three component mixtures. *International Journal of Heat and Mass Transfer*, 47:4637–4648, 2004.

[30] T. Setaro G. P. Celato, M. Cumo. A review of pool and forced convective boiling of binary mixtures. *Experimental Theral and Fluid Science*, 9:367–381, 1994.

[31] L. E. Scriven. On the dynamics of phase growth. *Chemical engineering science*, 10:1–13, 1959.

[32] J.R. Thome. Latent and sensible heat transport the boiling rates in binary mixtures. *Journal of Heat Transfer*, 104:474–478, 1984.

[33] M. Carne. Studies of the CHF of some binary mixtures. *Canadian Journal of Chemical Engineering*, 41:235–241, 1963.

[34] L. S. Fan Y. Ge. Three dimensional modeling of the dynamic and heat transfer characteristics of subcooled droplet impact on a surface with film boiling. *International Journal of Heat and Mass Transfer*, 49:4231–4249, 2006.

[35] R. Ponnappan P. Selvam, L. Lin. Direct simulation of spray cooling:effect of vapor bubble growth and liquid droplet impact on heat transfer. *International Journal of Heat and Mass Transfer*, 49:4265–4278, 2006.

[36] S. Osher M. Sussman, P. Smereka. A level set approach for computing solutions to incompressible two phase flow. *Journal of Computational Physics*, 114, 1994.

[37] V. K. Dhir G. Son. Numerical simulation of film boiling near critical pressures with a level set method. *Journal of Heat and Mass Tranfer*, 120:183–192, 1998.

[38] D. W. Stanton and C. J. Rutland. Multi-dimensional modeling of thin liquid films and spray-wall interactions resulting from impinging sprays. *International Journal of Heat and Mass Transfer*, 41(20):3037–3054, 1998.

[39] 3M. Fluorinert product information . *http://www.3m/3Msearch/3Msolutions/fluorinert-liquids*, 2000.

[40] Richard E. Sonntag and Gordon J. Van Wylen. *Introduction to Thermodynamics Classical and Statistical*. John Wiley and Sons, 1991.

[41] B. N. Taylor and C. E. Kuyatt. Guidelines for evaluating and expressing uncertainty of NIST measurement results. Technical Report 1297, National Institute of Standards and Technology, Bethesda, MD, 1994.

[42] Ryan K. Jester. Aggresive energy recovery from the waste heat of a hyrbid automobile powerplant. Master's thesis, University of Wisconsin-Madison, 2006.

[43] Timothy Shedd. Personal communication. Department of Mechanical Engineering, University of Wisconsin-Madison, 2006.

[44] C. Lane. Characterization and numerical modeling of momentum driven spray cooling. Master's thesis, University of Wisconsin-Madison, 2006.

[45] Vedat S. Arpaci and Poul S. Larsen. *Convection Heat Transfer*. Prentice-Hall, Inc., 1984.

[46] B.M. Regner and T.A. Shedd. An orientation independent,scalable spray cooling system for high heat flux removal. In *Space Technology & Applications International Forum*, Albuquerque, NM, U.S.A, 2006.

Appendix A

Gas-saturated Mixture Plots

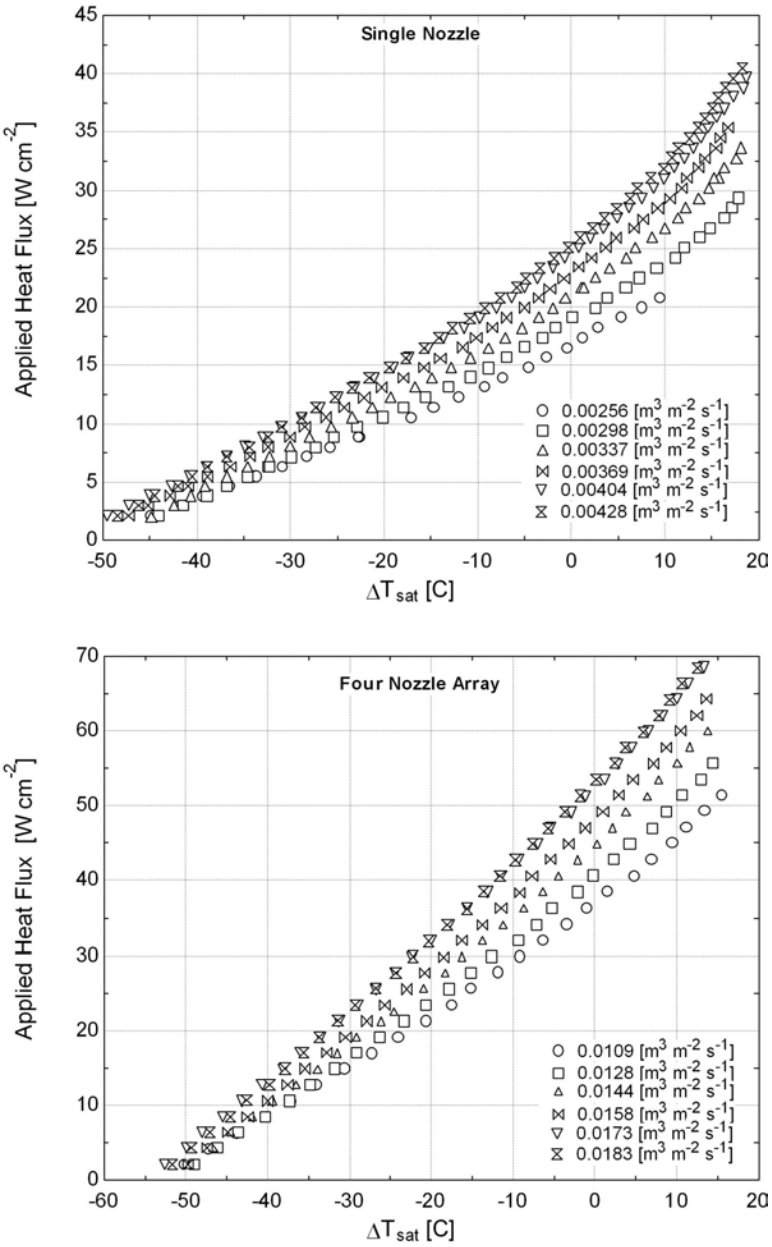

Figure A.1: Boiling curves for the 75-25 mixture of FC-72/FC-74 using the single nozzle and four nozzle array at 1 atm

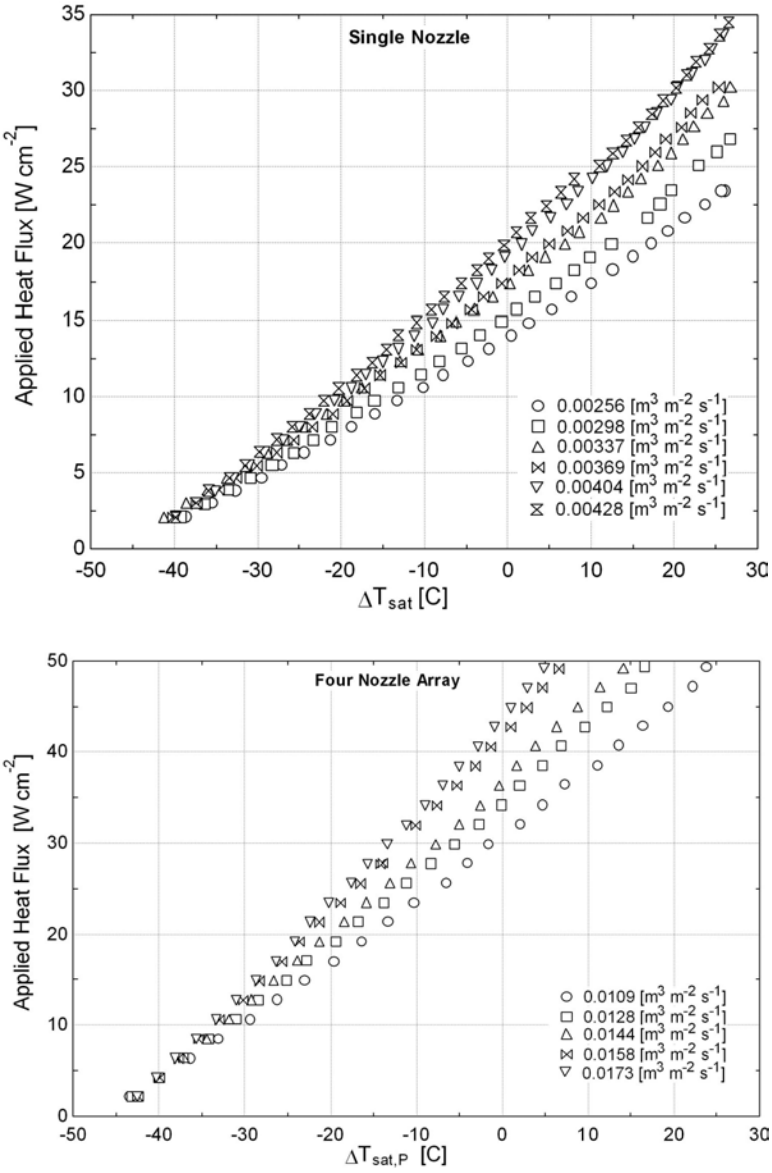

Figure A.2: Boiling curves for the 50-50 mixture of FC-72/FC-74 using the single nozzle and four nozzle array at 1 atm

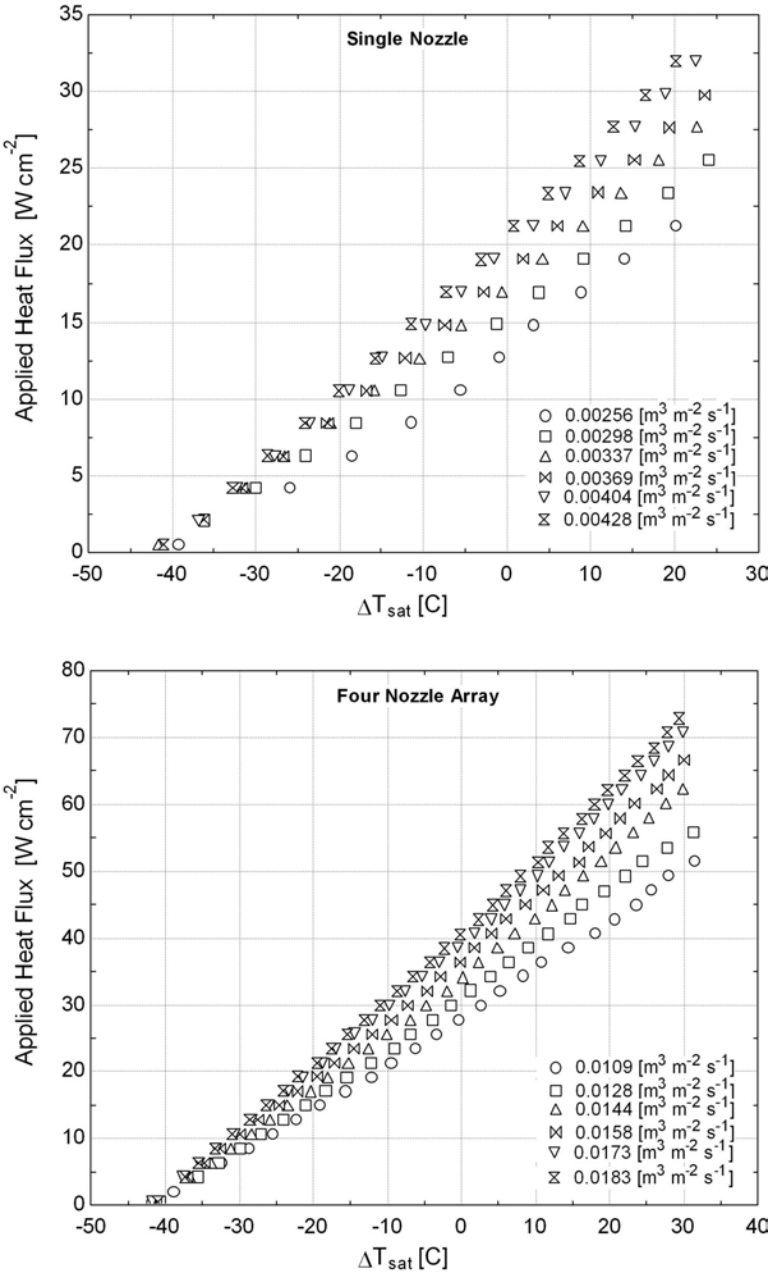

Figure A.3: Boiling curves for the 25-75 mixture of FC-72/FC-74 using the single nozzle and four nozzle array at 1 atm

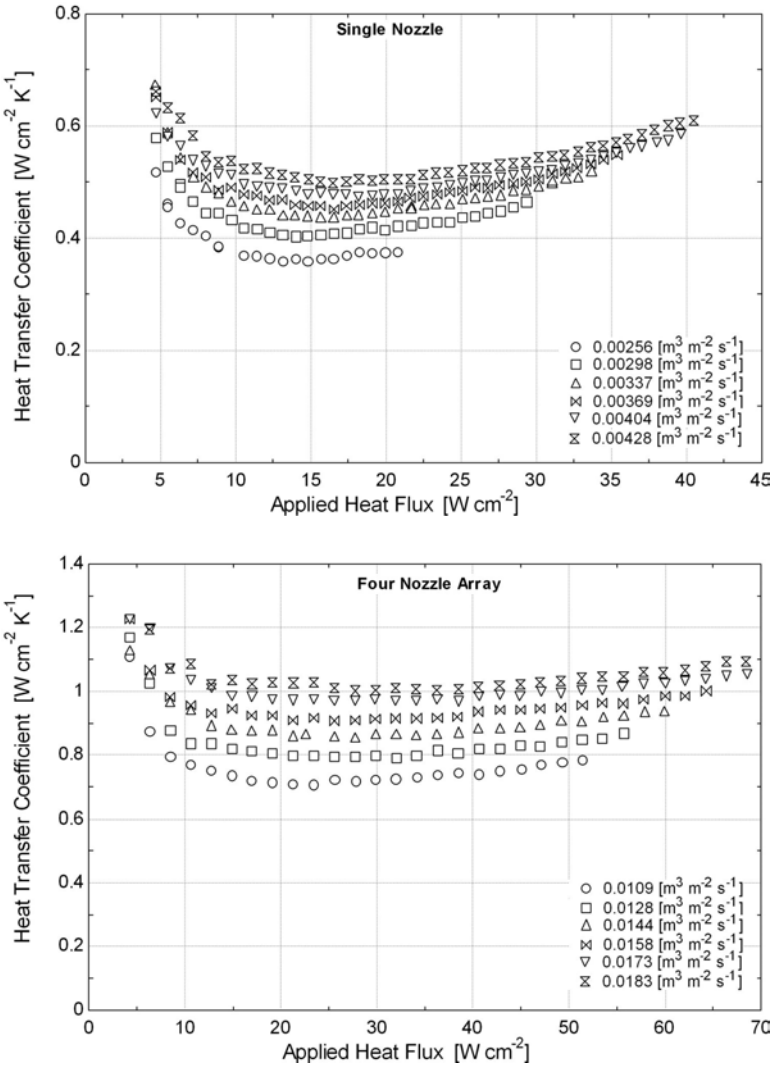

Figure A.4: Heat transfer performance for the 75-25 mixture of FC-72/FC-74 for the single nozzle and four nozzle array at 1 atm

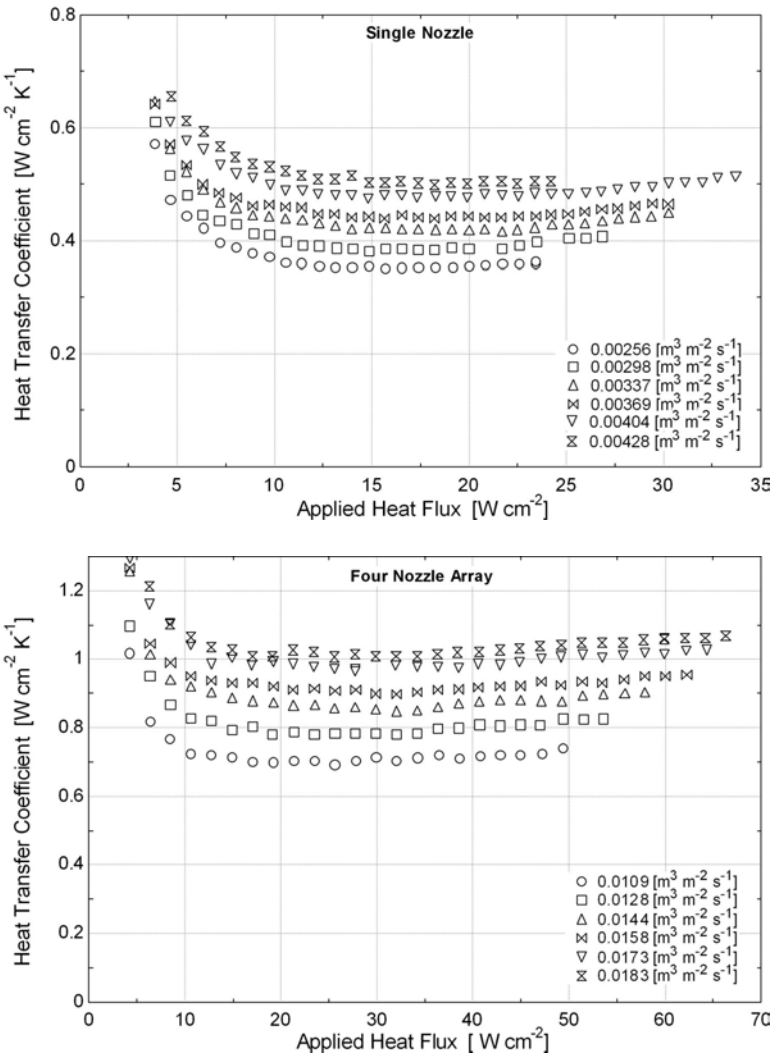

Figure A.5: Heat transfer performance for the 50-50 mixture of FC-72/FC-74 for the single nozzle and four nozzle array at 1 atm

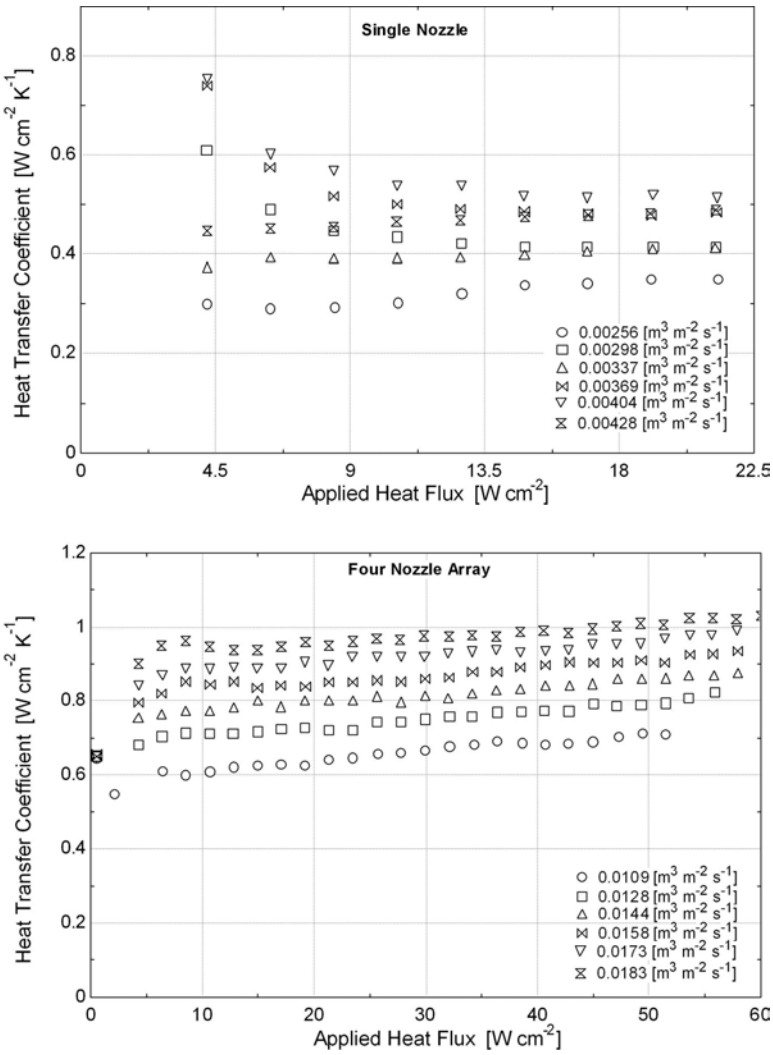

Figure A.6: Heat transfer performance for the 25-75 mixture of FC-72/FC-74 for the single nozzle and four nozzle array at 1 atm

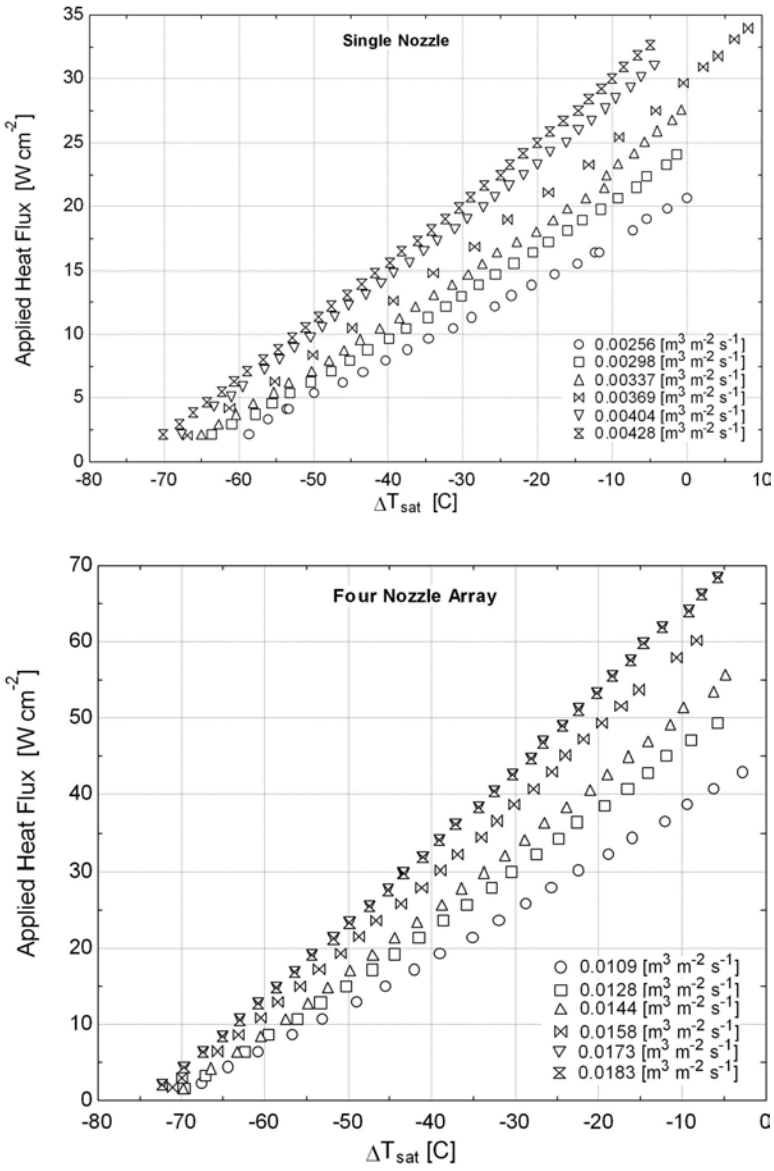

Figure A.7: Boiling curves for the 75-25 mixture of FC-72/FC-40 using the single nozzle and four nozzle array at 1 atm

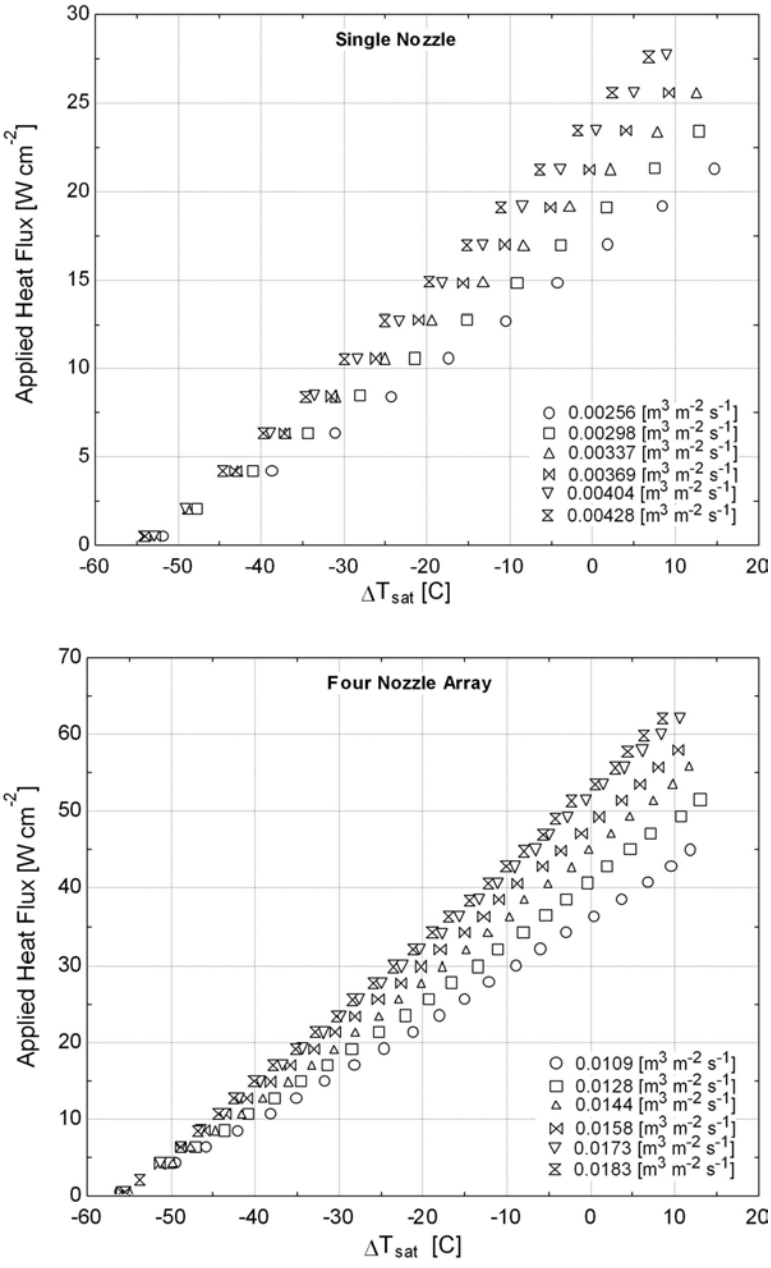

Figure A.8: Boiling curves for the 50-50 mixture of FC-72/FC-40 using the single nozzle and four nozzle array at 1 atm

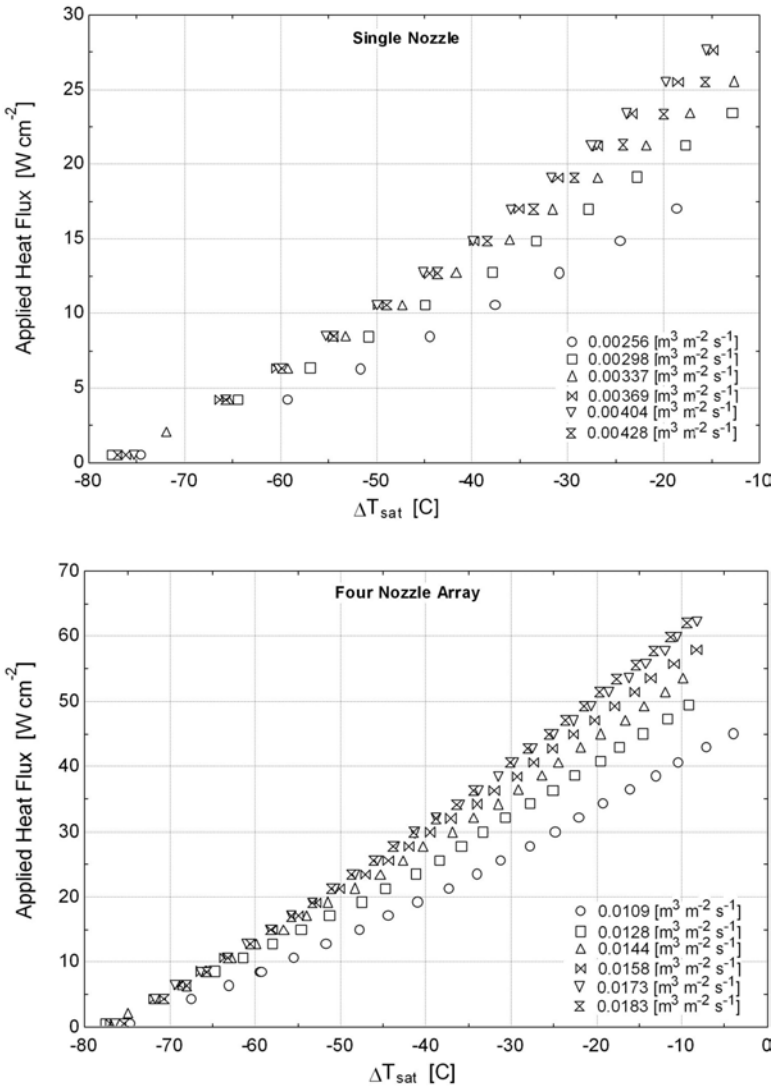

Figure A.9: Boiling curves for the 25-75 mixture of FC-72/FC-40 using the single nozzle and four nozzle array at 1 atm

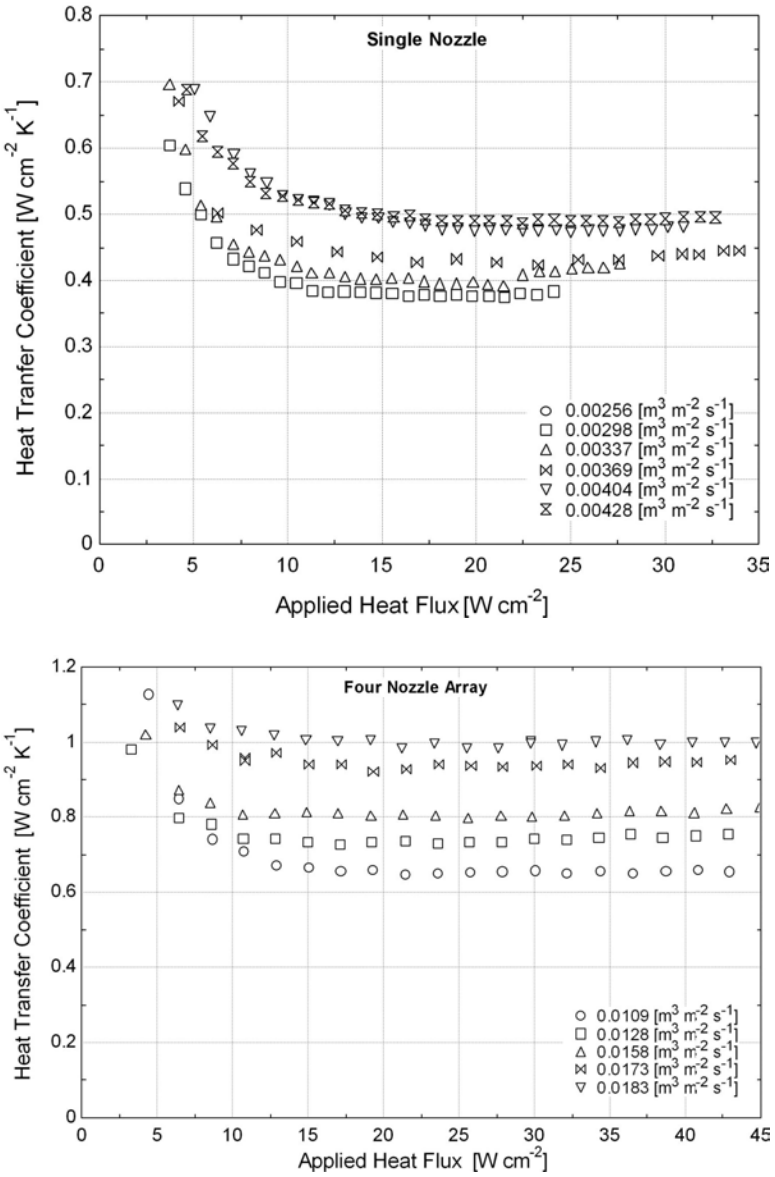

Figure A.10: Heat transfer performance for the 75-25 mixture of FC-72/FC-40 for the single nozzle and four nozzle array at 1 atm

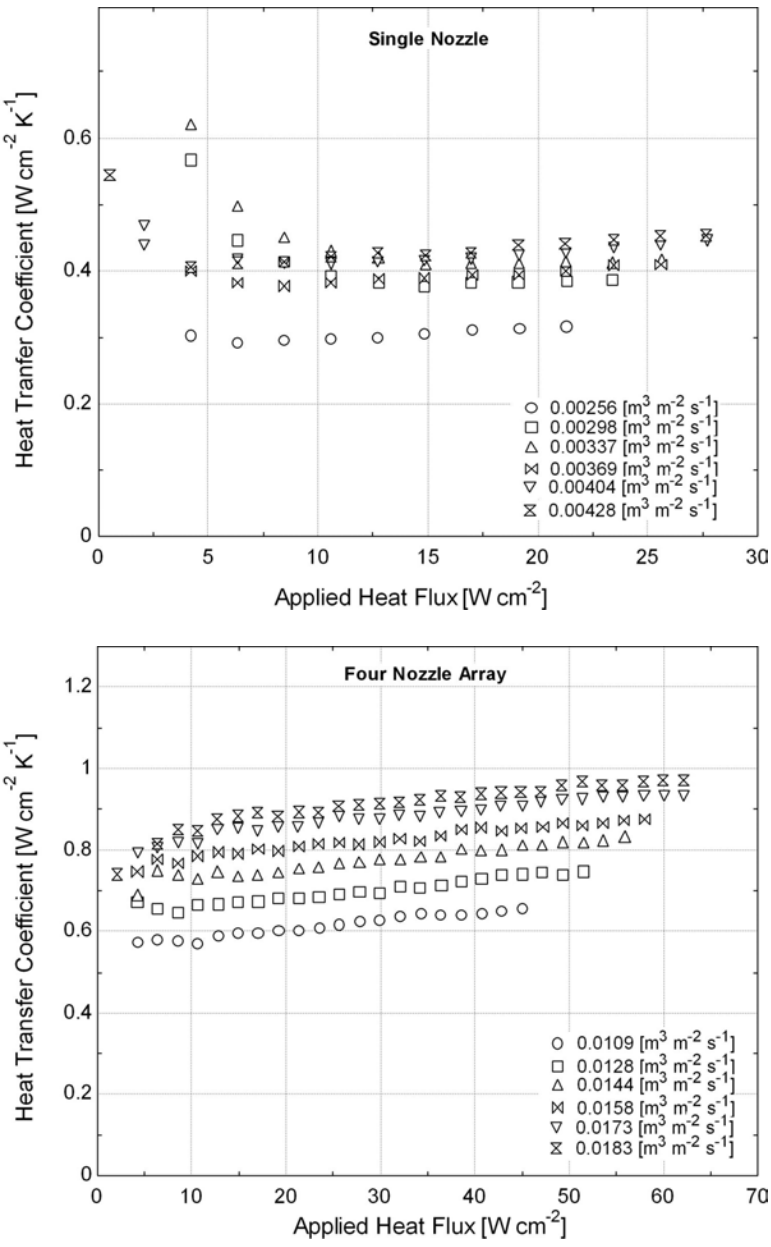

Figure A.11: Heat transfer performance for the 50-50 mixture of FC-72/FC-40 for the single nozzle and four nozzle array at 1 atm

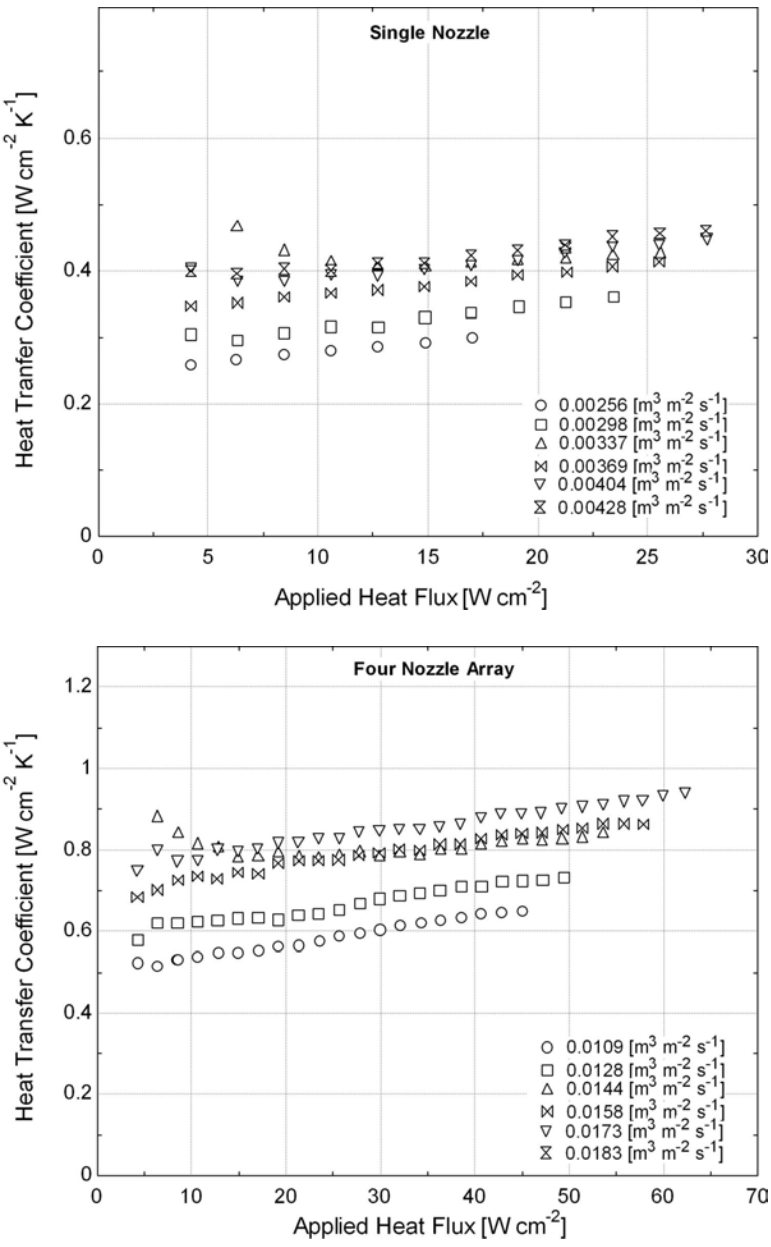

Figure A.12: Heat transfer performance for the 25-75 mixture of FC-72/FC-40 for the single nozzle and four nozzle array at 1 atm

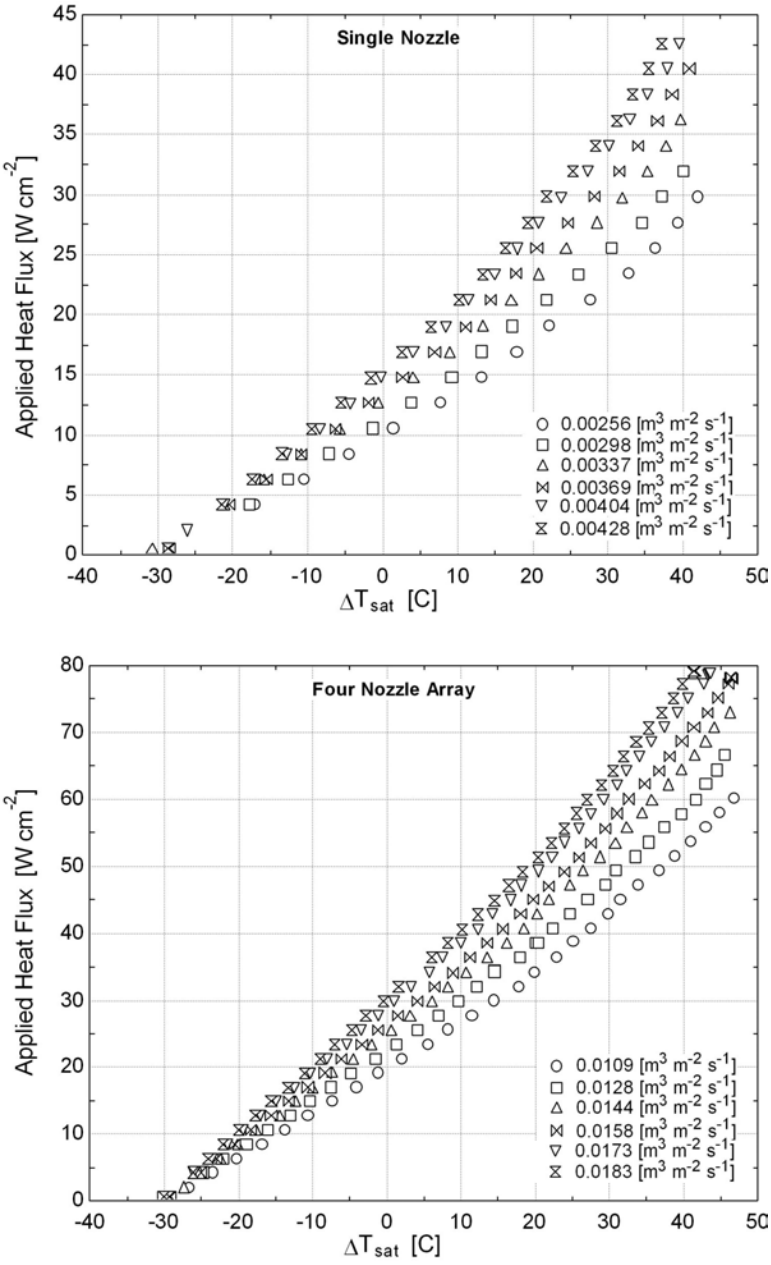

Figure A.13: Boiling curves for the 75-25 mixture of FC-72/HFE-7000 using the single nozzle and four nozzle array at 1 atm

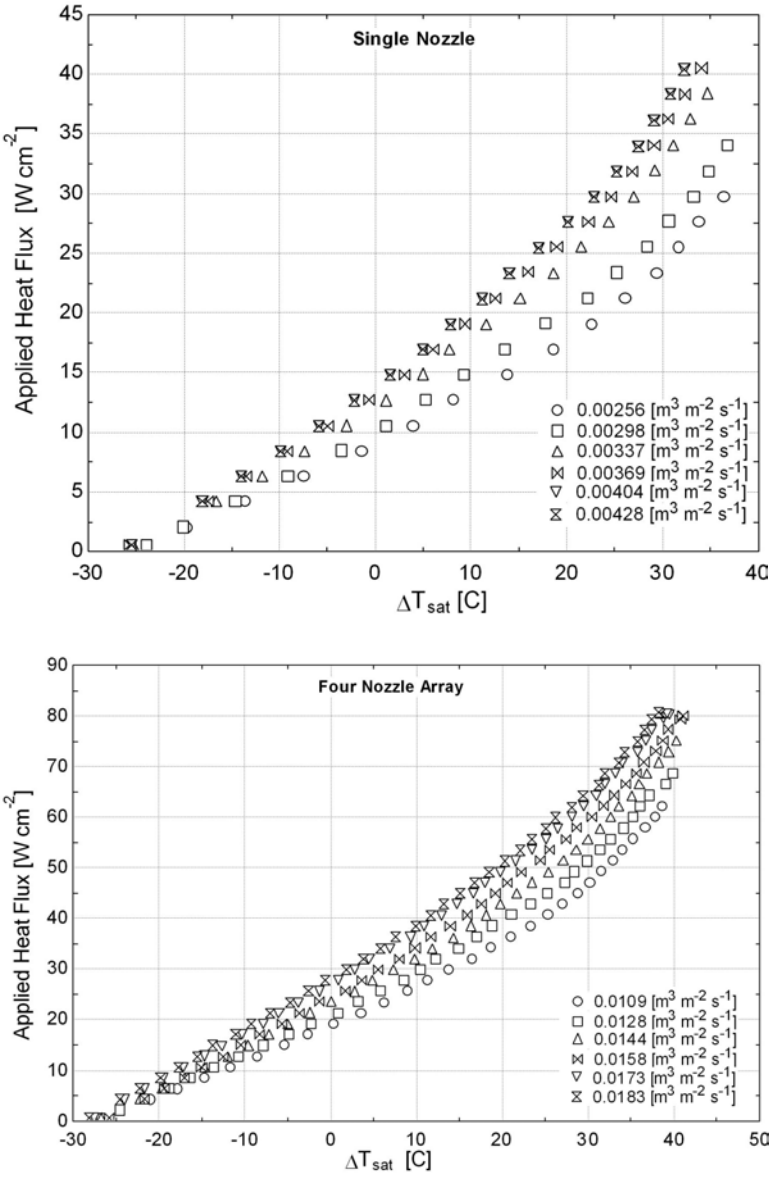

Figure A.14: Boiling curves for the 50-50 mixture of FC-72/HFE-7000 using the single nozzle and four nozzle array at 1 atm

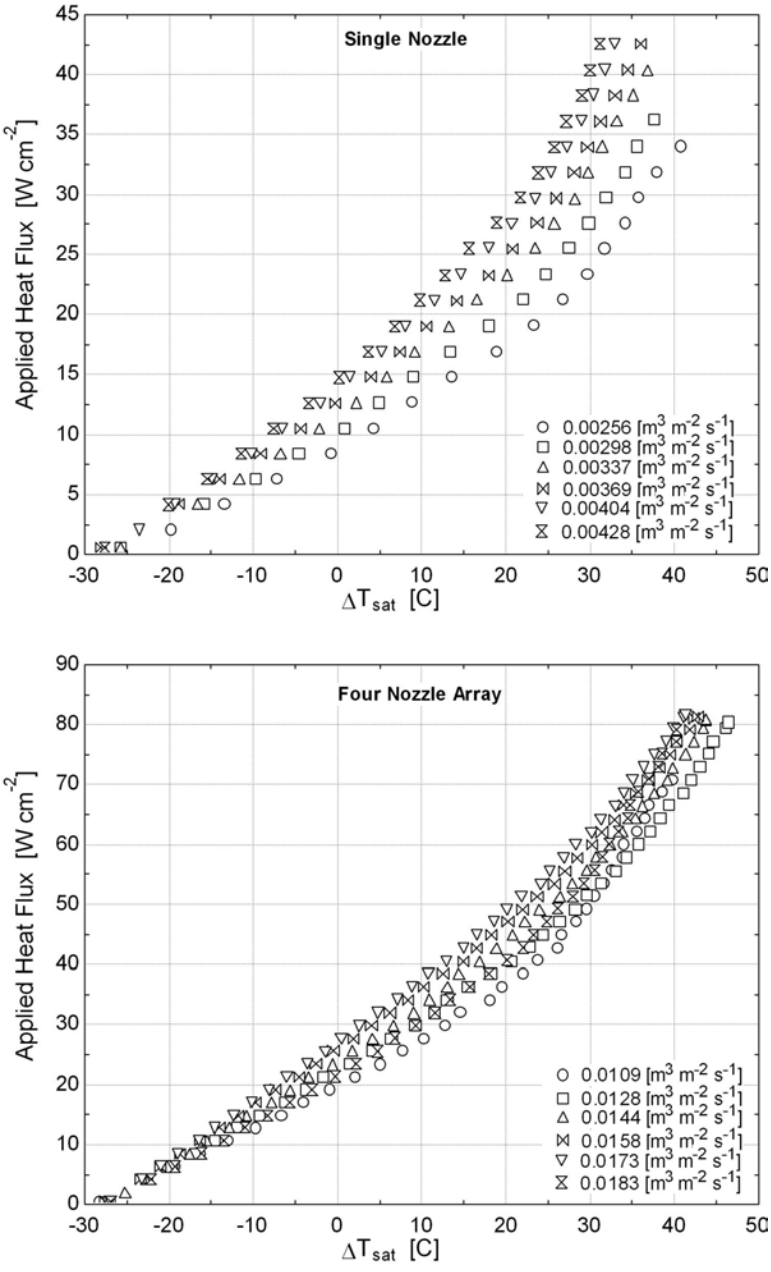

Figure A.15: Boiling curves for the 25-75 mixture of FC-72/HFE-7000 using the single nozzle and four nozzle array at 1 atm

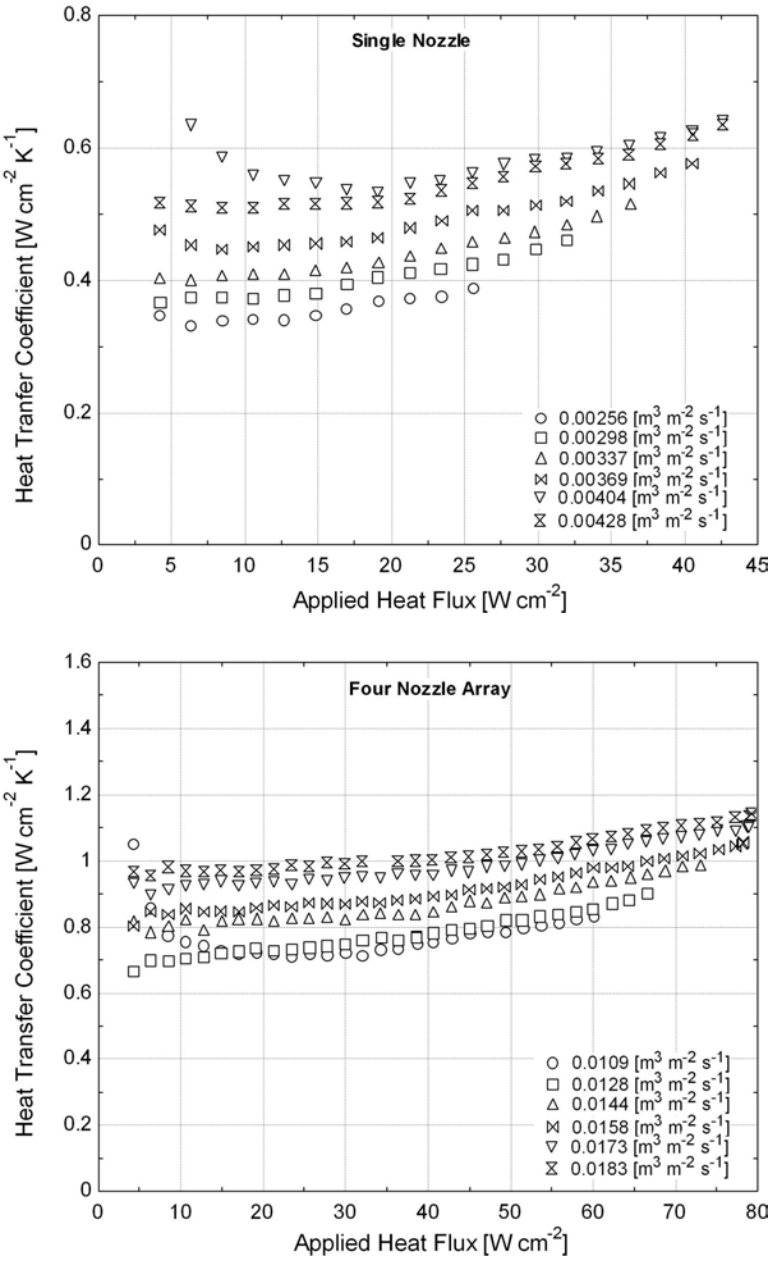

Figure A.16: Heat transfer performance for the 75-25 mixture of FC-72/HFE-7000 for the single nozzle and four nozzle array at 1 atm

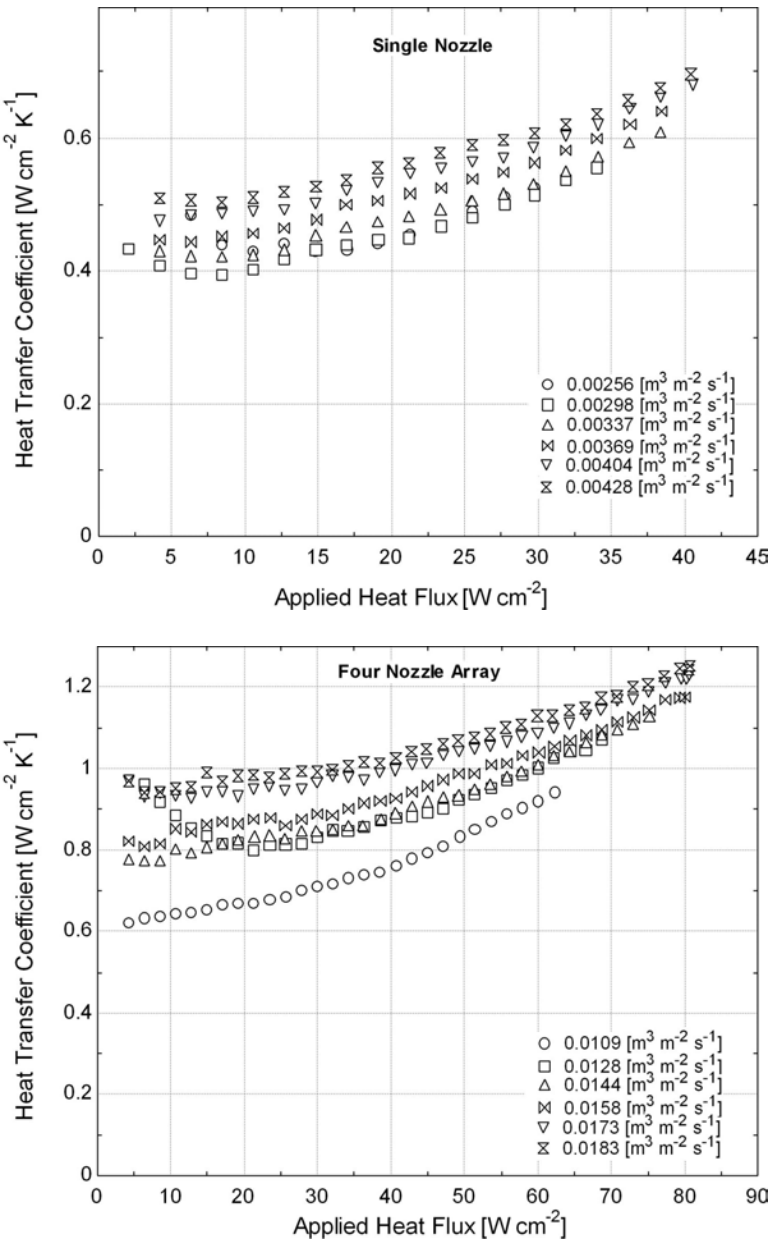

Figure A.17: Heat transfer performance for the 50-50 mixture of FC-72/HFE-7000 for the single nozzle and four nozzle array at 1 atm

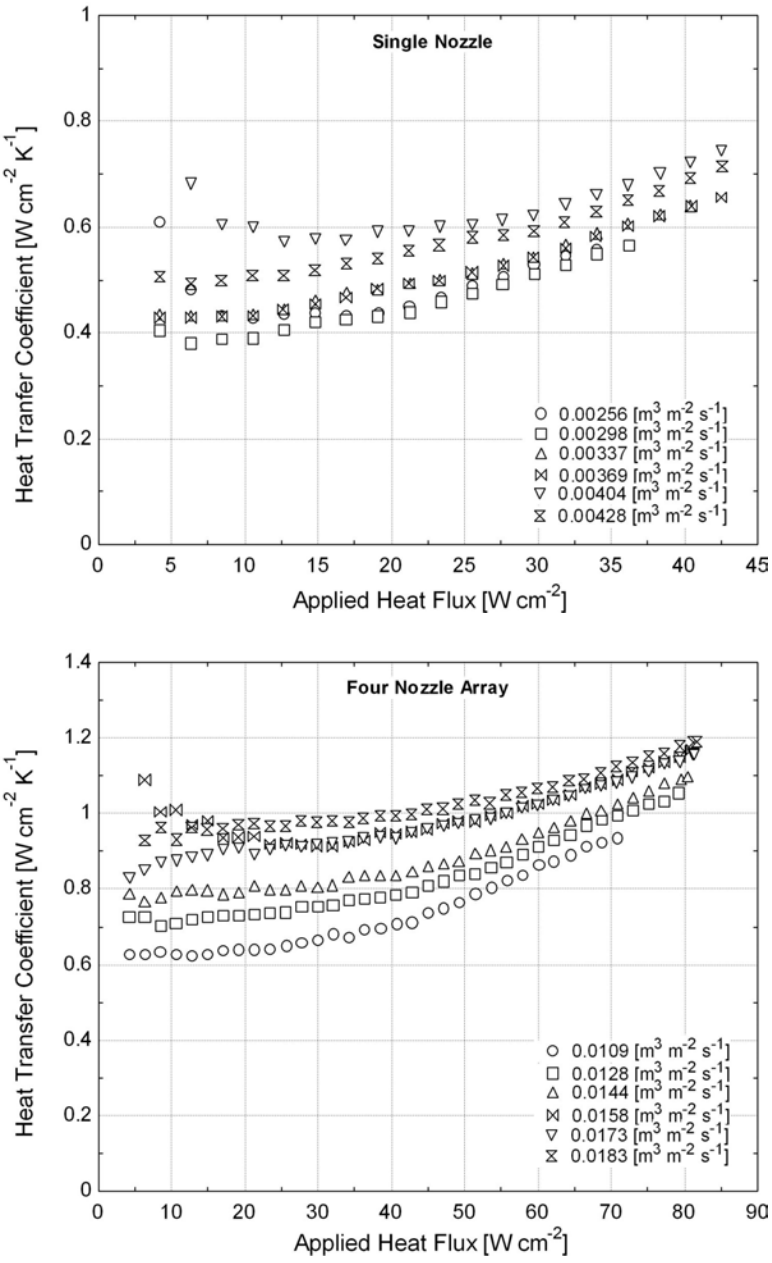

Figure A.18: Heat transfer performance for the 25-75 mixture of FC-72/HFE-7000 for the single nozzle and four nozzle array at 1 atm

Appendix B

Non-gas-saturated Mixture Plots

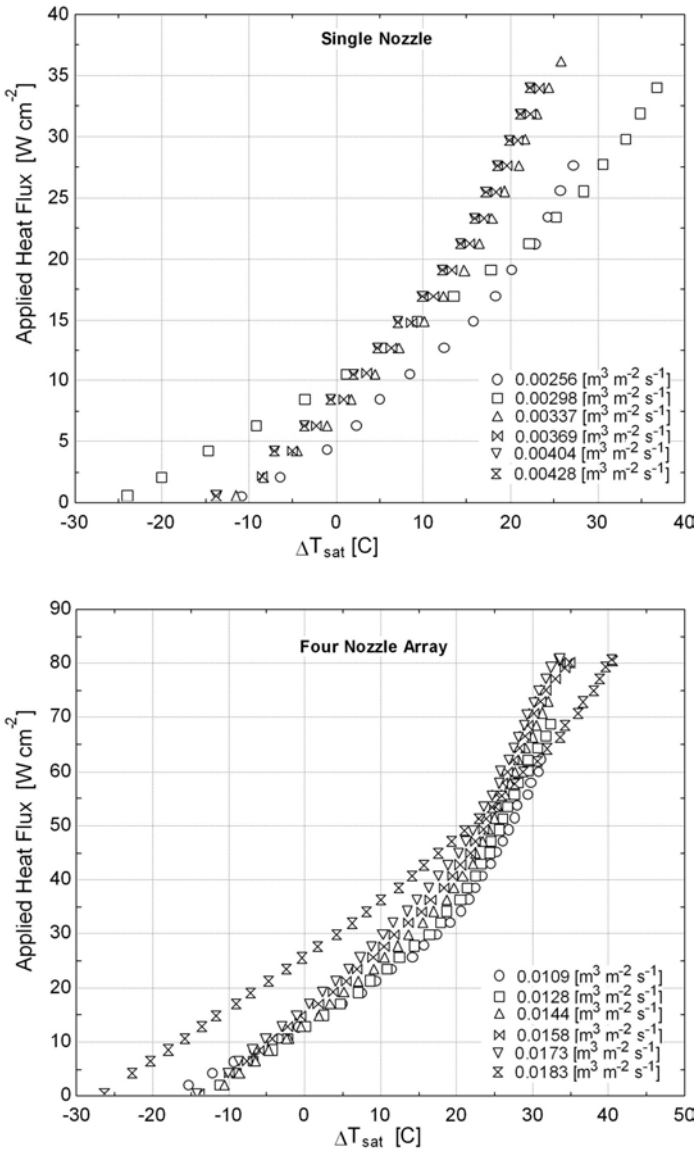

Figure B.1: Boiling curves for the 75-25 mixture of HFE-7000/HFE-7100 using the single nozzle and four nozzle array at 1 atm

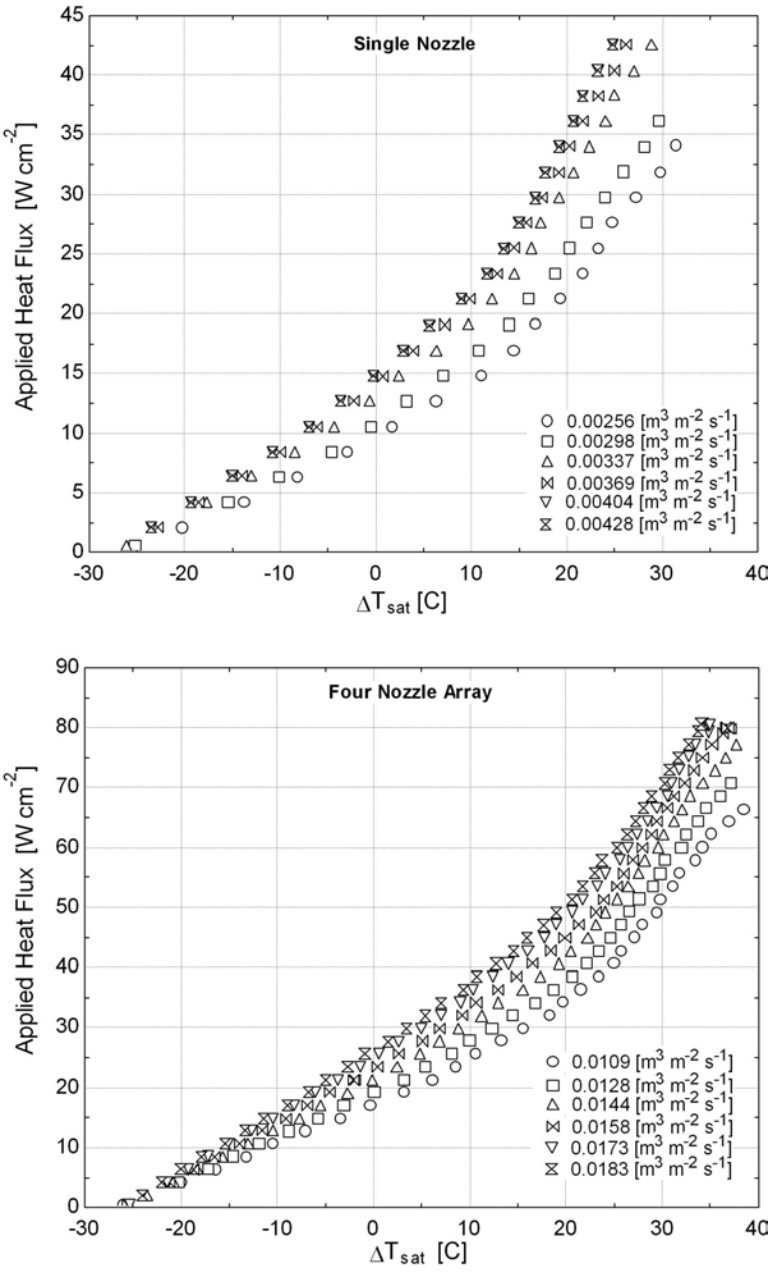

Figure B.2: Boiling curves for the 50-50 mixture of HFE-7000/HFE-7100 using the single nozzle and four nozzle array at 1 atm

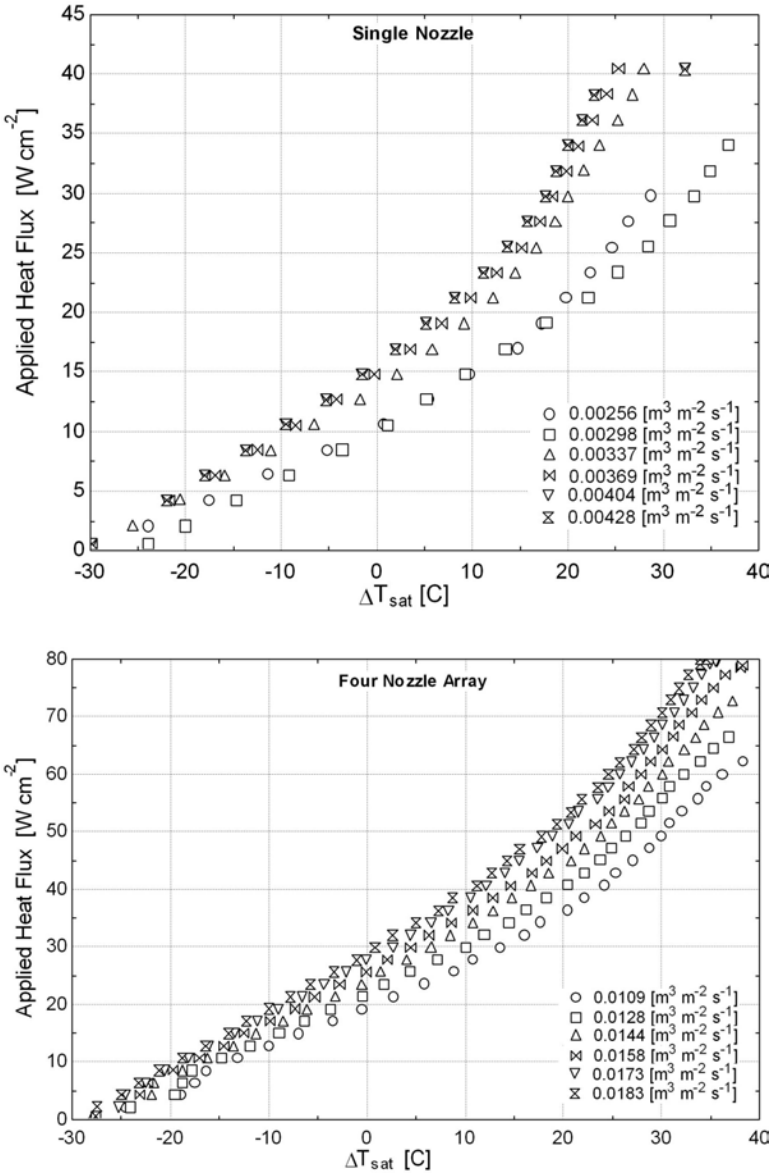

Figure B.3: Boiling curves for the 25-75 mixture of HFE-7000/HFE-7100 using the single nozzle and four nozzle array at 1 atm

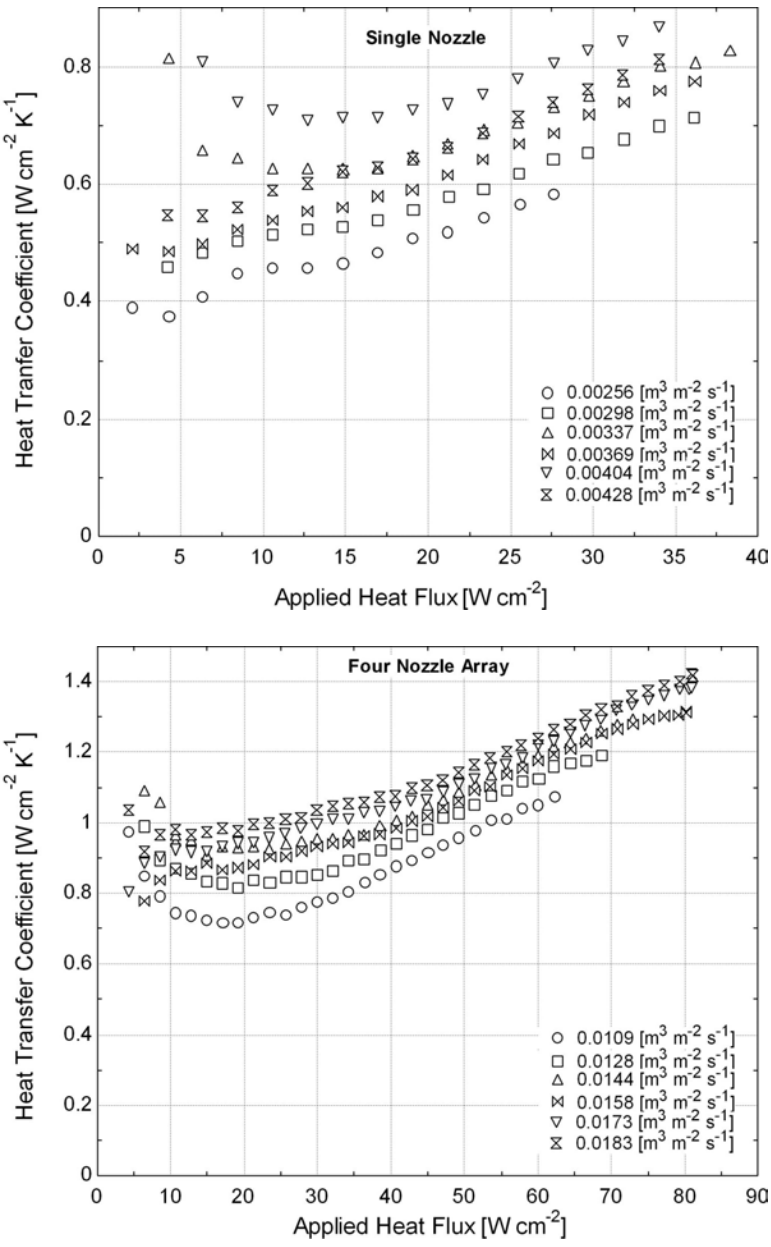

Figure B.4: Heat transfer performance for the 75-25 mixture of HFE-7000/HFE-7100 for the single nozzle and four nozzle array at 1 atm

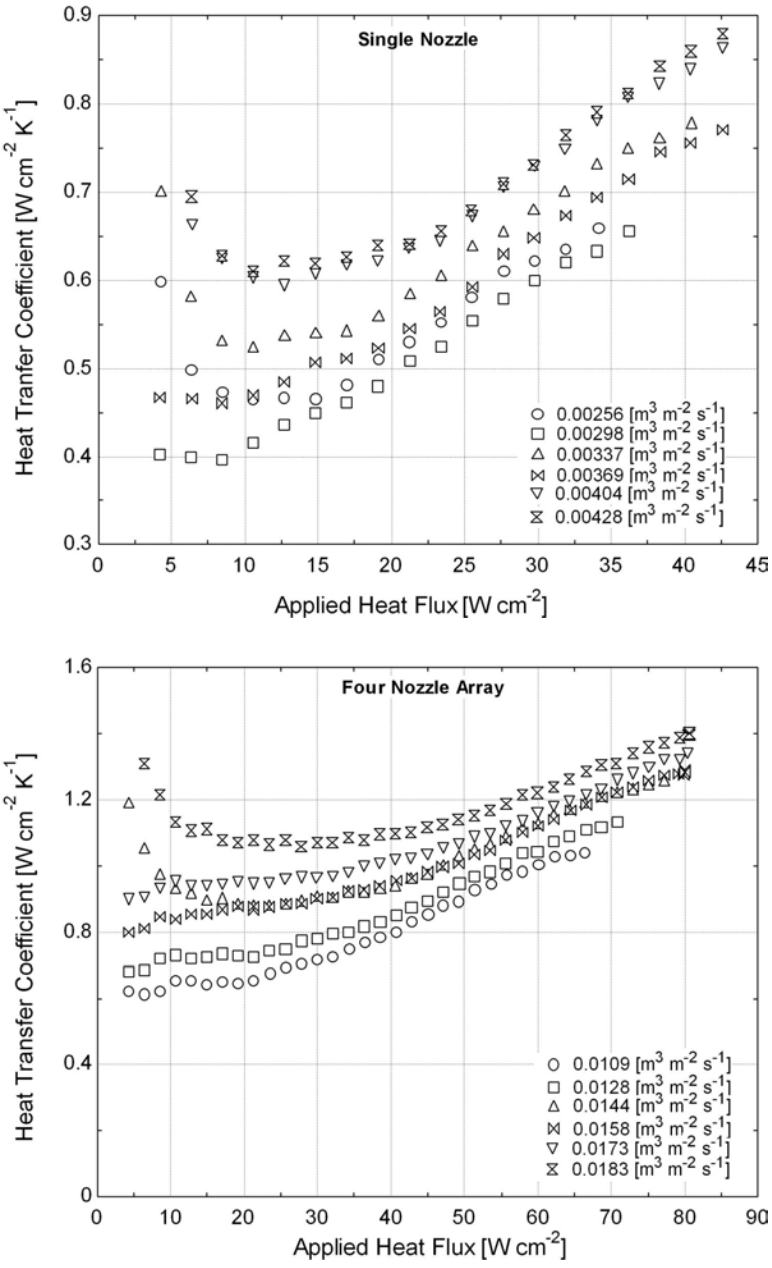

Figure B.5: Heat transfer performance for the 50-50 mixture of HFE-7000/HFE-7100 for the single nozzle and four nozzle array at 1 atm

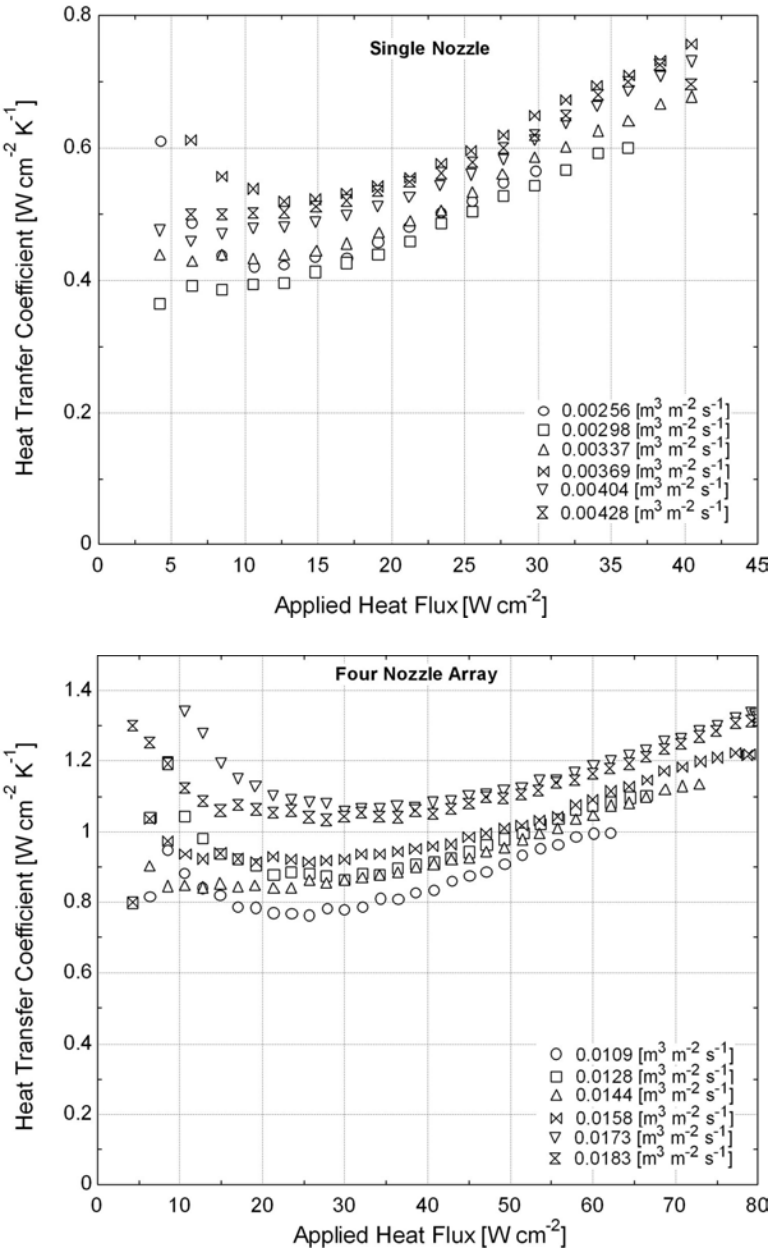

Figure B.6: Heat transfer performance for the 25-75 mixture of HFE-7000/HFE-7100 for the single nozzle and four nozzle array at 1 atm

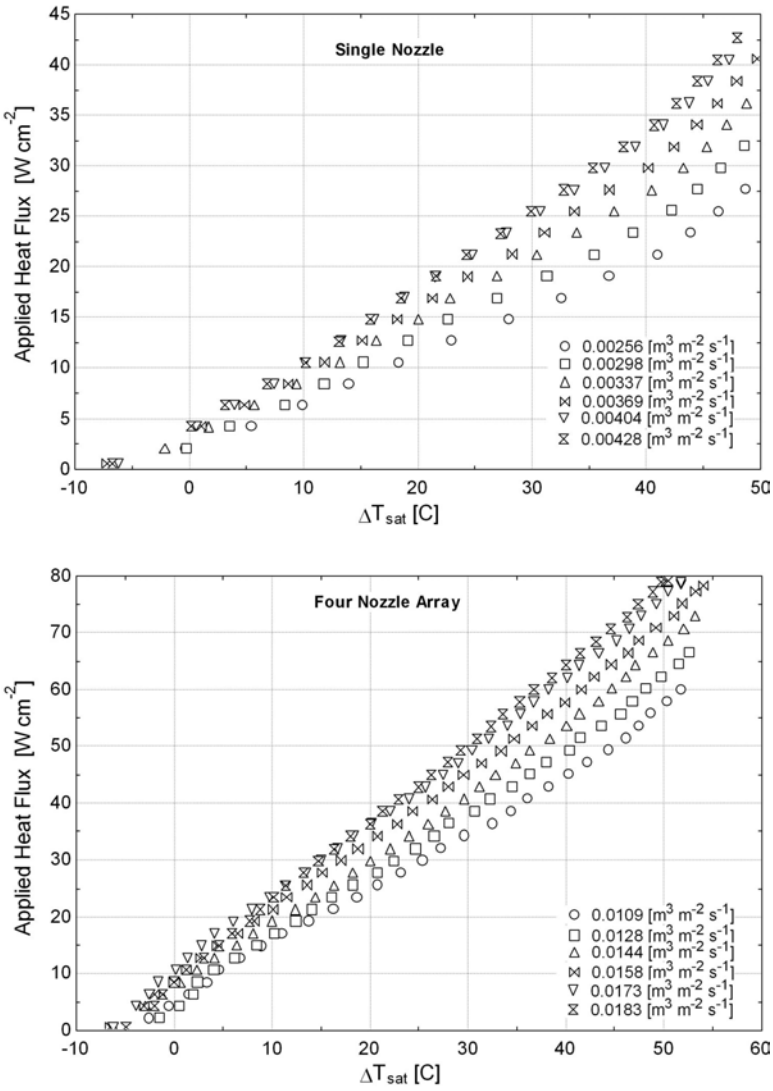

Figure B.7: Boiling curves for the 75-25 mixture of FC-72/HFE-7000 using the single nozzle and four nozzle array at saturation pressure

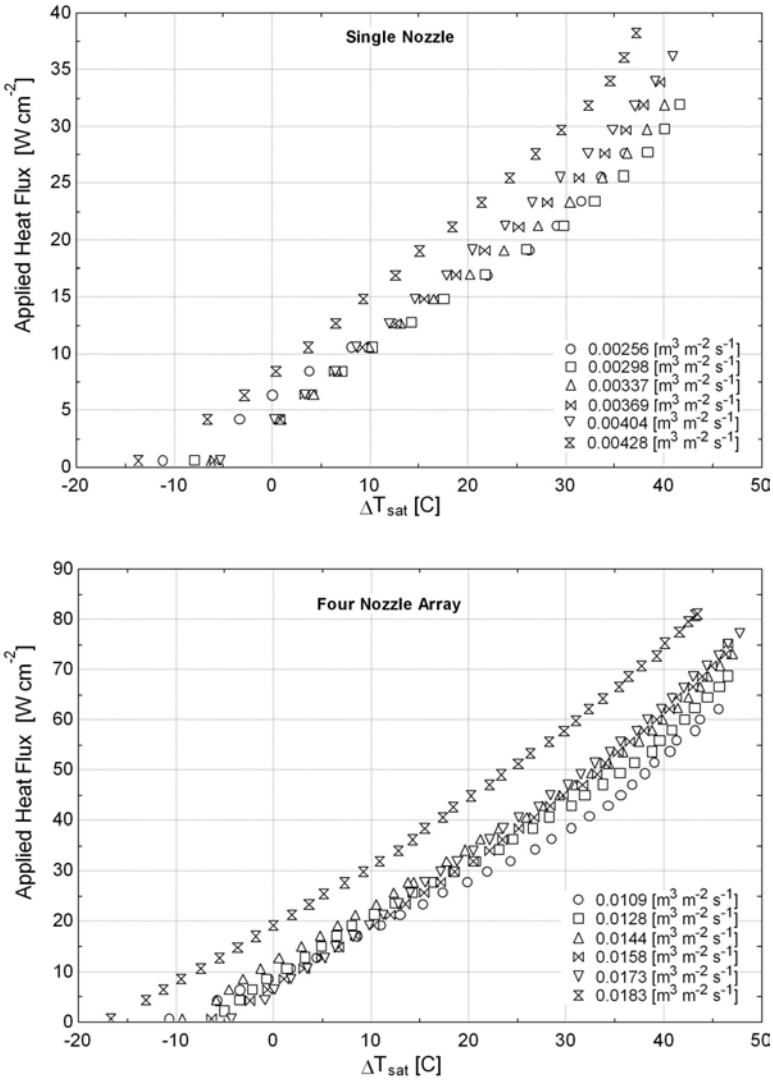

Figure B.8: Boiling curves for the 50-50 mixture of FC-72/HFE-7000 using the single nozzle and four nozzle array at saturation pressure

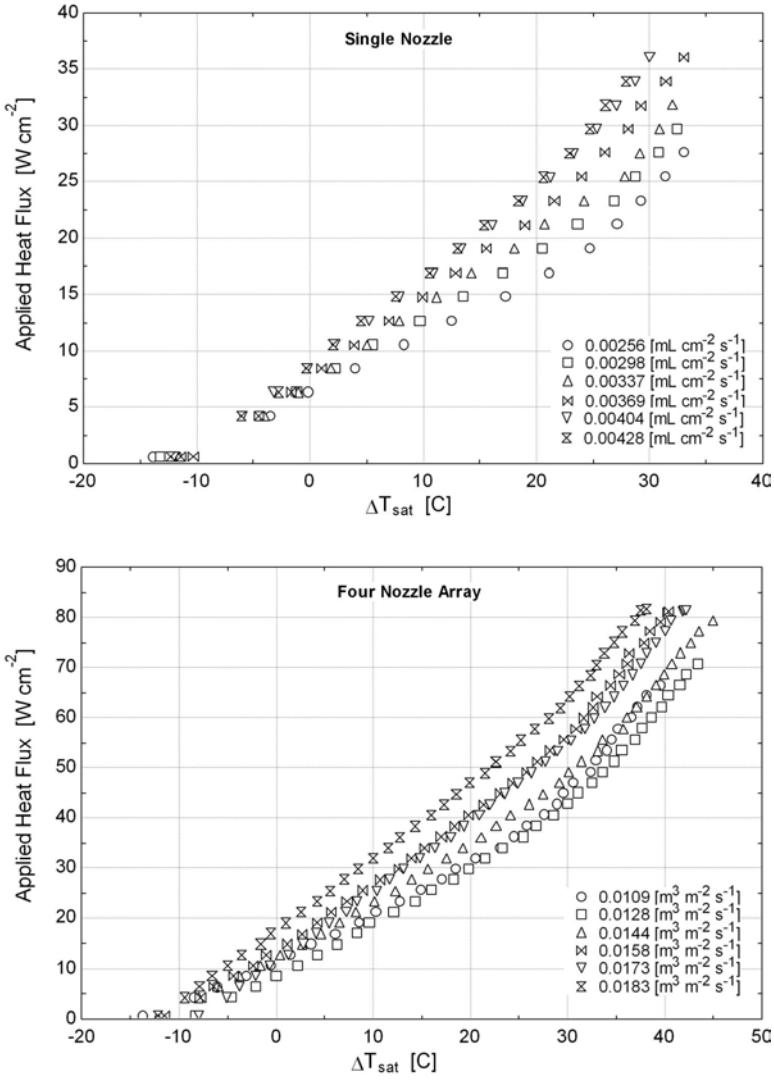

Figure B.9: Boiling curves for the 25-75 mixture of FC-72/HFE-7000 using the single nozzle and four nozzle array at saturation

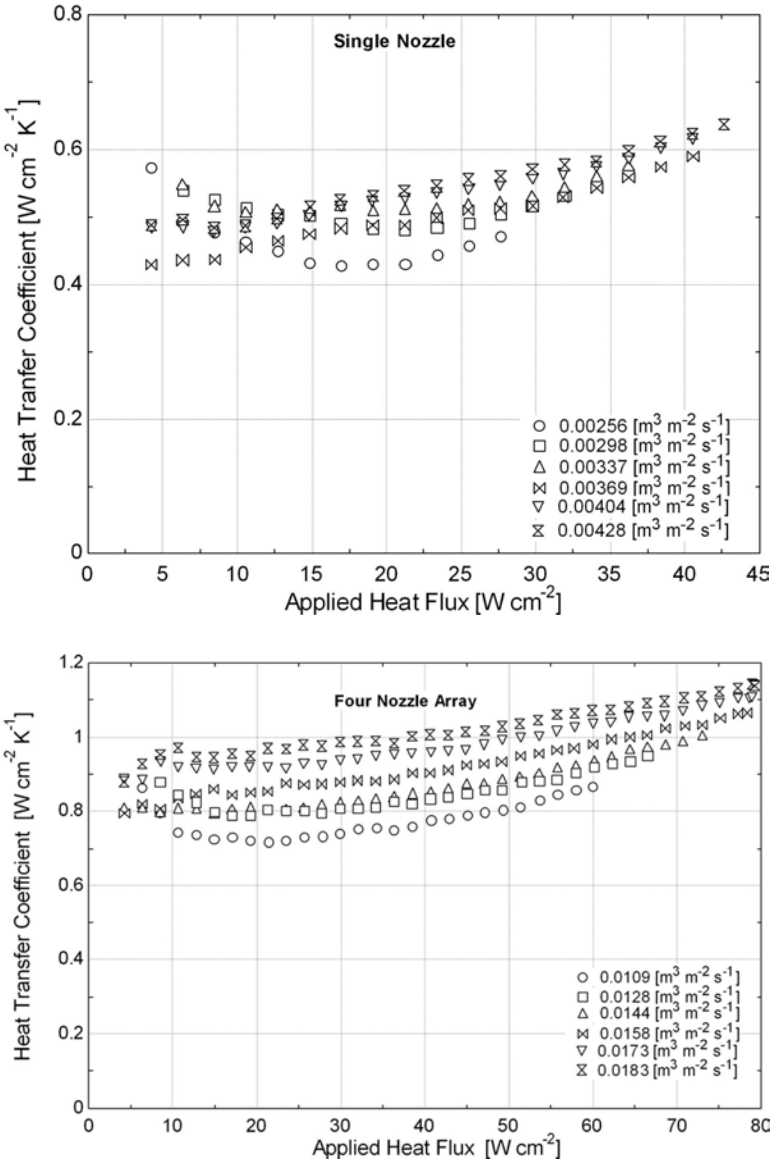

Figure B.10: Heat transfer performance for the 75-25 mixture of FC-72/HFE-7000 for the single nozzle and four nozzle array at saturation pressure

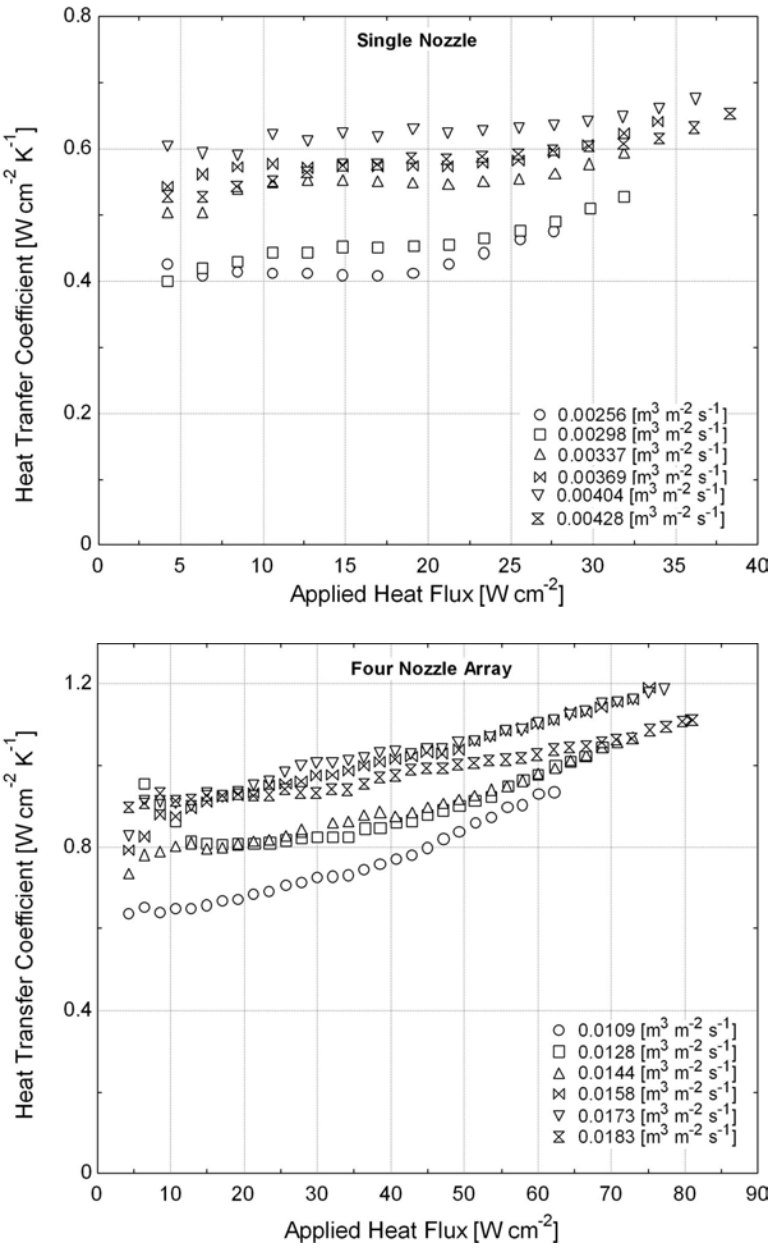

Figure B.11: Heat transfer performance for the 50-50 mixture of FC-72/HFE-7000 for the single nozzle and four nozzle array at saturation pressure

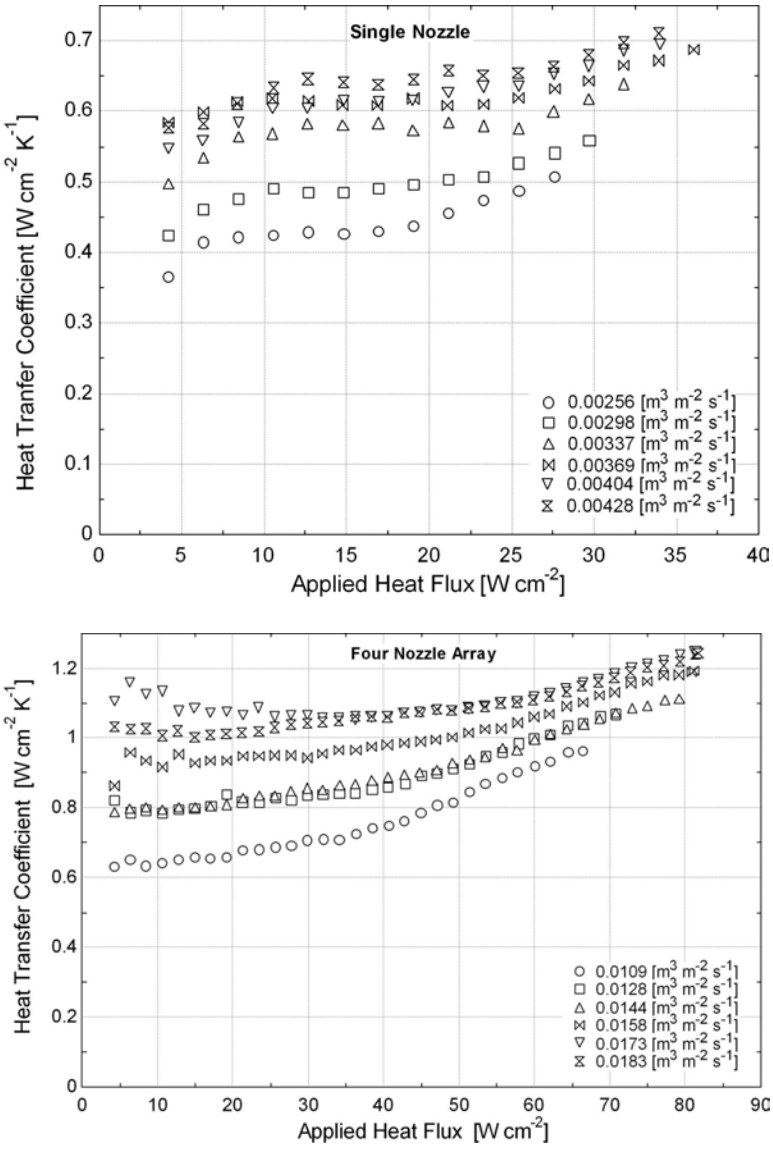

Figure B.12: Heat transfer performance for the 25-75 mixture of FC-72/HFE-7000 for the single nozzle and four nozzle array at saturation pressure

Appendix C

Numerical Model Equations

Equations

Parameters

$$A_h = w^2 \tag{C.1}$$

$$Q = q_{lpm}/A_h \cdot \left| 0.001666667 \ \frac{\text{mL/cm}^2 \cdot \text{s}}{\text{L/min} \cdot \text{m}^2} \right| \quad \text{droplet flux} \tag{C.2}$$

$$A = 22.7 \quad \text{A is y}_{crit} \text{ from cfd model} \tag{C.3}$$

$$C = 14.67 \quad \text{also from cfd model} \tag{C.4}$$

$$w = 2.54 \ \ [\text{cm}] \cdot \left| 0.01 \ \frac{\text{m}}{\text{cm}} \right| \tag{C.5}$$

$$ntn = 2 \ \ [\text{mm}] \cdot \left| 0.001 \ \frac{\text{m}}{\text{mm}} \right| \quad \text{distance between nozzles} \tag{C.6}$$

Fluid Properties

$$\rho = 1.68 \ \ [\text{g/mL}] \cdot \left| 1000 \ \frac{\text{kg/m}^3}{\text{g/mL}} \right| \tag{C.7}$$

$$\nu = 0.38 \ \ [\text{centiStoke}] \cdot \left| 1 \times 10^{\text{-}6} \ \frac{\text{m2/s}}{\text{centiStoke}} \right| \tag{C.8}$$

Variables

$$Area_{ratio} = 4 \cdot \frac{(d^2_{nozzle}) \cdot (\pi/4)}{(ntn \cdot w)} \quad 8 \text{ nozzles in 2.54 cm} \tag{C.9}$$

$$u_{drop} = \left(Q \cdot \frac{\left| 0.01 \ \frac{\text{m/s}}{\text{mL/cm2} \cdot \text{s}} \right|}{\text{Area}_{\text{ratio}}} \right) \quad \text{velocity of droplet} \tag{C.10}$$

$$\dot{m}_{flux} = Q \cdot \left| 0.01 \ \frac{\text{m3/m2} \cdot \text{s}}{\text{mL/cm2} \cdot \text{s}} \right| \cdot \rho \tag{C.11}$$

$$dx = w/N \tag{C.12}$$

$$N = 50 \tag{C.13}$$

$mom_{drop} = \dot{m}_{flux} \cdot w \cdot dx \cdot (u_{drop} \cdot MC)$ assuming that only 90% of momentum in direction of sprays (C.14)

Initial Condition

$$x_{in} = 0 \ \ [\text{mm}] \cdot \left| 0.001 \ \frac{\text{m}}{\text{mm}} \right| \tag{C.15}$$

$$x_0 = x_{in} \tag{C.16}$$

$$\dot{m}_0 = 0 \tag{C.17}$$

$$mom_0 = 0 \tag{C.18}$$

Analysis

$$\textsf{duplicate} \ \ i = 1, \ N \tag{C.19}$$

$$\dot{m}_i = \dot{m}_{i-1} + \dot{m}_{flux} \cdot dx \cdot w \tag{C.20}$$

$$\dot{m}_i = (1/2) \cdot \rho \cdot w \cdot \nu \cdot A^2 + (7/8) \cdot \rho \cdot C \cdot \nu \cdot w \cdot \delta_{plus,i}^{8/7} - (7/8) \cdot \rho \cdot C \cdot \nu \cdot w \cdot A^{8/7} \tag{C.21}$$

$$mom_i = mom_{i-1} + mom_{drop} - \tau_i \cdot dx \cdot w \tag{C.22}$$

$$mom_i = (1/3) \cdot \rho \cdot w \cdot \nu \cdot u_{\tau,i} \cdot A^3 + (7/9) \cdot \rho \cdot C^2 \cdot w \cdot \nu \cdot u_{\tau,i} \cdot \delta_{plus,i}^{9/7} - (7/9) \cdot \rho \cdot C^2 \cdot w \cdot \nu \cdot u_{\tau,i} \cdot A^{9/7} \tag{C.23}$$

$$u_{\tau,i}^2 = \frac{\tau_i}{\rho} \tag{C.24}$$

$$\delta_{plus,i} = \delta_i \cdot \frac{u_{\tau,i}}{\nu} \tag{C.25}$$

$$\delta_{mic,i} = \delta_i \cdot \left| 1000000 \ \frac{\text{micron}}{\text{m}} \right| \tag{C.26}$$

$$x_i = x_{i-1} + dx \tag{C.27}$$

$$\textsf{end} \tag{C.28}$$

$$\tau_{ave} = \text{Average}(\tau_{1..N}) \tag{C.29}$$